Late Quaternary volcanic activity in the New Ireland Basin: Distribution and geochemical evolution of tephra at the Tabar-Lihir-Tanga-Feni chain, Papua New Guinea

Dissertation
zur Erlangung des Doktorgrades
der Mathematisch-Naturwissenschaftlichen Fakultät
der Christian-Albrechts-Universität
zu Kiel

vorgelegt von
Kersten Horz

Kiel 2002

Kurzfassung

Diese Arbeit präsentiert die Ergebnisse einer sedimentologischen, petrologischen und geochemischen Studie von vulkanischen Gläsern, die aus Aschelagen in sieben Sedimentkernen gewonnen wurden. Die Sedimentkerne wurden während der EDISON II (SO−133) Forschungsfahrt in der Nähe der Tabar-Lihir-Tanga-Feni (TLTF) Inselkette, die im Neu Irland Becken von Papua Neuguinea liegen, gewonnen. Altersbestimmung, Korrelation der einzelnen Aschelagen, chemische Charakterisierung und mögliche Mantelquellen werden diskutiert.

Vor dieser Studie bestand die allgemeine wissenschaftliche Auffassung, dass die TLTF Vulkane die Hauptliefergebiete für die Aschen im New Ireland Becken sind. Eine weitere Quelle für die Aschen sind die aktiven Vulkane des New Britain Vulkanbogens, von denen man annahm, dass der vulkanische Eintrag von dort nur gering sei. In dieser Studie wird versucht, anhand geochemischer Signaturen die mögliche Herkunft der Aschenlagen zu rekonstruieren.

Die Altersbestimmungen der Sedimentkerne wurden mit Hilfe von Sauerstoffisotopenanalysen an planktischen Foraminiferen durchgeführt, aus denen sich dann durch Interpolation die relativen Alter der einzelnen Aschenlagen ermitteln ließen. Dabei konnten 37 Aschenlagen aus einem Zeitraum von 333 ka Jahren bestimmt werden.

Haupt- und Spurenelementzusammensetzung wurden an zahlreichen vulkanischen Glasscherben und Minerale der jeweiligen Aschenlagen mit einer Elektronenmikrosonde bzw. der ICP-MS analysiert. Die Elementzusammenset-zung der analysierten Gläser zeigen deutliche Unterschiede und können in drei Gruppen eingeteilt werden, die jeweils charakteristisch für ein Liefergebiet sind. Eine Gruppe besteht aus vulkanischen Gläsern deren Zusammensetzung von Tephriphonoliten über Phonoliten bis hin zu Trachyten reicht. Sie sind durch hohe Anreicherung an K, P, Pb, Sr, LILE (Grossionige, lithophile Elemente), LREE (Leichte Seltene Erden) und eine Verarmung an Ti und HREE (Schwere Seltene Erden) gekennzeichnet. Diese Zusammensetzung entspricht denen von den TLTF Vulkanen. Eine zweite Gruppe mit Daziten, Rhyoliten und Trachyten zeigt vergleichbare Anreicherungen an LILE und LREE aber wesentlich geringere P und

Sr Werte sowie eine negative Europiumanomalie. Deutliche Unterschiede liegen in der Anreicherung der HFSE (Elemente mit hoher Feldstärke) und den HREE. Aufgrund ihrer Zusammensetzung können die Gläser dieser Gruppe den Vulkanen in Rabaul (nordöstlich New Britain) zugeordnet werden. Die letzte Gruppe repräsentiert alle übrigen Vulkane in New Britain (ohne Rabaul). Sie bestehen aus Andesiten und Rhyoliten mit LILE, HFSE und REE Konzentrationen wie sie für Vulkanbögen typisch sind (z.B. Izu-Bonin, Mariana).

Die geochemischen Analysen zeigen, dass der größte Teil aller Aschenlagen in den obersten Sedimentschichten des New Ireland Beckens, einschließlich aller diskreten, aus hochexplosiven Vulkanausbrüchen stammenden Aschen, ihren Ursprung in Rabaul und allen anderen New Britain Vulkanen haben. Überraschenderweise können nur wenige Aschenlagen Eruptionen der TLTF Vulkanen zugeordnet werden. Dies könnte bedeuten, dass (i) nur kleine oder nicht explosive Ausbrüche in den letzten 333 ka stattfanden oder (ii) die TLTF Vulkane waren zum größten Teil überhaupt nicht aktiv. Beide Möglichkeiten decken sich mit den etablierten Datierungen von TLTF Vulkanereignissen, die alle wesentlich älter als 333 ka sind.

Durch die Unterschiede in der Geochemie lassen sich für die TLTF Vulkane auf der einen Seite und die Vulkane für Rabaul bzw. New Britain auf der anderen Seite unterschiedliche Mantelquellen postulieren. Vulkanische Gläser von den TLTF Vulkanen haben hohe Nb/Yb Verhältnisse, die weit über denen eines normalen MORB hinausgehen. Dieses charakteristische Merkmal teilen sie mit Basalten aus der Solomon See. Gläser vom New Britain Vulkanbogen sind sehr viel stärker verarmt im Vergleich zu N-MORB und haben geringere Nb/Yb Verhältnisse genau wie Basalte aus dem Manus Becken. Daraus lässt sich schlussfolgern, dass ein „Solomon See“ Mantelbereich mit einer angereicherten Zusammensetzung (relativ zu N-MORB) sich unter dem New Ireland Becken erstreckt. Vulkanische Gläser von Rabaul im Nordosten des New Britain Vulkanbogens haben eine sehr viel kompliziertere Übergangszusammensetzung. Diese besteht möglicherweise aus einer Mischung von „Solomon“ und „Manus“ Mantelkomponenten, bei der die fraktionelle Kristallisation von titanreichen Phasen möglicherweise eine größere Rolle spielt.

Abstract

This thesis presents the results of a sedimentological, petrological, and geochemical study of volcanic ash beds in sediment cores recovered during the EDISON II Cruise (SO–133) in the New Ireland Basin adjacent to the Tabar-Lihir-Tanga-Feni (TLTF) volcanic chain, east of Papua New Guinea. Age determination, correlation of the ash beds, attribution to possible provinces and the likely mantle sources are discussed. Before this study, the Tabar-Lihir-Tanga-Feni volcanoes were expected to be the main source of tephra in the New Ireland Basin. A further possible source for the tephras are the active volcanoes of the New Britain volcanic arc, but their contribution was expected to be minor. Here, the possible origins of the recovered ash beds in the New Ireland Basin will be discussed on the basis of their geochemistry.

Age determinations of the sediment cores, and the ash beds within them, were constrained through correlation and interpolation of foraminiferal oxygen isotope measurements. Thirty-seven ash beds in seven sediment cores dating back to 333 ka were identified.

Major and trace element compositions of numerous glass shards and minerals within the ash beds were determined using an electron microprobe and ICP-MS. The geochemical composition of the analyzed glass shards varies widely, but the shards can be cleanly split into three distinct compositional groups reflecting three different source provinces. One group consists of glass whose composition ranges from shoshonitic tephriphonolite through phonolite to trachyte, and is characterized by a strong enrichment in K, P, Sr, LILE, LREE, and depletion of Ti and HREE relative to MORB: these characteristics are shared by lavas from the TLTF volcanic chain. A second group consists of high-K dacite, rhyolite, and trachyte with similar enrichment in LILE and LREE as the TLTF lavas, but with markedly lower P and Sr concentrations, a negative Eu anomaly, and enriched HFSE and HREE concentrations: their characteristics and compositions closely resemble those of lavas from Rabaul. The last group consists of medium to low K series andesite and rhyolite, with LILE and REE concentrations very typical of island arc lavas and strongly depleted HFSE concentrations: these characteristics are

identical to those of the active New Britain island arc volcanoes (excluding Rabaul).

The geochemical analyses reveal that the great majority of all ash beds in the uppermost sediments of the New Ireland Basin, including all discrete prominent air-fall beds representing large highly explosive eruptions, are sourced from Rabaul and the other active New Britain arc volcanoes. Surprisingly, only a few thin tephra beds can be attributed to eruptions at the TLTF volcanoes. This suggests that either (i) only small, or non-explosive, eruptions have occurred at the TLTF volcanoes during the last 333 ka, or (ii) the TLTF volcanoes have been largely inactive since 333 ka. Both possibilities are consistent with the established record of volcanism on the TLTF islands, where all known volcanic events appear to be significantly older than 333 ka.

There is a clear distinction, on the basis of the observed geochemistry, between the mantle source of the TLTF volcanoes and that of Rabaul and the other New Britain volcanoes. Glasses from the TLTF volcanoes have high Nb/Yb ratios well above those of N-MORB, a characteristic shared by basalts from the Solomon Sea. In contrast, glasses from the New Britain arc volcanoes are strongly depleted relative to N-MORB and have low Nb/Yb values, as do basalts from the Manus Basin. Thus, it appears that a distinct "Solomon Sea" mantle domain with an enriched composition relative to MORB may extend to the northeast and underlie the New Ireland Basin. Glasses from Rabaul in the far northeast of New Britain have a more complicated transitional composition that may reflect a mix of both Solomon and Manus mantle components, and possibly a greater role for fractional crystallization of Ti-rich phases.

Contents

Figures

Tables

1 INTRODUCTION

1.1 Island arc systems

Island arc systems are formed when two oceanic plates converge and one subducts beneath the other. When the subducted oceanic lithosphere reaches a depth in excess of 80 km, an island arc is created at the surface by volcanic and plutonic activity 100–200 km from the trench axis. Island arcs are typical of the margins of shrinking oceans such as the Pacific, where the majority of island arcs are located. The generalized morphology of an island arc system is shown in Figure 1. Proceeding from the oceanward side of the system, the fore-arc region comprises the trench itself, the subduction complex (accretionary wedge) and the fore-arc basin.

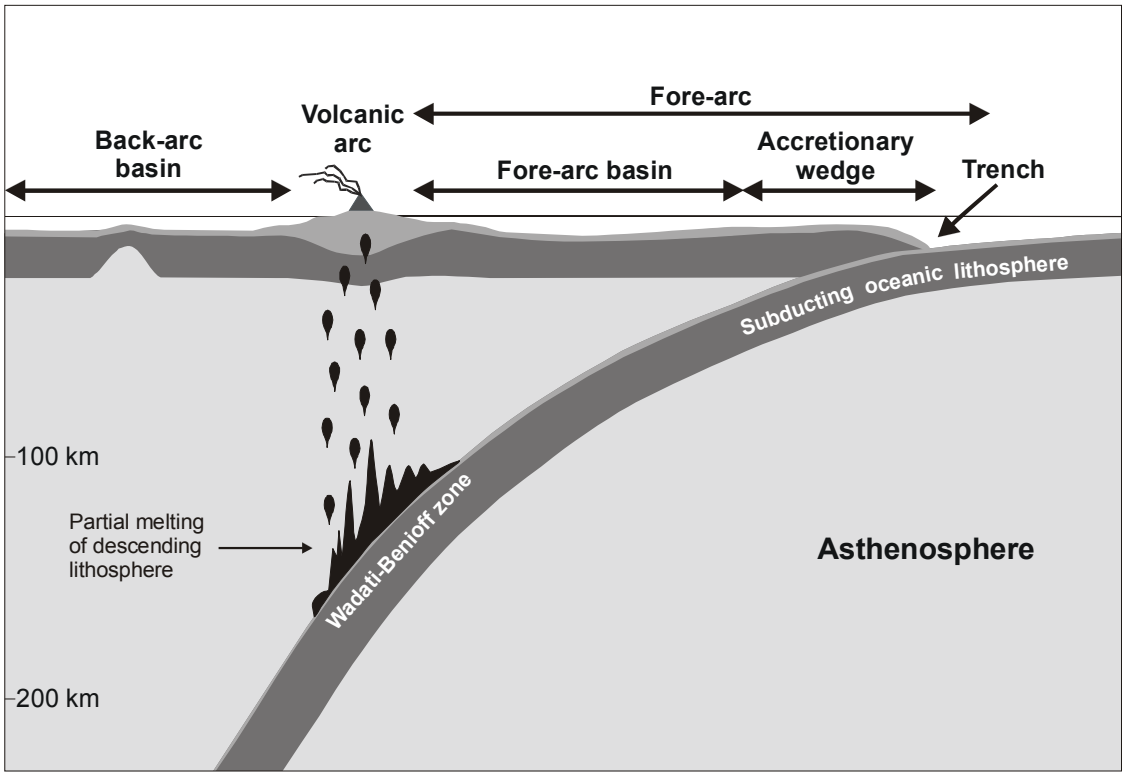

Figure 1: Idealized model of a subduction zone and a island arc.

The subduction complex is constructed of thrust slices of trench fill sediments and also possibly oceanic crust, which have been scraped off the downgoing slab by the leading edge of the overriding plate (Silver and Reed, 1988). A marginal

sea (back-arc basin) is often developed behind the island arc (Kearey and Vine, 1990, Figure 1). Three series of volcanic rocks occur in the island arc environment (Baker, 1982):

1. The low K (tholeiitic) series, which is dominated by basaltic lavas associated with lesser volumes of iron-rich basaltic andesites and andesites.
2. The medium K (calc–alkaline) series, which are more enriched in potassium, other incompatible elements and light rare earth elements (REE).
3. The high-K series, which includes the subgroups of alkaline basalts and shoshonitic lavas.

The tholeiitic series is found in intra-oceanic arcs (Aleutian, Mariana, Tonga–Kermadec, New Hebrides, Lesser Antilles). The tholeiites have been interpreted as being derived by the fractional crystallization of olivine from a primary olivine tholeiite magma originating at relatively shallow levels of 80–120 km. The calc–alkaline and alkaline series are encountered in continental margin arcs (Japan, Indonesia), and are believed to be derived from magmas generated at increasingly greater depths. There are also a systematic variations in trace element abundance, element and isotope ratios which correlate with the depth to the Benioff zone (Ringwood, 1974).

But how are volcanic islands generated if an active subduction system stalls, and the fore-arc turns into back-arc? The development of such an unusual volcanic island chain, generated by decompression processes, can be studied in the Bismarck Archipelago, east of Papua New Guinea. The Tabar-Lihir-Tanga-Feni (TLTF) island chain is the object of interest in this study (Figure 2).

1.2 Aims and objectives of this study

There exists little previous data on tephra layers in sediment cores from the New Ireland Basin. Therefore, detailed sampling and mapping near the Tabar, Lihir, Tanga, and Feni volcanic islands in the New Ireland Basin was undertaken during the EDISON I cruise of the R/V *SONNE* in mid-1994 (SO–94), followed by the EDISON II cruise (SO–133) in the summer of 1998 (Herzig et al., 1994; Herzig et al., 1998). During both expeditions, the bathymetry of the area was mapped using the HYDROSWEEP system. A number of young submarine volcanic cones

and hydrothermal systems were discovered near Lihir (Herzig et al., 1994; Herzig et al., 1998; McInnes et al., 2001). The following topics were investigated and interpreted on the basis of new geochemical data:

- Geochemical signatures of the tephra in the TLTF island chain.
- Chemical correlations between the TLTF-, Rabaul- and/or New Britain arc tephra.
- Provenance of the volcanic ash deposits based on their chemical and mineralogical composition.
- Are there temporal and spatial variations in the volcanic activity?
- Can the tephras be assigned to different magma sources through trace and rare earth elements?
- Are any evidence of the active subduction phases in the geological past?
- Is there any contribution to the magmatic source from lithospheric slabs subducted in the past?
- Is the mantle source beneath the Bismarck Archipelago homogeneous or heterogeneous in composition?

1.3 Organization of this study

This work is presented in eight chapters. Chapter 2 gives a general overview of the development, including tectonic setting and known geochemistry of the volcanic islands. The sedimentology, including sampling and sample site descriptions, detailed explanation of the sediment and the volcanic ash beds is presented in chapter 3. The results of the stable isotope analyses used for chronostratigraphy are discussed in chapter 4. Chapter 5 describes the mineralogy of the investigated samples. Major and trace elements of the volcanic glass is presented in chapter 6. The discussion in chapter 7 is subdivided into several sections. 7.1 pay attention to the volcanic activity. 7.2 gives a evolutionary model for the TLTF volcanoes. 7.3 identifies the slab component. 7.4 draw light on fractionation of incompatible elements. 7.5 gives a implication for possible mantle sources.

2 HISTORY

2.1 Introduction

The studied area is part of the Bismarck Archipelago, located approximately 600 km to the northeast of Papua New Guinea. It is a complicated microplate mosaic, which finds its expression in the island arc complexes of New Britain, New Ireland and New Hanover, Bougainville, the Solomon islands, and the area of investigation, the Tabar-Lihir-Tanga-Feni (TLTF) island chain (Figure 2).

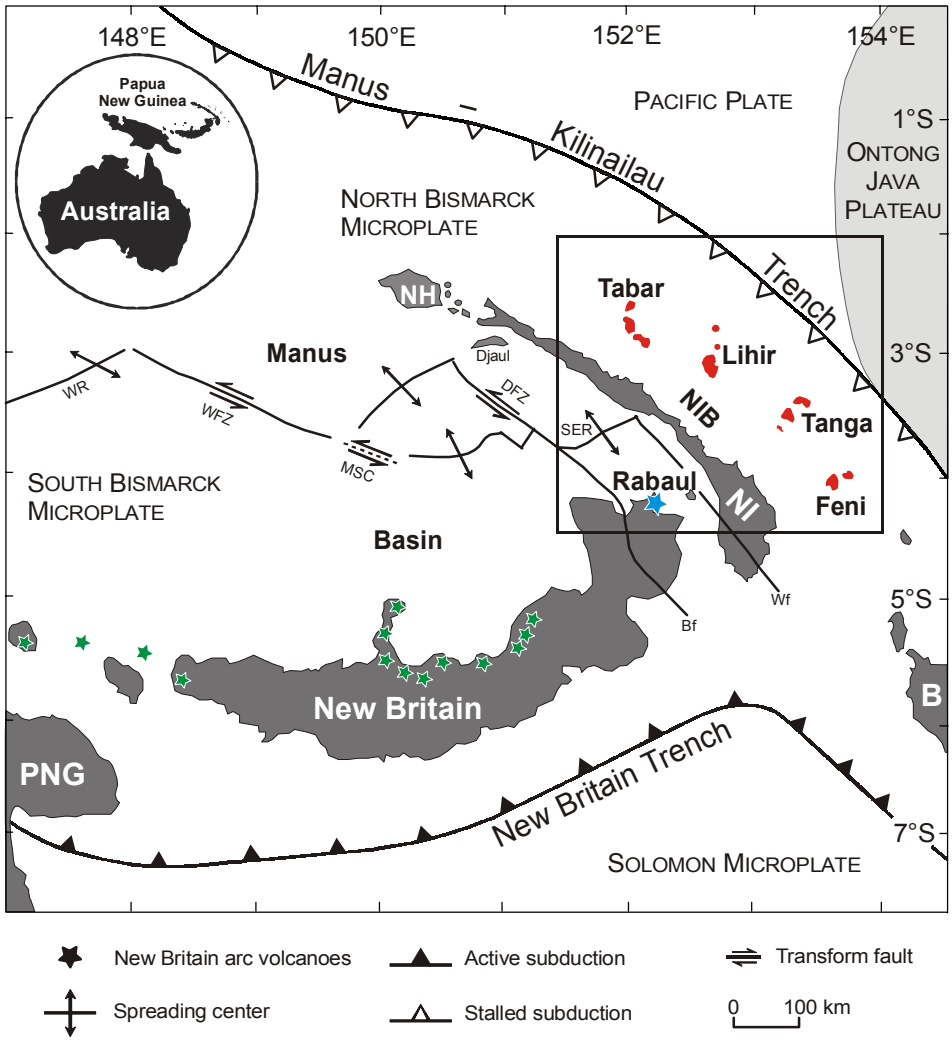

Figure 2: Location map showing the Bismarck Archipelago east of Papua New Guinea with the Tabar–Feni island chain (boxed area) and the principal structural elements of the New Ireland and Manus Basin (modified after Herzig et al., 1998). Abbreviations: WR = Wuillaumez Ridge, WFZ = Wuillaumez Fracture Zone, MSC = Manus Spreading Center, DFZ = Djaul Fracture Zone, SER = South East Ridge, Bf = Baining fault, Wf = Weitin fault, NH = New Hanover, NI = New Ireland, NIB = New Ireland Basin, PNG = Papua New Guinea, B = Bougainville.

The Tabar to Feni volcanic chain extends nearly 250 km parallel to New Ireland. The distance between the island chain and the Manus–Kilinailau Trench decreases from 125 km in the NW to less than 70 km in the SE. The peaks of the volcanoes at Tabar and Lihir rise to over 2000 m above the seafloor, whereas the Tanga and Feni volcanoes are situated in deeper water further to the SE and ascend 2500–2900 m above the seafloor. These volcanic massifs have volumes of 20–200 km^3 and altogether of more than 500 km^3 (Wallace et al., 1983).

The Tabar volcanic group exists of two islands, Simberi in the north and Tatau in the south. The Lihir group of islands consists of the main island of Lihir, the nearby islands of Mali and Sanambiet, and the smaller islands of Masahet and Mahur to the north. The Tanga Islands are midway between the Lihir and Feni island groups and are the smallest of the four groups in the Tabar–Feni chain. The Tanga group is composed of four inhabited islands of Malendok, Lif, Tefa, and Boang, and the two uninhabited volcanic islets of Bitlik and Bitbok. Finally the Feni Islands is a collective name for two adjacent islands, Ambitle and Babase. Those islands are at the southeastern end of the Tabar–Feni chain. All the islands consist mainly of Pliocene and Pleistocene lava flows and volcaniclastic deposits (Wallace et al., 1983). Present day thermal activity is found in each of the island groups, but best developed on Lihir and at the submarine seamounts discovered 1994 (e.g. Edison seamount, Herzig et al., 1994).

2.2 The New Ireland Basin

The convergence of the Indo–Australian and Pacific Plate at rates of 9-14 cm per year and the presence of at least two minor plates in the Bismarck Archipelago have produced one of the most tectonically and volcanically active regions on Earth (Curtis, 1973). The formation of island arcs in the Bismarck Archipelago is related to the westward subduction of the Pacific Plate under the Indo–Australian continent in the early Tertiary (Johnson, 1979; Stewart and Sandy, 1988). Throughout this period, the New Ireland Basin was a non-volcanic fore-arc basin. The collision of the buoyant oceanic Ontong Java Plateau with the 6000 m deep Manus–Kilinailau Trench in the middle Tertiary led to a reversal of subduction polarity (Figure 3), and to a reorganization of the plate tectonic regime with the

development of a mosaic of micro plates northeast of Papua New Guinea (Kennedy et al., 1990a; Kennedy et al., 1990b; McInnes and Cameron, 1994; Tregoning et al., 1998).

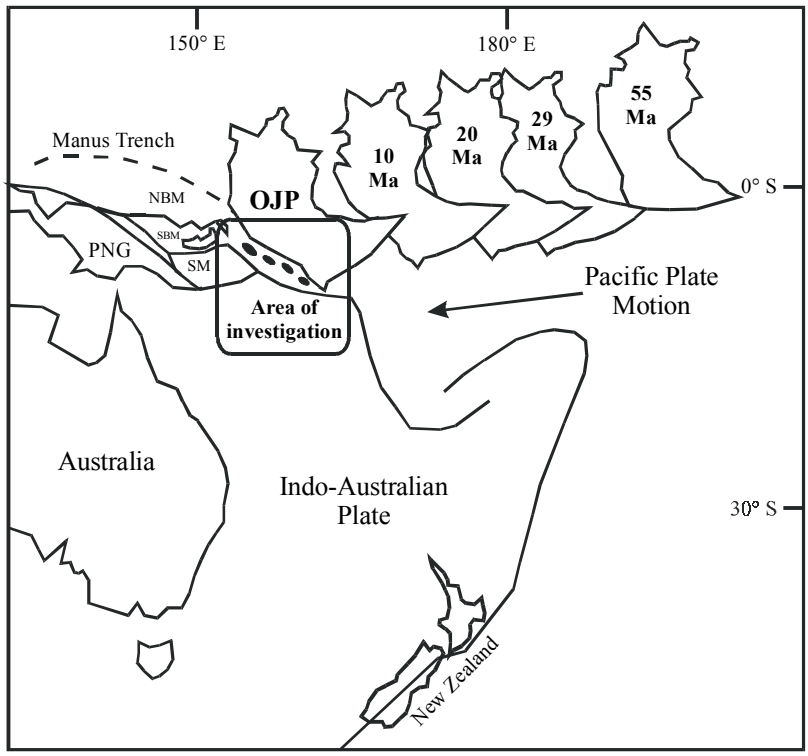

Figure 3: The westward motion of the Pacific Plate since the Tertiary (redrawn after Coleman and Packham, 1976) and late Miocene collision of the Ontong Java Plateau (OJP) with the Manus-Kilinailau Trench. PNG = Papua New Guinea, NBM = North Bismarck Microplate, SBM = South Bismarck Microplate, SM = Solomon Microplate.

This collision around 10 Ma blocked further subduction of the Pacific Plate (Kroenke, 1972; Moberly, 1972; Coleman and Kroenke, 1981). Spreading at the Manus back-arc spreading center caused faulting of the lithosphere and the development of small pull-apart basins in the New Ireland Basin and is possibly associated with initiation of the Pliocene to Recent volcanism at the TLTF islands.

At about 6 Ma, calc-alkaline volcanism commenced in the area of New Britain, New Ireland, Bougainville, and the Solomon Islands (Kroenke, 1984). Plate reorientation and fragmentation of the NE part of the Indo–Australian continent resulted in the formation of the Bismarck and Solomon microplates by back-arc spreading and the opening of the Manus Basin at 3.5 Ma (Taylor, 1979; Weissel, 1981; Marlow et al., 1991, Figure 4).

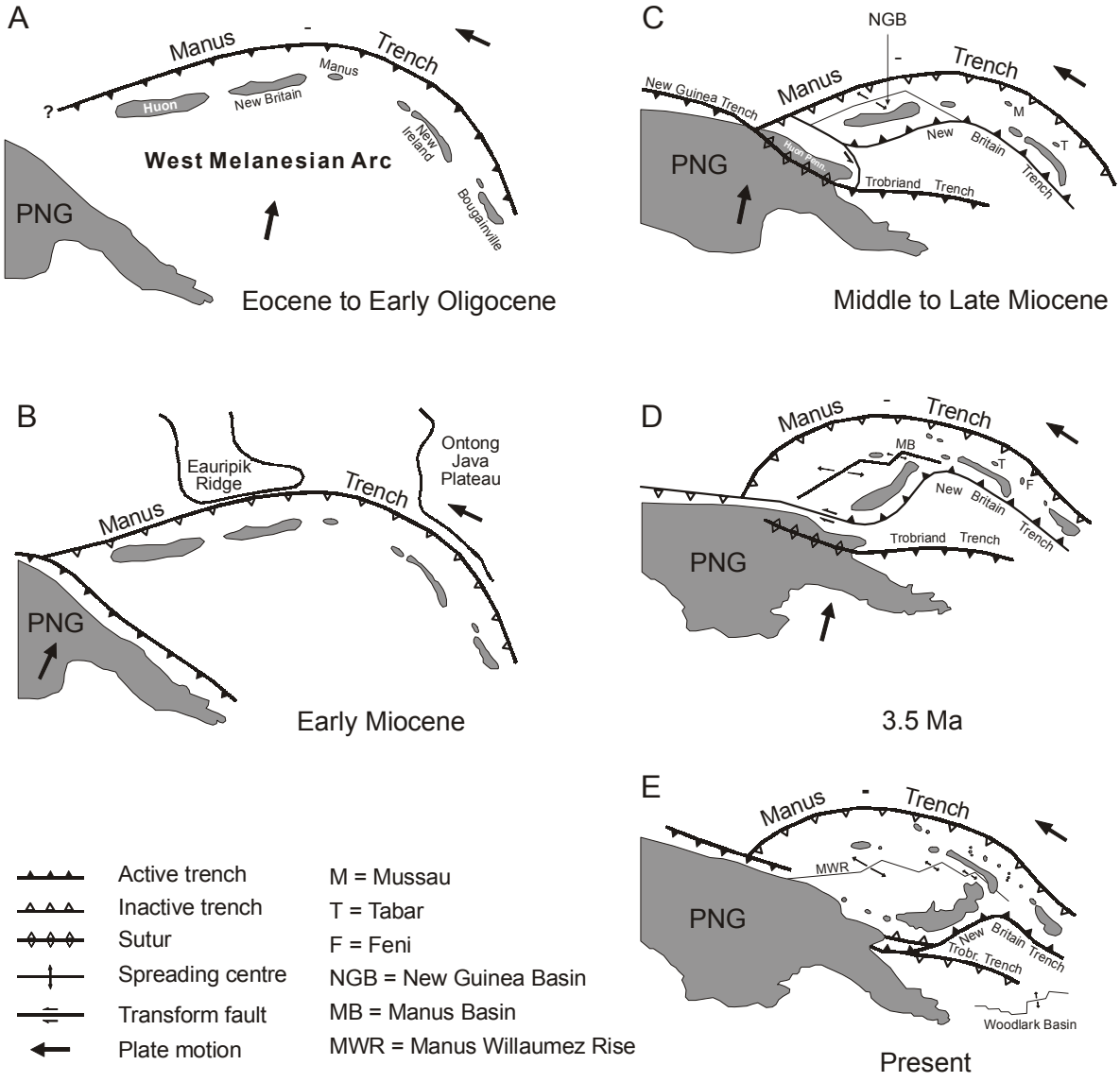

Figure 4: Schematic developing of the New Ireland area of the West Melanesian Arc from (Marlow et al., 1991). (A) In early Tertiary, the ancestral West Melanesian Island Arc (WMA) forms by southward-directed subduction initiated by underthrusting of the Pacific Plate as Australia and Papua New Guinea (PNG) moved north. The Ontong Java Plateau (OJP) is far to the southeast in the Pacific. The plateau migrated northwest on the Pacific Plate as convergence continued along the WMA. (B) By early Miocene, the OJP and the Eauripik Ridge collided with the trench along WMA, stopping subduction. The subduction zone then shifted south along mainland PNG at the New Guinea Trench. (C) At middle to late Miocene a fragment of the WMA, the ancestral Huon Peninsula, collided and rotated around PNG. The new northeast-directed subduction reversed the polarity of the WMA from the earlier southwest-directed subduction. About 5 Ma after subduction began along the New Britain Trench, back-arc spreading started between New Britain and the Manus Trench when the New Guinea basin began to open. (D) 3.5 Ma, the back-arc rifting jumped between Manus and New Britain Islands, opening Manus Basin and translating New Britain to the southeast relative to New Ireland, processes which still continue to the present (E). Further explanations are given in the text.

During back-arc spreading proto New Britain was transported at about 13 cm/yr to its present position in the southeast. Anti-clockwise rotation of proto New Britain resulted in collision with Papua New Guinea, and caused the formation of NW–SE striking transform faults and the left-lateral segmentation of the Manus spreading center. Transform-related, NW–SE striking faults now penetrated the island arc crust of New Ireland (Weitin and Baining fault, Stewart and Sandy, 1988) and appeared to extend into the New Ireland Basin. Distinct NW–SE trending faults occur on individual islands of the Tabar–Feni chain and have been recognized in offshore areas adjacent to the islands (Exon et al., 1986).

The youngest andesite-dacite volcanism in the area is of Pliocene–Pleistocene age and related to NNE striking faults which were probably formed as a result of extension parallel to the Manus back-arc spreading (Stewart and Sandy, 1988). The continued westward drift of the Pacific Plate could no longer be accommodated by the Manus–Kilinailau subduction zone, and caused plate rotation and stress relocation culminating in the formation of the active New Britain subduction zone. Although plate rotation has isolated the Tabar–Feni chain from the presently active arc of New Britain (Exon et al., 1986). The present volcanism on the islands is most likely related by some means to subduction from the south along the New Britain–Solomon Trench (Herzig et al., 1998). The major elements of the present tectonic regime are:

- northward subduction of the oceanic Solomon Microplate at the New Britain Trench with concomitant development of the New Britain volcanic arc,
- southward roll-back of the New Britain Trench and southward movement of New Britain relative to New Ireland and mainland Papua New Guinea,
- and crustal extension and seafloor spreading in the back-arc Manus Basin.

Thus, the New Ireland Basin is presently in a back-arc setting and the TLTF volcanoes do not overlie an active subduction system (Figure 2).

Volcanic activity on the islands, which began about 3.5 Ma ago and migrated in time from northwest to southeast, appears to have been related to extension along northeast-trending structures that cut across the New Ireland Basin (Kennedy et al., 1990a; McInnes and Cameron, 1994). The New Ireland Basin was shown by Exon and Tiffin (1984) to be a relatively simple downwarp with up to 5 km of Oligocene and younger sedimentary fill. Since Pliocene–Pleistocene time, partial

melts associated with extension in the thickened crust of the New Ireland Basin have risen through the old fore-arc crust along reactivated transfer faults to form the volcanic islands of the TLTF chain (Exon et al., 1986; Stewart and Sandy, 1988; McInnes, 1992; Herzig et al., 1998).

2.3 The Tabar-Lihir-Tanga-Feni volcanic chain

Previous geochemical studies of the Tabar-Lihir-Tanga-Feni (TLTF) islands made the striking observation that the TLTF volcanic chain is characterized by the occurrence of silica undersaturated, highly alkaline rocks with trace element and isotopic characteristics typical of modern island arc volcanism (e.g. Wallace et al., 1983; Kennedy et al., 1990b; McInnes and Cameron, 1994; Stracke and Hegener, 1998). These authors concluded that volcanism at the TLTF islands taps a sub-lithospheric mantle that has been enriched in incompatible trace elements during former periods of plate subduction. This observation is particularly significant since volcanic activity at the TLTF islands is not related to active plate subduction, but appears to be triggered by northeast–southwest trending extensional faults (Kennedy et al., 1990b; McInnes and Cameron, 1994; Herzig et al., 1998). Thus, for lavas produced in an extensional tectonic regime, the geochemical characteristics of the TLTF tephra are highly unusual.

The occurrence of alkaline, SiO_2-undersaturated volcanism in the Tabar–Feni area is unique among the island arcs of the Bismarck Archipelago. While alkali-olivine basalts, olivine nephelinite, basanite, tephrite, trachybasalts, and trachyandesites dominate the Tabar–Feni chain, the other island arcs are characterized by low- and medium-K andesitic volcanism (Johnson, 1979; Wallace et al., 1983; Johnson et al., 1988; Kennedy et al., 1990b; McInnes and Cameron, 1994).

Lava flows, interbedded lapilli tuffs, interlaminated ash beds, and volcaniclastic rocks, together with few domes and dykes, form the bulk of the TLTF islands. The older effusive rocks are subaerial in origin. Some rocks have prominent phenocrysts of green pyroxene and crystals of plagioclase up to 3 mm long (Wallace et al., 1983). Most of the younger volcaniclastic succession is mostly well consolidated, and consists of interbedded, angular to sub-angular, mafic clasts.

These are subordinate to a matrix of unsorted ash and breccia, containing fragments of pumice, and pyroxenite nodules (Wallace et al., 1983). Further geochemical analyses of glasses from these islands were beyond the scope of this study.

A model for the development of the Tabar–Feni islands based on extensional tectonics has been proposed by McInnes (1992). In this model, the onset of back-arc spreading in the Manus Basin at about 3.5 Ma, and the migration of New Britain to the SE caused the formation of NE–SW deeply penetrating extensional faults in the New Ireland Basin. The opening of pull-apart basins during this post subduction phase caused adiabatic decompression and local melting of the mantle wedge at depths of < 80 km. The alkaline melts rose along the same pull-apart structures, which initiated adiabatic decompression, and formed the alkaline volcanoes that now make up the Tabar to Feni island chain. In this model, it is postulated that volcanism in the Tabar island group must have been synchronous with the onset of back-arc spreading in the Manus Basin (McInnes, 1992). Alkaline melts were generated by partial melting of mantle material which had been subjected to metasomatism by water, carbon dioxide, and alkali-rich components released from sediments during the earlier subduction of the oceanic slab. Significant metasomatic contamination of the mantle wedge above the subduction slab is suggested by isotopic data, for instance high $\delta^{18}O$, high $^{87}Sr/^{86}Sr$, and significant Sr-enrichment, and mineral chemistry on carbonate-rich phlogopites and amphiboles from pyroxenite ejecta in the Tabar group (McInnes and Cameron, 1994).

The conventional opinion is that the age of volcanism in the Lihir and Feni island group must be younger due to the SE migration of the locus of extension as it followed the transport of New Britain. Radiometric age data from the Tabar island group are scarce and range from 3.7 - 1.9 Ma (Johnson, 1979; Wallace et al., 1983; Licence et al., 1987; Rytuba et al., 1993). Further to the south the volcanic activity has been lasted from 1.1 Ma to 2.2 Ka. The most recent eruption on land occurred about 2300 yr ago on Ambitle Island in the Feni group to the extreme southeast (Licence et al., 1987).

2.4 The EDISON I Cruise (SO–94)

In March 1994 the research vessel *SONNE* mapped the largely uncharted offshore areas of the Tabar-Lihir-Tanga-Feni island chain in the New Ireland Basin of Papua New Guinea. The Epithermal Deposits Southwestern Pacific Ocean (EDISON) cruise was a multidisciplinary program. The objectives of this program were to study the tectonic setting, to document recent submarine volcanism, and hydrothermal activity, as well as ore-forming processes in an area of young, alkaline seamounts (Herzig et al., 1994). Detailed mapping and sampling was carried out in the vicinity of each of the four island groups of the Tabar-Feni chain. On the southern flank of Lihir island, a group of three volcanic cones (Edison, Conical, and TUBAF Seamounts) were discovered at water depths of 1000–1500 m. The volcanoes are located in a narrow zone of recent seismic activity and elevated heat flow (up to 100 mW/m^2). The recovered volcanic rocks consist of fresh alkali-olivine basalts, clinopyroxene-rich basalts (ankaramites), and porphyritic phlogopite basalts. One of the volcanoes has a recently erupted ejecta blanket containing abundant mafic to ultramafic xenoliths, ranging from spinel lherzolite, dunite and harzburgite, to wehrlite, gabbro, anorthosite, serpentinite, and amphibolite. This suite appears to represent a unique cross-section of subduction-modified mantle material sampled by volatile-rich primary magma during its ascent to the seafloor. A fourth large volcano (New World Seamount) northeast of Lihir measures 2500 m at its base and has a 100 m deep pit crater about 1200 m depth. The most spectacular findings were the discovery of an active hydrothermal system with associated vent fauna and mineralization at “Edison Seamount”, and the recovery of unusual gold-rich (up to 43 ppm Au) hydrothermal precipitates in 1050 m water depth at the top of “Conical Seamount”, only 25 km south of the epithermal Ladolam gold deposit on Lihir. The discovery of submarine hydrothermal vents associated with highly alkaline, quartz-undersaturated fore-arc volcanics represents a significant departure from similar hydrothermal systems associated with MORB type and felsic calc-alkaline lavas on the mid-ocean ridges and in back-arc basins. The high gold grades in hydrothermal precipitates at “Conical Seamount” may indicate the first example of a shallow marine epithermal system analogous to those on land, and has

important implications for understanding the origin of large Ladolam-type epithermal gold deposits (Herzig et al., 1994).

As part of the multidisciplinary program marine sediment cores were raised during this cruise to investigate and document the volcanic activity during the Late Quaternary and the Holocene (Stoffers et al., 1994). The interpolated ages of the tephra layers in the known $\delta^{18}O$-event stratigraphy showed that the volcanic activity was particularly intensive in the whole island chain around 75 to 73 ka. Tanga was continuously active to around 31 ka and then sporadically to the present, with two major eruptive phases at around 18 ka and 3 ka. The Tabar group was quiescent during the $\delta^{18}O$-Stage 4 but became more active after 51 ka continuing to the present. The youngest major outbreak as recorded in the sediment cores occurred in Tanga/Feni Group at about 2 to 3 ka (Dr. K. Winn, personal communication).

2.5 The EDISON II Cruise (SO–133)

Cruise SO–133 of R/V *SONNE* conducted detailed mapping and sampling in the active tectonic zone south of Lihir Island, Papua New Guinea, between July and August 1998 (Herzig et al., 1998). This research cruise was a follow-up program of the above mentioned survey SO–94, conducted in 1994 (Herzig et al., 1994). The objectives of this cruise were to establish the nature and extent of volcanism, hydrothermal activity, and biological communities associated with active extension of the crust of the New Ireland Basin in the vicinity of Lihir Island. The main focus was the detailed investigation of epithermal gold mineralization at several young volcanic cones originally discovered during cruise 1994 (Edison-, TUBAF-, and Conical Seamount), and nearby fault zones associated with the uplift of the pedestal of Lihir (Herzig et al., 1998; Herzig et al., 1999).

As part of the SO–133 cruise eight sediment cores were completed to sample the recent record of subaerial volcanic activity especially along the northwest part of the New Ireland Basin, which hasn't been investigated on the EDISON I cruise.

3 SEDIMENTOLOGY

3.1 Sample sites

Eight sediment cores were collected at several stations in the New Ireland Basin in the vicinity of the Tabar, Lihir and Tanga volcanoes. Detailed lithological, petrological, and geochemical analyses were undertaken on seven representative sediment cores to study the abundant ash beds within all cores. Two stations were located NW of Tabar, one station was between Tabar and Lihir, three stations were NE of Lihir, and the last station was west of Tanga (Figure 5, Table 1). Core 17678, without any prominent ash input, is not shown here (see Herzig et al., 1998; Schmidt et al., in press.).

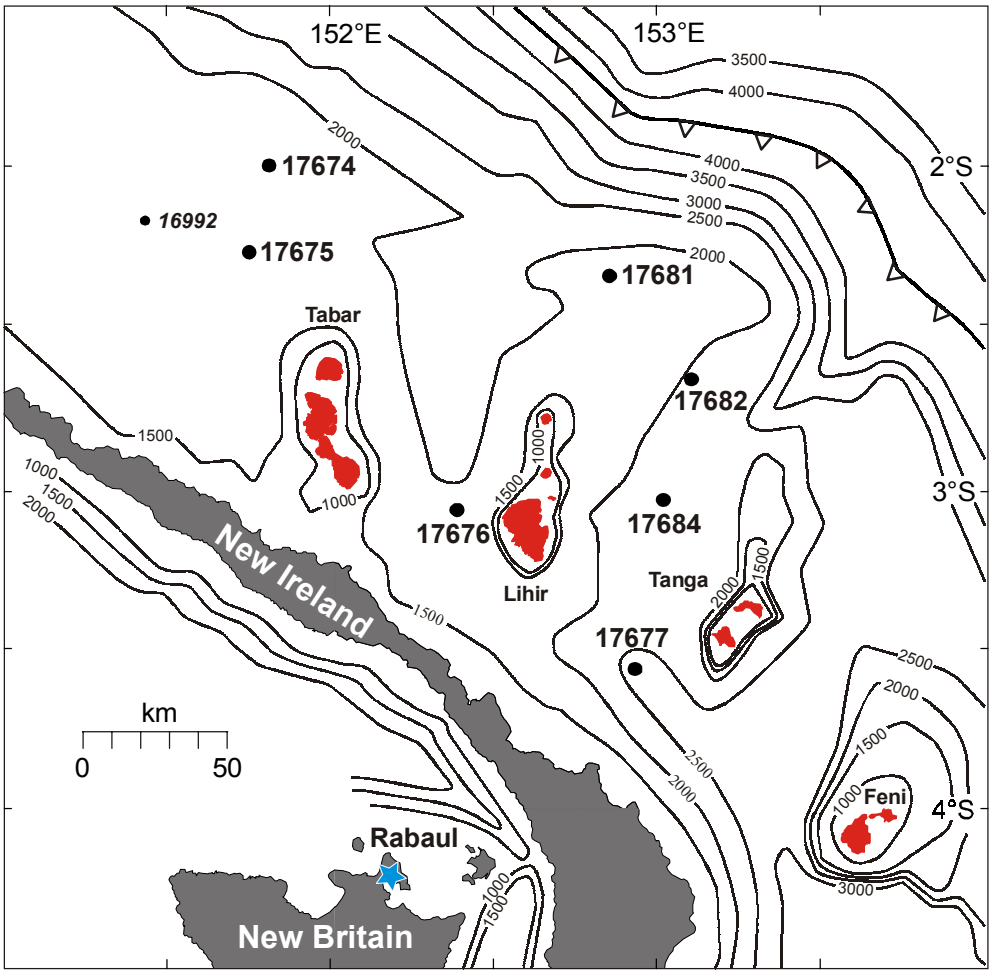

Figure 5: Location of the sediment stations. Core *16992* from cruise SONNE–94 (Herzig et al., 1994). Star = Rabaul volcanoes.

Table 1: List of sample stations in the New Ireland Basin

Core	Latitude	Longitude	Water depth	Core length	Distance from the nearest island group		
					Group	Shore	Volcano base
	(°S)	(°E)	(m)	(m bsf)		(km)	(km)
17674-1*	2°07.17'	151°33.98'	1716	0.5	Tabar	68	58
17674-2**	2°07.15'	151°34.01'	1716	1.2			
17675-1*	2°29.95'	151°33.28'	1898	0.4	Tabar	45	32
17675-2**	2°29.97'	151°33.25'	1897	2.1			
17676-1*	3°02.00'	152°21.02'	1860	0.5	Lihir	16	13
17676-2**	3°02.00'	152°21.01'	1861	2.9			
17677-1*	3°37.24'	152°57.29'	2516	0.4	Tanga	29	24
17677-2**	3°37.28'	152°57.18'	2516	3.6			
17681-1*	2°23.99'	152°50.83'	1831	0.4	Lihir	53	45
17681-2**	2°23.95'	152°50.85'	1830	7.4			
17682-1*	2°38.96'	153°01.93'	2040	0.5	Lihir	50	42
17682-2**	2°38.98'	153°01.90'	2045	8.3			
17684-1**	3°06.40'	152°59.86'	2387	3.2	Lihir	34	32

* Box core, ** Piston/Gravity core

3.2 Sample preparation

As part of the EDISON II program, eight sediment cores were collected at several stations in the New Ireland Basin next of the Tabar, Lihir and Tanga volcanoes using a box corer in conjunction with either a gravity or piston corer (Figure 5). Seven representative sediment cores were chosen to study the abundant ash beds within all cores. The cores were opened, documented, sampled and analyzed in the Institute of Geoscience, University Kiel.

Sampling of the sediment with 10 ml syringes was made for basic physical parameters, as well as for oxygen/carbon isotope measurements and ash bed determinations at close intervals of 3 to 5 cm in the uppermost of the succession, and between 7 to 10 cm in the lower part of the cores. Furthermore all cores were investigated every 10 cm with a binocular microscope for discrete, thin (<2 mm) ash beds. In addition subsamples of prominent ash layers were also taken for geochemical purpose. These samples of known volume were weighed, freeze-dried and weighed again for the calculation of water content and bulk densities, and then wet-sieved using a 63 μm polyester mesh sieve. The samples were cleaned with distilled water, dried and splitted into several grain size fractions (<63 μm, 63–125 μm, 125–250 μm, 250–500 μm, 500–1000 μm, and >1000 μm) for statistical evaluations, and isotope investigation. For geochemical analyses a composite grain size fraction of 125–500 μm were used to guarantee sufficient

sample material. Sediment structures were studied in detail in selected core segments using radiographic films and photographs.

3.3 Sediment

Photographic documentation, detailed lithological descriptions, PARASOUND records, and magnetic susceptibilities were measured for all sediment cores which are presented here and are listed in the Appendices → 9.1, 9.2, and 9.3. The sediment succession is given as composite depth by which the depths in the gravity and piston cores were corrected for surface sediment loss. All available sedimentological, acoustical, and magnetic data were used for a accurate core fit (core fit values are given in the appendices → 9.4). The records generally follow the correlations and descriptions given in the SONNE−133 cruise report with minor corrections based on stable isotope data (Winn et al., 1998). In the following a short description of all investigated sediment cores is listed below.

3.3.1 Core 17674

This core station is located on a slope to the north of a broad flat basinal area northeast of the Tabar group (Figure 5). Core recovery was 1.2 m. The sediment consists mainly of grayish orange to yellowish brown foraminiferal sand with minor amounts of dispersed volcanic glass throughout the sediment sequence. Bioturbation was common Thin ash beds were found at 0.27 m and 0.44 m and the latter ash bed was chosen for background information of the ash and pumice (volcaniclastics) distribution in the New Ireland Basin (Figure 23, 30, 37).

3.3.2 Core 17675

Core station 17675 is positioned on top of the south slope of the above broad and flat basinal area. The core recovery was 1.8 m. Grayish orange to pale yellowish brown clays predominate in this core with occasional forams in layers and nests. Bioturbation was rare beneath 0.70 m and was not observed below 1.40 m. Four volcanic ash layers are found at 0.12, 0.18, 0.22, and 1.38 m (Figure 24, 31, 38).

3.3.3 Core 17676

17676 is placed on top on a flat slope SW Lihir penetrating 2.9 m sediment. Yellowish brown to olive gray clays are the main component in this core. Foram sand, volcanic and shell debris are inter-layered. Five prominent ash beds are found at 0.10 m, 0.20 m, 0.22 m, 1.48 m, and 3.00 m (Figure 25, 32, 39).

3.3.4 Core 17677

Core 17677 is located SW of Tanga on a basinal area and yield numerous ash horizons. The 3.6 m long core consists of yellowish brown to olive brown foraminiferal sand and ooze with minor clay content. Bioturbation is consistent throughout the core. Graded turbidites (predominantly D and E sequence of Bouma, 1969), widespread reworking of sediment, and primary fine grain flows were recognized. Furthermore, the highest amount of ash input with 15 prominent ash beds were encountered in this core (Figure 26, 33, 40).

3.3.5 Core 17681

Core station 17681 was raised NNE of the Lihir Islands at a distance of 53 km, and penetrated the axis of a local depression. The 7.4 m long core is composed of yellowish brown to orange mud in the upper 0.50 m section, changing into gray clays in the deeper part of the core, typical of normal deep sea sediments. Bioturbation is observed throughout the core. Two prominent ash beds are located at 3.45 m and 4.44 m depth (Figure 27, 34, 41).

3.3.6 Core 17682

Station 17682 NE of the Lihir Islands is situated on a submarine basin at a distance of 50 km from the shore line. The sediment composition changes from yellow silty mud and foraminiferal sand in the upper 0.30 m to more homogeneous olive gray clays towards the bottom of the 8.44 m long core. Five ash beds were observed at 0.09 m, 0.39 m, 3.11 m, 3.28 m, and 7.13 m. Sample 17682-23.2 cm are analyzed for background information of the ash distribution in the New Ireland Basin (Figure 28, 35, 42).

3.3.7 Core 17684

Core 17684 is situated on top of a local promontory (~10 km wide, and ~40 m deep). The upper 1.10 m sediment in this 3.18 m long core consists of moderate yellowish brown to brown silty sands and clays with organic debris (e.g. molluscan fragments). Below 1.10 m, the sediment changes to compact, dark olive grayish to black sandy, ash rich clays. Bioturbation is common through the whole core. Prominent ash beds were found at 0.30 m, 1.30 m, 2.39 m, 2.48 m, and 2.91 m (Figure 29, 36, 43).

3.4 Volcanic ash

Analyzing the ash particle morphology via scanning electron microscopy (SEM) is the preferred method of determining the type of volcanic eruptions and the transport mode. To identify and differentiate the ash beds, more than 300 grains were counted in each sample to assess the proportion of glass shards, minerals, lithic fragments and biogenic components in the 125–500 μm grain-size fraction. Such counts allow the identification of the variance in the supply of glass shards to the sediment from the general background (Table 2).

3.4.1 Scanning electron microscope (SEM) technique

Scanning electron microscope observations were made on Au-coated glass samples using a JEOL JSM-5410LV and a CamScan electron microscope coupled with an X–Ray energy dispersive spectrometer at the Institute of Geoscience, University Kiel. Analytical conditions were 20 kV beam voltage, 10 eV channel width, 30° take-off angle, 10 μm beam diameter (defocussed), count times of 40 seconds (peaks) and ZAF normalized computation method.

3.4.2 Results

To avoid common problems in naming important types of volcaniclastic particles, a short definition is given as follows:

- A *pyroclastic* fragment/particle originates from rapidly expanding magma that loses cohesion and breaks into bits when overburden pressures are exceeded. Magmatic expansion creates a glass foam that break into glass shards from broken vesicles (Fisher and Smith, 1991; Heiken and Wohletz, 1991).
- *Hydroclasts* form by magma-water interactions that produce chilled glass particles by either explosive or nonexplosive means. Thermal contraction of hot magma or lava in water leads to the formation of shattered, angular, poorly vesiculated shards (Fisher and Smith, 1991).
- *Epiclastic* particles are lithic clasts and crystals derived by any type of pre-existing rock by weathering and erosion (Fisher and Smith, 1991).
- *Tephra* is applied to pyroclastic accumulations irrespective of size and is synonymous with pyroclastic material (Thorarinsson, 1974).
- In this study, the term *ash bed* is used to refer to a distinct zone in a sedimentary core, frequently several centimeters to millimeters thick, that contains abundant glass shards and associated crystals (Table 2).

Ash beds with >25% glass or lithic fragments were classified as either glassy ash (**GA** beds) or lithic ash (**LA** beds), and the remainder as ash-bearing sediment (**AS** beds; Table 2). The grain-size distribution displays a fine to very fine-grained (<63 μm in diameter) nature that is characteristic of the surrounding volcanic ash deposits of the TLTF area.

The discrete **GA** ash beds consist mainly of clear glass shards (28–88%) and fresh pumice (1–38%). The crystal portion is mostly feldspar (<1–20%), pyroxene (1–14%), and minor phlogopite (<1–9%). The biogenic component in the single ash beds varies between <1 to 69% (Table 2). In contrast there are seven prominent discrete GA beds (17677-117 cm, -229 cm; 17681-345 cm, -444 cm; 17682-311 cm, -328 cm, -713 cm) containing 50–88% clear glass shards and up to 34% pumice, <5% organic material, and rare crystals (Table 2). These seven GA beds stand out through their relatively homogeneous composition and the high amount of clear glass shards. All GA glass shards consist of walls of tiny broken bubbles or the junctions of the bubbles developed by the vesiculation of silica magma. There are essentially three types of morphology : (1) flat plates from the glass walls separating large flattened vesicles (Figure 6-1), and (2) cuspate or lunate-shaped fragments of broken bubble walls that are commonly y-shaped (in

cross-section) representing remnants of three bubble junctions, or concave plates that formed the wall adjoining bubbles (Figure 6-2). Both types are called “bubble wall shards” (Fisher and Schmincke, 1984; Heiken and Wohletz, 1985). Type (3) are spheroidal bubbles completely enclosed in glass and are frequent in the seven prominent GA beds (Figure 6-2). The bubble wall and bubble junction shards tend to develop from lower viscosity rhyolitic magmas at temperatures >850 °C, whereas pumice shards tend to develop from relatively high viscosity rhyolitic magmas with temperatures <850 °C (Izett, 1981). The seven prominent GA beds are interpreted as fallout tephra from explosive eruptions of a more distal source as the TLTF volcanoes.

The major constituent of the **LA** beds was glass shards (4–29%), microvesicular pumice (<1–5%), crystals, particular plagioclase (2–15%), and pyroxene (<1–11%) plus rock fragments of various lithologies (eroded volcanic debris; up to 69%). The pumice is composed of highly vesiculated volcanic glass (Table 2). Two types of silicic pumice are found in the investigated LA beds: (1) fibrous fragments with tubular, subparallel vesicles (Figure 6-3, 4.2-4) and (2) varieties of fragments with spherical vesicles suggesting conditions of higher vapor pressure during eruption (Figure 6-2 to 6-5, Ewart, 1963).

The ash-bearing sediment beds (**AS**) contain a significant proportion of forams (70–97%) and/or a mixed glass shard population ranging from transparent (clear), flat, curved, and tricuspate (y-shaped) varieties (<1–22%) to pumice (<1–9%; Table 2), and rare brown blocky hydroclasts (Figure 6-6) Microcrysts are scarce and rock fragments of volcanic debris are also found in the AS beds (up to 15%; Table 2). It is very likely that these beds represent mixtures of several eruptions that were closely spaced (months to decades) in time.

Plagioclase, olivine, clinopyroxene, and titanomagnetite were the main inclusions in the glass matrix of all analyzed glass samples (→ 5). Petrographically the volcanic glass shards and associated crystals appear fresh and unweathered.

Figure 6: SEM photomicrographs of the most abundant types of glass particles

6-1: A typically glass fragment (vitric pyroclast) that has been broken from a vesicle wall.

6-2: A characteristic glass vesicle formed during a cavity within a magma chamber caused by a volatile phase diffusing from solution in a magma toward growing bubbles.

6-3: Details of a highly vesicular pumice pyroclast showing elongate, parallel vesicles with thin (<3 μm) vesicle walls. Additionally most of the elongate vesicles show considerable coalescence.

6-4: Cross section of photomicrograph no. 3. Note the typical elongate and tubular structure.

6-5: Pumice variety with small (5 – 40 μm) ovoids. Most of the ovoid vesicles show collapse of mutual vesicle walls and coalescence to form larger vesicles. The entire texture of this pyroclast gives the impression of a “bubble wall”.

6-6: Brown blocky hydroclast showing fractures characterized by sharp shapes and curviplanar surfaces outlining minor grain modification during transport abrasion from the volcanic source.

1

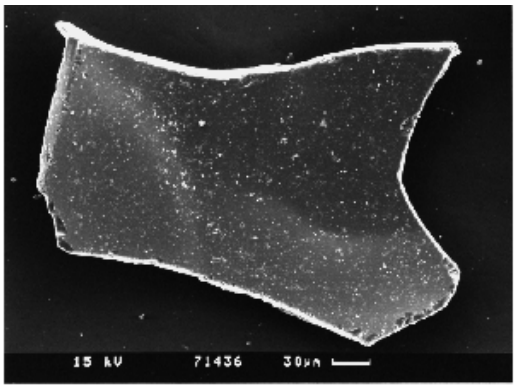
15 kV 71436 30µm

2

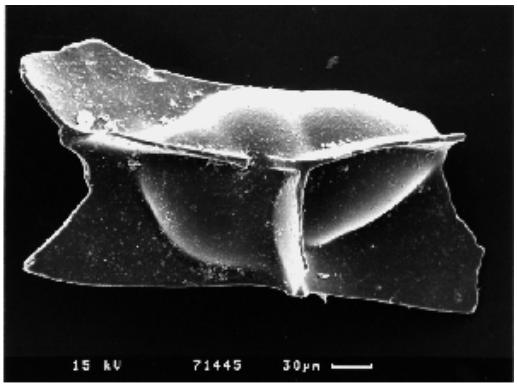
15 kV 71445 30µm

3

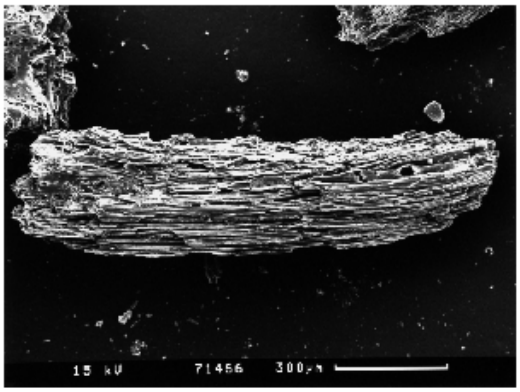
15 kV 71456 300µm

4

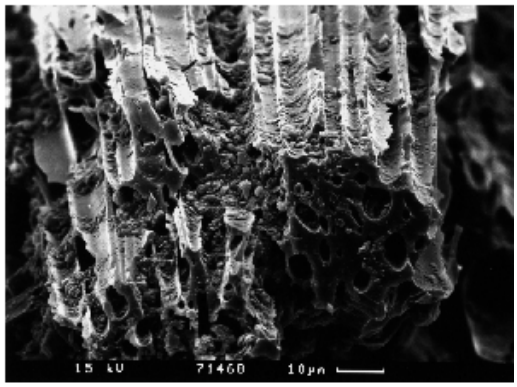
15 kV 71460 10µm

5

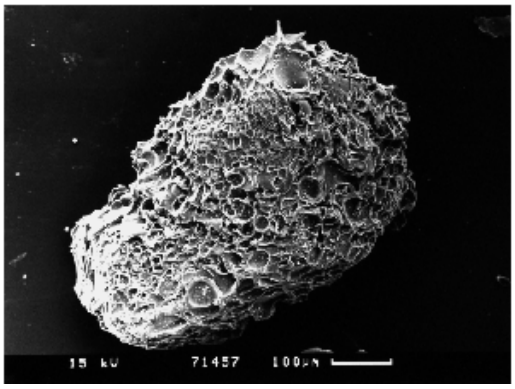
15 kV 71457 100µm

6

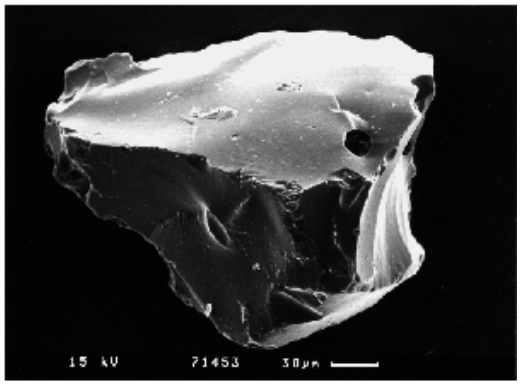
15 kV 71453 30µm

Table 2: Ash bed components (%)

Core	Bed base (cm)	Thickness (cm)	Glass shards	Lithics		Crystals				Bioclasts	Classification
				Pumice	Others	Feldspar	Pyroxene	Phlogopite	Others		
17674	27.2	1.0	3.4	-	-	-	-	-	-	96.6	AS
	44.4 *	0.5	17.2	0.3	0.2	0.5	-	-	-	81.8	AS
17675	12.1	3.3	22.0	1.6	4.8	1.3	-	-	-	70.3	AS
	18.3	2.9	3.7	8.5	0.6	0.4	-	-	-	86.8	AS
	21.5	0.9	10.8	1.2	0.2	3.4	-	-	-	84.4	AS
	138.4	15.9	31.9	0.8	-	0.5	-	-	-	66.8	GA
17676	10.3	1.4	2.9	1.3	3.3	0.4	-	-	-	92.1	AS
	20.3	1.7	39.1	1.4	0.6	1.4	-	-	-	57.5	GA
	22.2	1.8	28.4	1.1	1.3	0.5	-	-	-	68.7	GA
	147.5	0.5	0.7	-	13.5	1.3	0.6	0.3	0.6	83.0	AS
17677	6.8	3.4	41.4	6.0	2.2	2.2	1.0	0.2	0.2	46.8	GA
	51.5	0.5	42.8	21.8	2.6	11.4	5.0	3.3	2.6	10.5	GA
	56.8	0.5	42.0	37.6	1.5	10.0	-	8.5	0.2	0.2	GA
	75.0	18.2	49.0	12.5	5.2	9.6	14.1	4.0	3.8	1.8	GA
	116.6	5.8	53.1	22.0	20.5	2.6	-	-	-	1.8	GA
	154.3	2.5	28.5	4.8	30.1	15.0	4.8	1.2	1.0	14.6	LA
	157.6	3.3	7.5	2.6	63.8	12.8	8.7	0.5	1.3	2.8	LA
	160.2	2.6	67.6	2.3	-	19.8	0.2	-	8.4	1.7	GA
	183.3	2.0	9.5	1.6	68.7	11.2	7.5	-	0.4	1.1	LA
	228.9	11.1	75.5	19.1	4.3	0.2	-	-	0.2	0.7	GA
	231.1	1.6	8.8	0.4	32.4	2.7	2.2	1.2	0.2	52.1	LA
	264.8	7.2	24.4	0.7	55.3	4.5	3.7	-	-	11.4	LA
	270.0	2.5	7.9	2.6	31.2	14.3	8.6	0.2	0.6	34.6	LA
	272.4	1.5	82.1	1.7	-	2.3	1.7	0.4	-	11.7	GA
	345.5	8.2	5.7	-	67.0	2.3	24.6	0.2	0.2	-	LA
17681	344.6 *	2.8	78.8	4.2	9.9	2.3	-	-	-	4.8	GA
	444.0	3.7	87.5	7.7	0.2	-	-	-	-	4.6	GA
17682	9.2	1.1	6.2	1.1	0.9	0.5	-	0.2	-	91.1	AS
	38.6	2.0	2.0	1.1	14.7	1.6	-	-	0.2	80.4	AS
	311.2	2.0	73.6	6.9	2.2	1.2	-	-	-	16.1	GA
	327.8	5.8	64.3	33.5	1.8	0.4	-	-	-	-	GA
	712.6	7.5	82.1	10.9	1.8	0.2	-	-	-	5.0	GA
17684	29.9	6.2	27.8	14.7	19.5	9.4	4.7	6.8	2.1	15.0	GA
	129.6	1.7	4.0	-	59.3	2.0	7.0	-	1.2	26.5	LA
	239.2	12.6	17.2	0.4	34.6	2.5	10.9	-	0.4	34.0	LA
	248.4	1.0	14.3	-	30.2	4.1	5.9	0.2	0.6	44.7	LA
	290.7	1.1	28.7	0.5	24.2	3.7	4.2	-	-	38.7	GA

* Mixed glass population

(AS) = Ash-bearing sediment, (GA) = Glassy ash, (LA) = Lithic ash

3.5 Sedimentation environment in the New Ireland Basin

Marine volcaniclastic deposits occur in the New Ireland Basin around the TLTF volcanoes and were sedimented in a back-arc setting related to the Manus Basin and the stalled Manus–Kilinailau Trench system. These deposits are interbedded with hemipelagic clays and foraminiferal ooze, and correspond to mm to cm thick sporadic turbiditic D and E sequences (Bouma, 1969). The furthermost deposition mechanisms are grain or gravity flows (density separation within a moving sediment) characterized by very fine grain size, fine-bedding, and irregular upper and/or lower boundaries. The cause for this sedimentational process is the far distal locations of the sample stations. Figure 7 illustrates the differences between typical sediment facies near the volcanic flanks and the basin facies in the distal apron of the TLTF volcanoes, respectively.

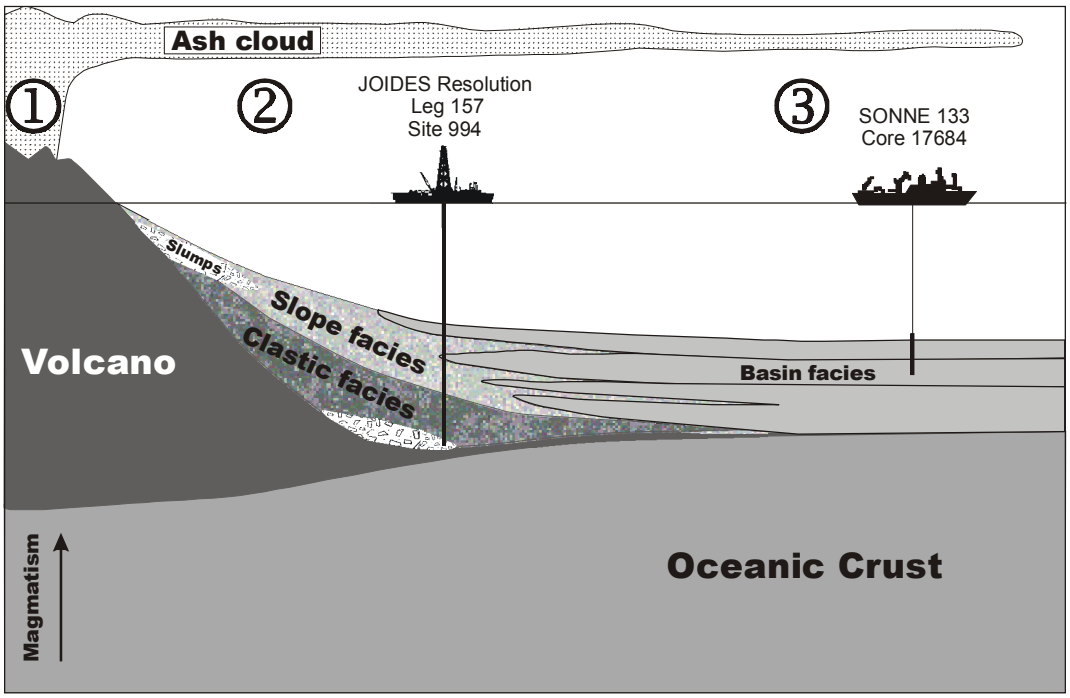

Figure 7: Sketch illustrating connection between magmatism and sedimentation. 1. Source volcano: debris-, lava-, and pyroclastic flows, fallout tephra. 2. Volcano margin: shelf- and slope environments. Slumps, debris flows, turbiditiy currents and deposits. 3. Basins of deposition: sediment gravity flows, fallout/pelagic sedimentation. No. 3 is the predominating sedimentation type found in the sediment cores from the TLTF area. In comparison thereto ODP Leg 157, Gran Canaria, is a good example fore a typical slope facies proximal the submarine flanks of a volcano characterized by volcano margin sedimentation listed above (modified after Schmincke and Sumita, 1998).

Fallout deposits come to rest after aerial fragment transport by initial trajectory (for large fragments) close to the eruption source, or after scattering by wind (and currents ?) from turbulent eruption clouds to more distal parts. The latter mechanism is the predominant sedimentation type of all ash beds from far distal sources in the New Ireland Basin. In contrast, flows of pyroclastic material originate from collapsing eruption columns, by the “boiling over” from vents (Fisher and Schmincke, 1984), and from laterally directed eruptions frequently associated with crater, domes and dome collapse. They comprise the main source of volcaniclastic material from the TLTF islands, especially Lihir and Tanga (Wallace et al., 1983; Müller et al., 2001). The most important pyroclastic deposit type for the ash beds found in the SO−133 cores are the pyroclastic surge deposits from the TLTF volcano sources which are better sorted, finer-grained, thinner, and more well-bedded than pyroclastic flow deposits (Fisher and Schmincke, 1984).

4 CHRONOSTRATIGRAPHY

4.1 Oxygen isotope ($\delta^{18}O$) determinations

The ages of the sediment cores, and the ash beds within them, were constrained through correlation and interpolation with foraminiferal $\delta^{18}O$-values of the established global $\delta^{18}O$-event stratigraphy (Winn et al., 1991; Bassinot et al., 1994; Stuiver et al., 1998). No $\delta^{18}O$-analyses of forams were made on samples of core 17674 because Parasound and magnetic susceptibility profiles showed a good correlation with the neighboring core 16992 of the SONNE–94 cruise (Stoffers et al., 1994).

4.1.1 $\delta^{18}O$-isotope techniques

15 tests (100–160 µg carbonate) of the planktonic foraminifera *Globigerinoides ruber* (white) were selected from the 250–400 µm grain-size fraction for oxygen isotope measurements. Cores 17675, 17676, 17677, 17681, 17682 and 17684 were sub-sampled at 3–5 cm intervals (uppermost part) and 7–10 cm intervals (lower part). The carbonate tests were placed in ethanol, and cleaned in a sonic bath for 30 to 120 seconds to remove all contamination. In the CARBO-Kiel device, the tests were treated with H_3PO_4, the released CO_2 gas was purified twice using liquid nitrogen traps, and then analyzed with the Finnigan MAT 251 mass spectrometer at the Leibniz Laboratory for Radiometric Dating and Isotope Research, University of Kiel. Analytical precision for the $\delta^{18}O$ values is ±0.03‰ (2σ).

4.1.2 Results

Globigerinoides ruber (white) in all of the cores show an initial increase in $\delta^{18}O$ from the present day value –2.9 ‰ to around –1.0 ‰ during the last glacial, followed by fluctuations in $\delta^{18}O$ that can be matched to the established global isotopic record for the Quaternary (Figure 8, e.g. Bassinot et al., 1994). This enables specific ages to be assigned to the sediment successions and the ash

beds within them (assuming constant sedimentation rates). The correlation reveals that cores 17675, 17676 and 17677 provide a record from the present day to the earliest part of $\delta^{18}O$ Stage 2 at about 26 ka, whereas the other cores extend back to ~120 ka and beyond. The longest record is provided by core 17681, which terminates in $\delta^{18}O$ Stage 9 at 333 ka (Figure 8). Reliable ages cannot be assigned to the lower part of core 17677 below 0.45 m. In this lower segment, the tephra deposits show irregular upper and lower boundaries with the overlying and underlying sediments respectively, indicating extensive sediment reworking at this site. These values are presented as a bar by plotting the $\delta^{18}O$-values between 0.45 – 3.60 m with an arbitrarily chosen age of 18,000 years BP. On this account no ages can be given for the two prominent ash beds (17677-117 cm and 17677-229 cm) representing large explosive volcanic events. Glass shards of the five prominent ash beds in cores 17681 and 17682 correspond likewise to large explosive eruptions, two have ages of 164 ka and 214 ka (core 17681-345 cm and -444 cm) and the other three have ages of 72 ka, 75 ka and 161 ka (core 17682-311 cm, -328 cm and -713 cm; Table 4). It is obvious that between 70 ka and 75 ka a period of brisk volcanic activity occurred, also confirmed through ash datings in the SO–94 cruise. Additionally, the stable isotope profiles from core 16992 of the SONNE cruise 94 indicated that core 17674 reached down to 25 ka (Dr. K. Winn, personal communication, Herzig et al., 1994).

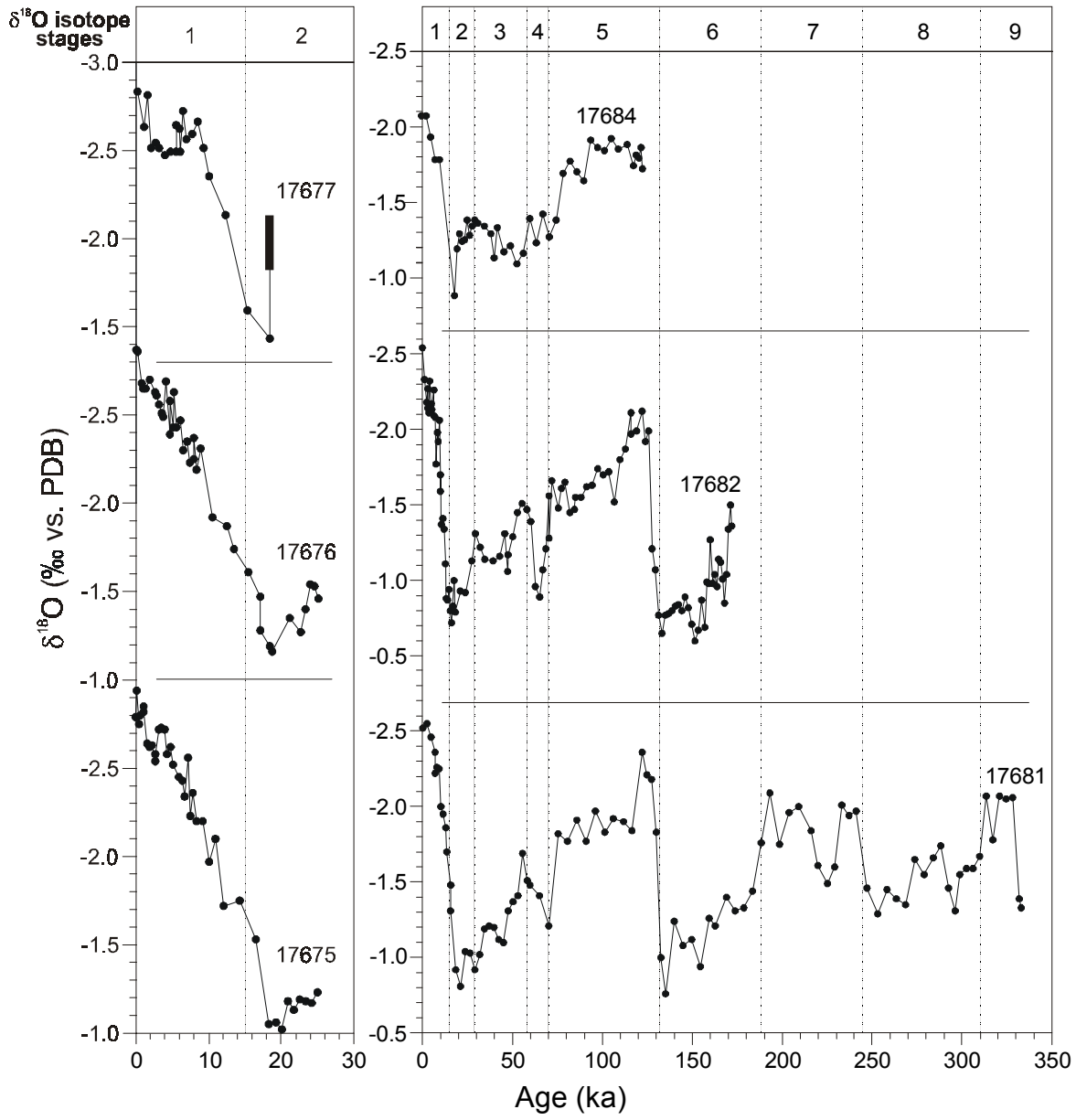

Figure 8: Oxygen isotope profiles of cores 17675, 17676, 17677, 17681, 17682, and 17684. Grey dotted lines show the boundaries of δ^{18}O-Stage numbers. The δ^{18}O-records of the foraminifera *G. ruber* in core 17677 below 0.45 m is presented as a bar with an arbitrarily chosen age of 18.000 years BP. For details see text.

4.2 AMS ^{14}C-age determinations

Local control on the $\delta^{18}O$-stratigraphy was exercised by AMS ^{14}C-age determinations.

4.2.1 AMS ^{14}C-technique

Up to 1600 *Globigerinoides ruber* tests (1–1.3 mg carbon) were picked from the 250–400 µm-size fraction, and cleaned with H_2O_2 in a sonic bath for 5 minutes, dried, and then converted into CO_2 (via combustion). Next the CO_2 was reduced to graphite on a Fe catalyst followed by analysis of the graphite at the AMS facility of the Leibniz Laboratory, University Kiel (Nadeau et al., 1998). All samples supplied the minimum carbon weight of 1 mg necessary for good quality dating with analytical precision better than 0.5% (2σ)

4.2.2 Results

Differences in the reservoir effect are observed both locally and regionally. In the northwestern part of the New Ireland Basin, the conventional ^{14}C-ages of the undisturbed surface sediment are 480±30 BP in core 17675 and 645±25 BP in core 17676 (Table 3). The older age in the latter core may reflect the presence of reworked foraminifera, which could not always be separated from autochthonous forams. Therefore, the same age correction have been applied to the older ^{14}C-datings, assuming that the environmental conditions in this area have not significantly changed through geologic time.

Table 3: AMS ^{14}C-determinations

Core	Core depth (cm)	AMS ^{14}C age	Calendar age	Calendar age (corrected***)	Reference
17675	0	480 ± 30	520 ± 30	0	Stuiver et al., (1998)
	49 *	7625 ± 40	8380 ± 40	7860 ± 40	Stuiver et al., (1998)
	65 **	10285 ± 55	11485 ± 55	10965 ± 55	Winn et al., (1991)
17676	0	675 ± 25	645 ± 25	0	Stuiver et al., (1998)
	30 **	8475 ± 50	9445 ± 50	8800 ± 50	Stuiver et al., (1998)
	55 **	14140 ± 80	17640± 80	16995 ± 80	Winn et al., (1991)

*Box core, **Gravity core, ***for reservoir effect

4.3 Calculated ages of the submarine ash beds

Thirty-seven individual ash beds from cores 17675, 17676, 17677, 17681, 17682, and 17684 were dated through their stratigraphic position in the δ^{18}O-records. By applying the δ^{18}O-event stratigraphy and through interpolation, their ages could be determined. Because of a lack of TLTF island tephra data no correlation could be made between the investigated submarine ash beds and tephra on the islands. However, as shown in Figure 9 only a few ash beds appear to correlate with each other.

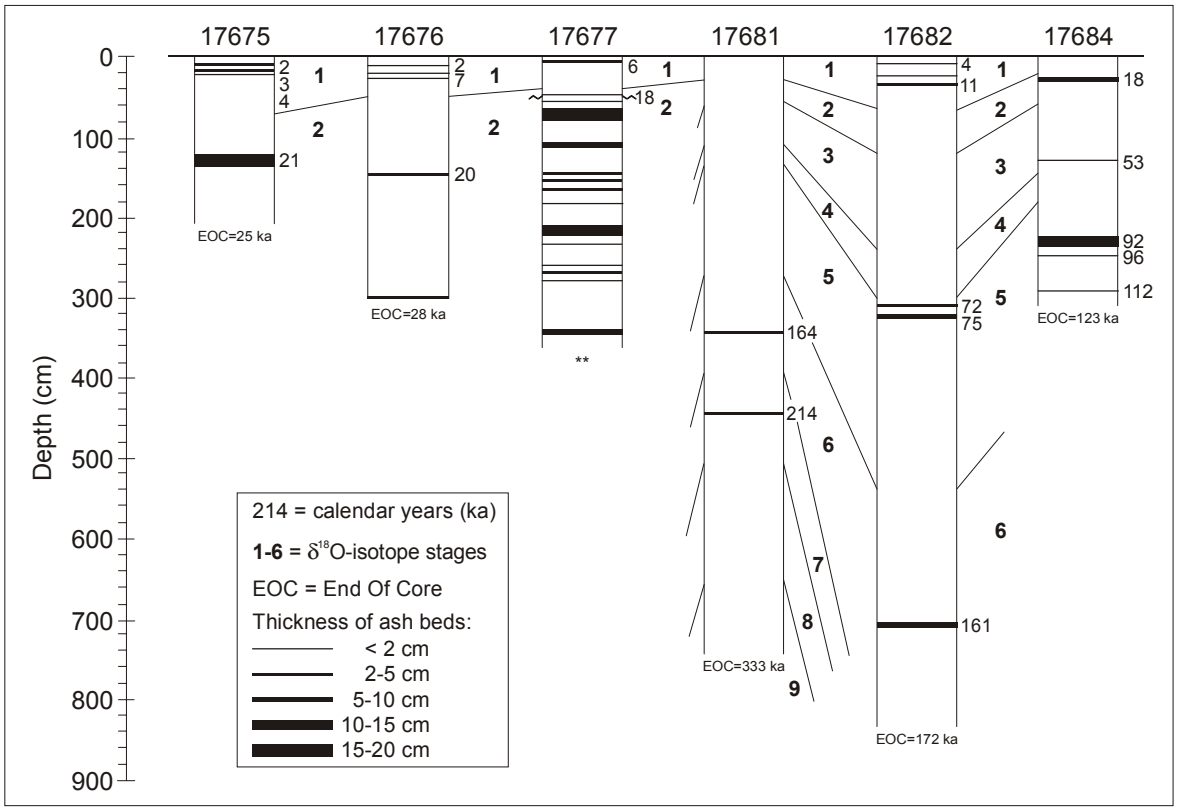

Figure 9: Calculated ages of the ash beds in the investigated sediment cores.

A accordance of ash beds can be observed at 2 ka (δ^{18}O-Stage 1) for samples 17675-12 cm, 17676-10 cm as well as 4 ka for samples 17675-22 cm, and 17682-9 cm. Another accordance can be assigned to sample 17675-138 cm and 17676-148 cm, which represent probably the same event at ~20 ka (δ^{18}O-Stage 2). Additionally ash beds 17677-52 cm and 17684-30 cm at 18 ka also linked to δ^{18}O-Stage 2. δ^{18}O-Stage 5 include ash beds from core 17682-311 cm (72 ka) and 328

cm (75 ka), and core 17684-239 cm (92 ka), -248 cm (96 ka), and -291 cm (112 ka). These samples are independent events in δ^{18}O-Stage 5 and can't be linked among each other. Ash beds 17681-345 cm at 164 ka and 17682-713 cm at 161 ka (δ^{18}O-Stage 6) pointing to two eruptions closely in time. The youngest major outbreak as recorded in the sediment cores occurred at about 2 to 4 ka which match strongly observations made at the SO–94 cruise (Dr. K. Winn, personal communication).

4.4 Sedimentation rates in the New Ireland Basin

Bulk sedimentation rates vary by a factor of five from a maximum of 9.7 cm / 1000 years in core 17676 to a minimum of 2.1 cm / 1000 years in core 17681 (Table 4). As expected, very high sedimentation rates occur near the volcanic islands (>5 cm / 1000 years), whereas the rates progressively decrease to the NE with increasing distance from the islands. These distal sedimentation rates are still higher than given sedimentation rates for the Ontong Java Plateau with <2 cm / 1000 years (Berger and Killingley, 1977; Herguera et al., 1992).

Table 4: Relative ash bed ages and sedimentation rates

Core	Depth (cm)	Calendar years (ka)	δ^{18}O-Stages	Sed. rate (cm / ka)	Core	Depth (cm)	Calendar years (ka)	δ^{18}O-Stages	Sed. rate (cm / ka)
17675	12.1	2.0	1V-2	6.1	17681	344.6	164.0	6V-1	2.1
17675	18.3	3.2	1V-2	5.7	17681	444.0	214.0	7V-1	2.1
17675	21.5	3.7	1V-2/1V-3	5.8	17682	9.2	3.3	1V-2	2.8
17675	138.4	21.0	2V-2	6.6	17682	23.2	7.9	1V-4	2.9
17676	10.3	1.7	1V-1	6.1	17682	38.6	11.0	1V-5	3.5
17676	20.3	6.8	1V-4	3.0	17682	311.2	72.0	4V-4/5V-1	4.3
17676	22.2	7.1	1V-4	3.1	17682	327.8	75.0	5V-2	4.4
17676	147.5	21.0	2V-2	7.0	17682	712.6	161.0	6V-1	4.4
17676	300.0	31.0	3V-1	9.7	17684	29.9	3.6	1V-2	8.3
17677	6.8	6.0	1V-3	1.1	17684	129.6	53.0	3V-6	2.4
17677	51.5	18.0	2V-1	2.9	17684	239.2	92.0	5V-6	2.6
17677	56.8-345.5	mixed			17684	248.4	96.0	5V-7	2.6
					17684	290.7	112.0	5V-8	2.6

5 MINERALOGY

5.1 Preparation and Electron microprobe (EMP) technique

Minerals were embedded in an epoxy resin perspex carrier. These carriers were then polished in two steps with Buehler Micropolish® B (0.1 μm) and C (0.05 μm) Gamma Alumina powder to obtain an even surface and to avoid compositional variations due to superficial alteration processes. Major elements were analyzed using a four-spectrometer CAMECA Camebax SX electron microprobe of the Institute of Geoscience in Kiel. Analytical conditions were 15 kV accelerating voltage, 12.5 mA beam current, 5–10 μm beam diameter (defocussed), and count times of 20 seconds (peaks) and 10 seconds (backgrounds). A variety of internal synthetic standards and MPI-DING glass standards of the Max-Planck-Institute of Chemistry in Mainz were used for the calibration of the microprobe (Jochum et al., 2000). Glass measurements are the average of a minimum of two to three individual spots per sample. The reproducibility of the results of the major elements was calibrated by measuring one standard after five samples. Analytical precision (2σ) was better than 1 % for most elements (Table 12). Totals varied from 94 to 101 wt.%, reflecting the presence of a few percent volatiles in most shards, and all analysis are recalculated to 100 wt.% volatile free. Magnesium number (Mg# = $100Mg/Mg+Fe^{2+}$) is calculated by using $Fe_2O_3/FeO = 0.4$ (Middelmost, 1989).

5.2 Results

5.2.1 Feldspar

Plagioclase varies in composition from An_{69}-An_{29} (Andesin - Labradorit) and could be found in all investigated ash beds of all cores (Figure 10). In core 17677 plagioclase crystals are the dominant phenocryst phase, and it occurs as a microphenocryst with up to 20% abundance in all GA and LA beds (Table 2). Furthermore no differences in the An content of phenocrysts and matrix plagioclase could be determined (Table 20).

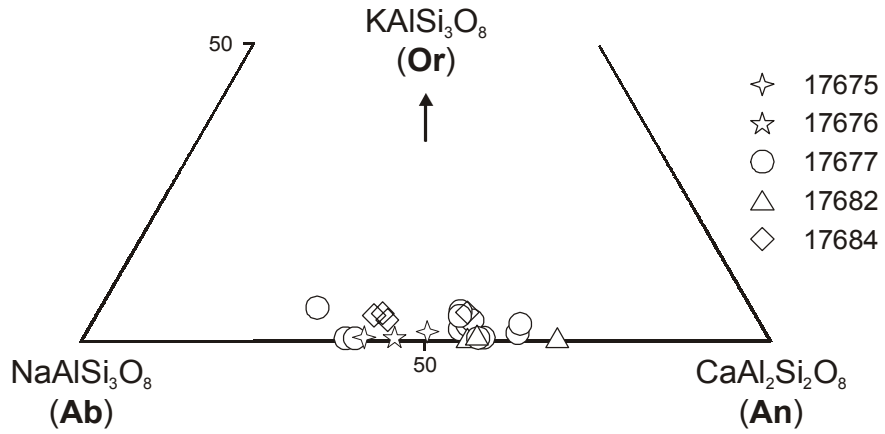

Figure 10: Ternary-feldspar system of investigated ash bed samples in the triangle Albit-Anorthite-Orrthoclase (Ab-An-Or in mol%).

5.2.2 Pyroxene

Clinopyroxene forms pale to dark green, prismatic crystals that can be classified in general as augite except samples 17677-158 cm and -183 cm which tend more to diopside (Figure 11, Morimoto et al., 1988). The idiomorphic crystals range in composition with $Wo_{50-36}En_{42-34}Fs_{15-7}$ (Table 21). Orthopyroxene could not be observed in the samples.

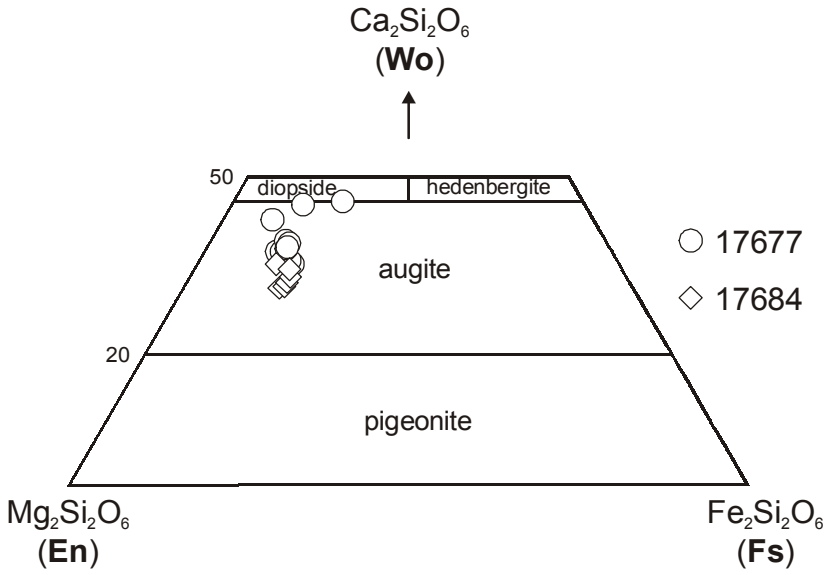

Figure 11: Composition of clinopyroxenes (Fs, Wo, En in mol%).

5.2.3 Olivine

Olivine is confined to samples 17676-20 cm and 17677-7 cm, -75 cm, and –183 cm. Euhedral olivine crystals have a fosterite content of Fo_{64-50} including high CaO concentration of up to 1.6 wt.%. Common inclusions are titanomagnetite microphenocrysts. The olivine crystals show no significant differences in composition between core and rim analyses (Table 22). Moreover no distinct composition between phenocrysts and glass matrix crystals could be observed.

5.2.4 Other mineral phases

Phlogopite (< 1 mm, brownish in color) with Mg# between 89 – 91 could be observed primarily in samples of cores 17677 and 17684 (Table 2) and is commonly associated with clinopyroxene, which is consistent with observations made by McInnes and Cameron (1994), Müller et al. (2001), and Franz et al. (2002). In addition limited crystals of hornblende, and titanomagnetite could also be observed, the latter crystal primarily as inclusions both in glass matrix and in phenocrysts (Table 23).

6 VOLCANIC GLASS GEOCHEMISTRY

6.1 Glass shard preparation

Major element composition of 37 representative glass samples are presented in this section. Fresh glass shards and crystals were hand-picked from each of the ash beds using a binocular microscope. Representative shards (2–35 from each ash bed) were embedded in an epoxy resin perspex carrier. The glass shard analyses were carried out on the same electron microprobe (EMP) with identical conditions used for the mineral analyses (→ 5.1). Detailed composition are listed in the appendices → 9.6.

6.2 Results

6.2.1 Major element composition and classification of the glass shards

Glass shard major element compositions cluster tightly about an average value for each ash bed (Table 13-19). The only exceptions are two ash beds (17674-44 cm and 17681-345 cm) that contain two compositionally distinct glass shard populations. For those beds, each population was averaged separately, and differences in shard color and texture enabled them to be separated for major and trace element analyses. It is evident that all other ash beds contain a single homogeneous glass shard population derived from a single homogeneous source. The ash beds are cleanly split into three distinct compositional groups on a K_2O versus SiO_2 plot (Figure 12), and the same grouping is apparent on a total alkalis versus silica plot (Figure 13). Glass shards from the Group A ash beds have 5–7 wt.% K_2O at 51–64 wt.% SiO_2, and can be classified as members of the shoshonite series, and range from tephriphonolites, phonolites to trachytes. Glass shards from the Group B beds have 3–5 wt.% K_2O at 66–75 wt.% SiO_2, belong to the high-K series, and are dacites, rhyolites, and two samples are trachytes (17677-117 cm and 17681-345 cm). Glass shards from the Group C beds have <2 wt.% K_2O at >70 wt.% SiO_2, straddle the boundary between the medium and low-K series, and are exclusively rhyolites.

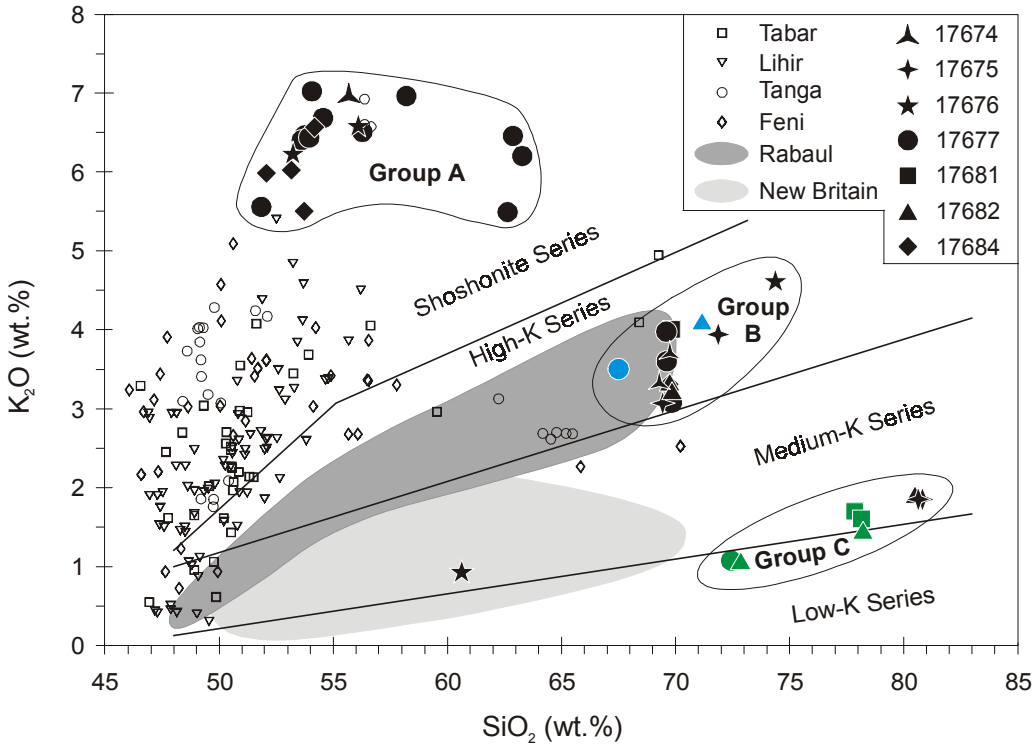

Figure 12: K_2O versus SiO_2 diagram to classify the discovered glass shard composition. Bold symbols represent data from this study and open symbols correspond to Müller et al. (2001), and Wallace et al. (1983). Rabaul data set are from Wood et al. (1995), and New Britain data from Gill et al. (1993), and Woodhead and Johnson (1993). Boundary lines from Rickwood (1989). Colored symbols denote the seven prominent, homogeneous GA beds (see also → 3.4).

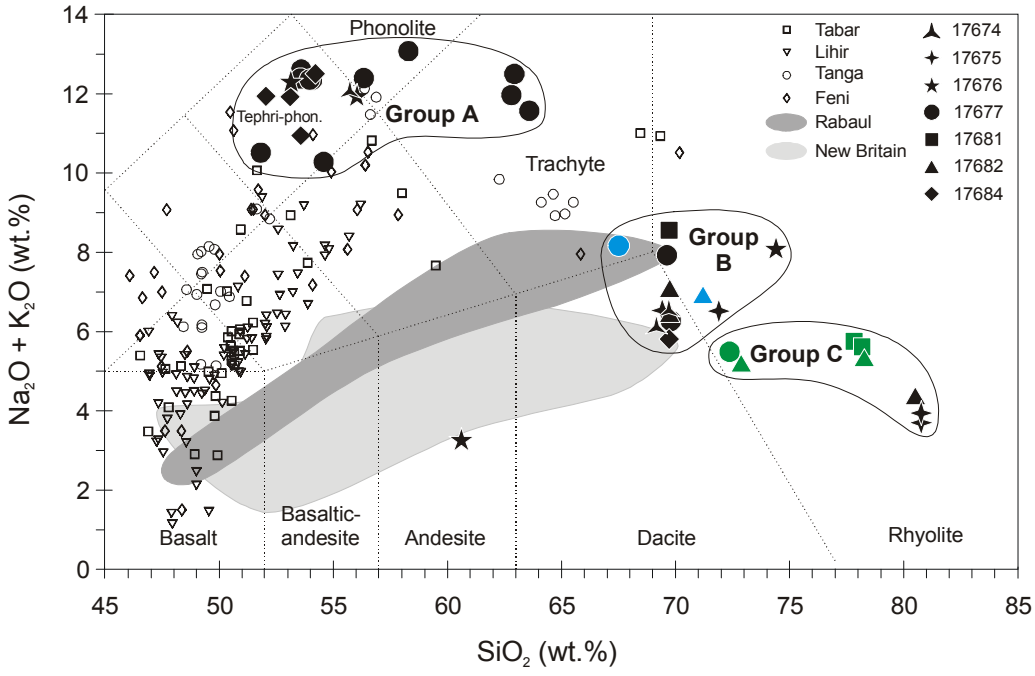

Figure 13: Total alkalis versus silica plot (Le Bas et al., 1986). Literature data and symbols as Figure 12.

Ash bed 17676-148 cm contains glass shards with Group C affinities (0.8 wt.% K_2O), but markedly lower SiO_2 (59 wt.%) than all other Group C beds. Sample 17674-44 cm includes shards with Group A and Group B compositions, while sample17681-345 cm contains glass shard populations from Group B and C.

Because of a lack of published glass shard data from the TLTF volcanoes and New Britain a comparison with land-based volcanic glass data was not possible. Therefore the major element chemistry of the samples are compared with published analyses of hard rocks (e.g. alkali-basalts, basanite, tephrite) from the TLTF volcanoes and the adjacent volcanoes of the New Britain arc, including Rabaul in the far northeast (e.g. Wallace et al., 1983; Gill et al., 1993; Woodhead and Johnson, 1993; Wood et al., 1995; Müller et al., 2001).

All analyzed glass samples represent highly evolved end member compositions at the silica-rich end of the published literature analyses for the TLTF volcanoes, the Rabaul volcanoes, and volcanoes at the New Britain arc listed above. The Mg numbers of all groups are low to moderate (23 – 44) suggesting high degrees of melt fractionation. The TiO_2 content is less than 1 wt.% for all glass samples.

Group A samples are from cores 17674, 17676, 17677, and 17684 nearby Tabar, Lihir, and Tanga Figure 5. The main part of ash beds yield core 17677 and 17684 next to Tanga, whereas ash beds from cores 17674 and 17676 are most likely volcanic background from more distal eruptions at Tabar and/or Lihir. It seems that Tanga is the most recently active Island in the volcanic chain. The primary part of crystals, and lithic rich ash beds (LA) are also found in those cores ($\rightarrow$ 3.4.2, Table 2). Furthermore, a separation of three trachytes (17677-52 cm, -57 cm and -160 cm) with > 60 wt.% SiO_2 at 11–12 wt.% alkalis is noticeable. The Mg numbers are the highest of all groups at up to 44, and with FeO^T/MgO ratios of 3.2–3.9. Exceptions are here again the three trachyte samples with the lowest Mg number (29) and highest FeO^T/MgO ratios (5.9–6.0).

Single ash beds from all investigated cores are represented in Group B which closely resembles the geochemical signature of Rabaul (dark gray field in Figure 12 and 13). Additionally two of the discrete, homogeneous glassy ash (GA) beds (17677-117 cm and 17681-345 cm) are also placed in this group (blue bold circles in Figure 12 and 13). Mg numbers in this group are lower (34–39) than in Group A in contrast to FeO^T/MgO ratios of 4.2–4.8, which are little higher as in Group A.

One exception is sample 17676-22 cm with the lowest Mg number of 23 and the highest FeO^T/MgO ratios of 8.3, which is attributed to an erroneous measurement.

Group C harbor the largest proportion of the discrete GA beds (17677-229 cm, 17681-444 cm; 17682-311 cm, -328 cm, -713 cm), and two samples from core 17675 and 17676. This group corresponds geochemically to the New Britain volcanoes exclusive of Rabaul (light gray field Figure 12 and 13). Mg numbers are the lowest of all groups (30–33) at >70 wt.% SiO_2 with FeO^T/MgO ratios of 4.0–6.1.

All representative GA samples of Group B and C were also analyzed for F, Cl, and SO_2. These samples bear only traces of F (< 0.08 wt.%), Cl (< 0.3 wt.%), and < 0.1 wt.% for SO_2 (Table 16, 17, 18).

On Harker diagrams the major elements are plotted against SiO_2 and demonstrate in detail the chemical distinction of Group A, B, and C tephra (Figure 14).

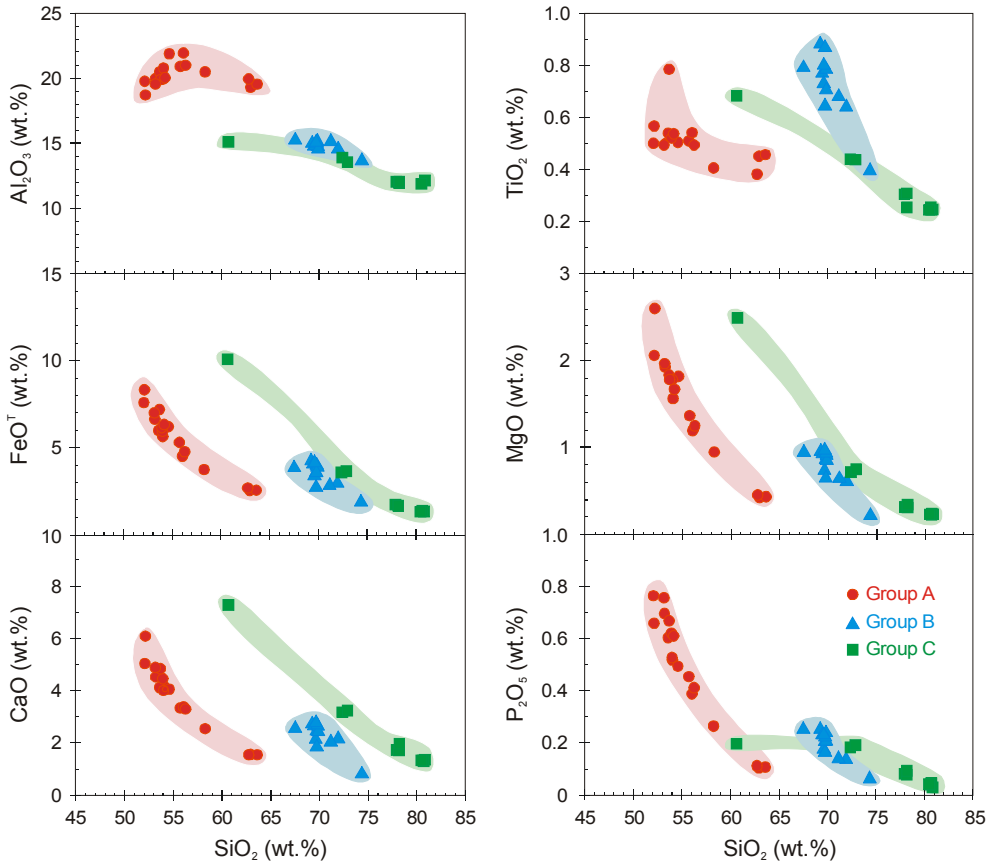

Figure 14: . Al_2O_3, FeO^T, CaO, TiO_2, MgO, P_2O_5 versus SiO_2 Harker diagrams for Group A, B, and Group C.

FeO^T, CaO, MgO, and P_2O_5 show coherent negative trends with increasing SiO_2, while Al_2O_3 exhibits a slightly positive correlation (values up to 22 wt.%,) turning into a negative trend caused by fractional crystallization of mainly phlogopite and K-feldspar (trachytes samples 17677-52 cm, -57 cm and -160 cm).The evolved crystal fractionation trends in the CaO, Al_2O_3 and MgO versus SiO_2 are produced by removal of (1) clinopyroxene + plagioclase, minor olivine, and (2) clinopyroxene + plagioclase ± titanomagnetite ±amphibole, respectively. Removal of those elements in the evolved tephra produces a relatively rapid increase in SiO_2 (Figure 14, Kennedy et al., 1990b). The crystal fractionation trend in the K_2O versus SiO_2 plot (Figure 12) focused in Group A with trachytes 17677-52 cm, -57 cm and -160 cm (> 60 wt.% SiO_2 at 5.5–7 wt.%) displaying fractional crystallization of K-feldspar + phlogopite ± hornblende ± titanomagnetite as an important factor during differentiation of the evolved TLTF tephra. P_2O_5 show a clear negative trend with increasing SiO_2 for Group A but less for Group B and C. It is most likely, that apatite has influenced the Group A tephra but plays no significant role in B and C.

6.2.2 Conclusion

The major element composition of the investigated glass shards show a significant distinction from each other and can be classify into three main geochemical Groups reflecting three different provinces of origin. The major distinctions are:

Group A ⇒ The TLTF tephra.

- 5–7 wt.% K_2O at 51–64 wt.% SiO_2
- tephriphonolites, phonolites, trachytes (SO–133), + latites and dacites (SO–94)
- Mg#: 29.3–43.9
- FeO^T/MgO: 3.2–6.0 (ave. 4.0)
- Al_2O_3: 18.5–21.9 wt.% (ave. 20.1)

→ phl + K-fsp ± cpx ± ol ± ti-mt fractionation

- CaO: 1.5–6.9 wt.% (ave. 3.7)

→ cpx + plag fractionation

- Na_2O: 3.5–6.4 wt.% (ave. 5.6)
- P_2O_5: 0.1–0.8 wt.% (ave. 0.5)

→ sparse apatite attendance

Group B ⇒ The Rabaul tephra.

- 3–5 wt.% K_2O at 66–75 wt.% SiO_2,
- dacites, rhyolites, trachytes (SO–133), + basaltic andesites, and dacites (SO–94)
- Mg#: 23.1–39.4
- FeO^T/MgO: 4.2–4.8, (ave. 4.2)
- Al_2O_3: 13.9–15.1 (ave. 14.7)
- CaO: 0.9–2.8 wt.% (ave. 2.3)
- Na_2O: 2.4–4.7 wt.% (ave. 3.3)
- P_2O_5: 0.1–0.3 wt.% (ave. 0.2)

Group C ⇒ The New Britain arc tephra.

- <2 wt.% K_2O at 59–79 wt.% SiO_2
- rhyolites, andesites
- Mg#: 30.2–38.2
- FeO^T/MgO: 4.0–6.1 (ave. 5.3)
- Al_2O_3: 11.5–14.7 (ave. 12.3)
- CaO: 1.3–7.1 wt.% (ave. 2.4)
- Na_2O: 1.9–4.2 wt.% (ave. 3.1)
- P_2O_5: 0.03–0.2 wt.% (ave. 0.1)

It is obvious that all samples of all three distinct groups are far more evolved than the existing database of Wallace et al. (1983), and Müller et al. (2001) for the TLTF volcanoes, and also for Rabaul and New Britain (Gill et al., 1993; Woodhead and Johnson, 1993; Wood et al., 1995). This effect is explainable by the chemical differences between lavas (= glass + diluting phenocrysts) and (evolved) magmas.

Furthermore, the largest eruptions are likely to be the most volatile-rich and thus the most evolved sources affecting in particular Group B and C.

6.3 Trace element composition of the ash beds

Trace element composition of 21 representative glass samples are described in this section. Trace elements were analyzed using the VG PlasmaQuad PQ1 instrument at the University, Kiel. A complete list of chemicals, laboratory instruments and apparatus, and the dissolution procedure is described in Garbe-Schönberg (1993). Detailed composition are listed in the appendices → 9.8, element ratios are given in Table 5.

6.3.1 Preparation and analytical technique

1.6 up to 3 mg of handpicked glass shards were weighed in teflon beakers and dissolved in 2 ml HF and 2 ml freshly prepared aqua regia (HNO_3:HCl, 1:3) on a hotplate at 140 °C for 14 hours. 0.5 ml $HClO_4$ was added and the solution was evaporated at 180 °C. Shortly before complete dryness, 0.5 ml HNO_3 and 1.5 ml deionised H_2O were added and the solution dried afterwards. The residue was taken up in 0.5 ml HNO_3 and 2.5 ml deionised H_2O on a hotplate at ~140 °C. Finally, the solutions were brought up with deionised H_2O to a fixed volume of 3 ml. All utilized chemicals for dissolution are subboiled or supra pure, and the water is deionised. Sample 17682–710 cm was prepared in duplicate. The duplicate analysis show a reproducibility of the dissolution method generally better than 1% for most elements (Table 24). Exceptions are Ba that displays an error to 13% as well as Sr and Zr with errors of 7% and Rb and Y with 2%. Prior the measurement process the sample solutions were diluted 1/200 with 2% HNO_3 and a 50 ppb spike of Re, In, and Be was also used as an internal standard to compensate for physical interferences over the whole mass range. Oxide interferences occur for several elements (e.g. CeOH on Gd and BaO on Eu). The actual correction factor for each element was calculated from the measured concentrations of the interfered isotopes in a 100 ppb calibration solution. The oxide pattern was checked to be less than 0.5% CeO/Ce before the run of each sample (Garbe-

Schönberg, 1993). The blanks for all elements are negligible compared to the concentration in the samples. Reproducibility and accuracy of the MPI DING glass standard StHs6/80 and the BHVO-1 standard are shown in Table 25. The reproducibility for trace elements of the StHs6/80 glass standard is generally better than 6% except Co, Ni, Zn, Ga, and Cs with errors up to 18%. The rare earth elements (REE) show reproducibility better than 2%. The accuracy for the BHVO-1 standard is for most elements better than 4% of all analyzed Kiel standards compared to values of (Jenner et al., 1990; Govindaraju, 1994).

6.3.2 Results

K/Rb ratio in the volcanic glass of the distinct Groups A, B, and C have approximately similar averages of 656, 663, and 710 (Table 5). They are much lower than N-MORB (1578) and well below that of Mariana arc lavas (456±85, Lin et al., 1989; 365±90, Sun and Stern, 2001). More depleted Izu-Bonin arc lavas have similar K/Rb ratios, with a mean value of 693±105 (Taylor and Nesbitt, 1998). In contrast, a clear distinction is obvious for K/Ba ratio. The shoshonites of Group A with a mean of 157 are only little beyond MORB (140) but thrice as high as in Group B (52) and more than twice as high as in Group C (66). Izu-Bonin arc lavas (27±8, Taylor and Nesbitt, 1998), other Mariana arc lavas (27±7, Lin et al., 1989), high-K lavas from Southern Italy (29±1, Ellam et al., 1989), and even Fiji shoshonites (49±11, Gill and Whelan, 1989) show significantly lower K/Ba ratios.

Although TLTF samples have a Cs/Rb ratio of 0.018 and approach the mantle value (0.013, Sun and McDonough, 1989), Rabaul tephra (0.030) and New Britain arc tephra (0.047) are far higher. U/Nb in the TLTF shoshonites (0.52) are equivalent to Mariana shoshonites (0.56, Sun and Stern, 2001), regardless of the absolute concentration of Nb. Rabaul (0.41) and New Britain (0.47) are little lower than Group A.

Variation of selected incompatible elements versus SiO_2 reveals systematic differences between the TLTF shoshonites (Group A), Rabaul glasses (Group B), and New Britain glasses (Group C, Figure 15). Additionally a comparison of TLTF shoshonites with selected global shoshonites and high-K lavas are also included in Figure 15.

Among the large ion lithophile elements (LILE), Rb reflects a very similar behavior to that of K_2O with increasing SiO_2 (→ Figure 12). Ba illustrates a higher enrichment of both TLTF samples (417 ppm) and Rabaul glasses (514 ppm) than New Britain glass samples (221 ppm). This probably reflects highest fluxes of slab-derived fluids below Rabaul, whereas TLTF tephra archive an high flux input since the active subduction phase 15 Ma ago.

Table 5: Element ratios of Group A, B, and C glasses. MORB values after Pearce and Peate (1995)

	Group A	ave.	Group B	ave.	Group C	ave.	N-MORB
K/Rb	571-742	656 ±80	474-851	663 ±134	611-811	710 ±83	1578
K/Ba	130-183	157 ±18	27-77	52 ±29	58-73	66 ±6	140
Cs/Rb	0.016-0.019	0.018 ±0.001	0.026-0.034	0.030 ±0.003	0.037-0.057	0.047 ±0.009	0.016
Sr/Nd	62.0-86.8	79.40 ±14	5.9-14.3	10.1 ±3	16.9-34.2	25.6 ±7	12.33
Sr/Y	74.7-133.7	104.2 ±23	3.2-7.0	5.1 ±1	5.7-12.3	8.9 ±3	3.21
Ba/La	17.5-21.0	19.3 ±1	31.6-53.2	42.4 ±7	45.8-58.6	52.2 ±5	2.52
Ba/Nb	75-183	129 ±40	103-229	166 ±42	195-248	221 ±20	2.7
Ba/Th	136-201	169.0 ±26	141-397	269.0 ±86	395-461	428.0 ±28	52.5
U/Th	0.7	0.7 ±0.02	0.6-0.7	0.65 ±0.03	0.9-1.1	0.96 ±0.07	0.39
U/Nb	0.39-0.65	0.52 ±0.1	0.37-0.46	0.41 ±0.03	0.42-0.52	0.47 ±0.04	0.02
Pb/Ce	0.26-0.43	0.35 ±0.06	0.31-0.38	0.35 ±0.03	0.54-0.67	0.61 ±0.05	0.04
Pb/Th	4.2-6.5	5.40 ±0.8	3.5-5.7	4.60 ±0.8	10.5-14.2	12.40 ±1.8	2.50
Pb/Sm	2.3-4.0	3.10 ±0.6	1.7-2.5	2.10 ±0.3	2.3-2.7	2.50 ±0.2	0.11
Pb/Nb	2.4-5.2	3.80 ±1.4	2.6-3.3	2.90 ±0.2	5.4-7.1	6.30 ±0.8	0.13
Th/Nb	0.55-0.91	0.73 ±0.1	0.58-0.75	0.66 ±0.07	0.46-0.54	0.50 ±0.05	0.05
Th/Sm	0.46-0.71	0.59 ±0.09	0.35-0.72	0.53 ±0.14	0.17-0.26	0.21 ±0.04	0.05
Zr/Nb	16.8-25.8	21.3 ±4	44.2-67.9	56.0 ±8	67.4-96.4	81.9 ±13	31.8
Zr/Hf	42.6-51.9	47.2 ±4	35.4-39.9	37.7 ±1	33.7-35.6	34.7 ±1	36.1
Nb/Ta	20.3-47.1	33.7 ±10	19.2-27.4	23.3 ±3	15.4-18.9	17.2 ±1	17.9
Nb/Yb	1.56-3.40	2.48 ±0.66	0.57-1.28	0.92 ±0.27	0.30-0.52	0.41 ±0.08	0.76
La/Th	7.2-9.6	8.4 ±0.9	4.3-7.9	6.1 ±1.4	7.9-9.5	8.7 ±0.6	20.8
La/Nb	3.9-8.7	6.3 ±1.7	3.1-4.6	3.90 ±0.5	4.1-4.5	4.30 ±0.2	1.07
Ce/Yb	21.6-27.7	24.6 ±2	5.8-8.7	7.21 ±1	3.4-5.2	4.34 ±1	2.46
$(La/Sm)_N$	2.63-3.17	2.90 ±0.2	1.73-2.01	1.87 ±0.1	0.93-1.39	1.16 ±0.2	0.95
$(La/Yb)_N$	7.75-10.11	8.93 ±0.8	1.78-2.78	2.28 ±0.4	0.94-1.61	1.28 ±0.3	0.82
Ce/Ce*	0.89-1.22	1.05 ±0.1	0.93-0.94	0.93 ±0.01	0.28-0.95	0.62 ±0.3	0.28
Eu/Eu*	0.92-0.98	0.95 ±0.03	0.61-0.74	0.68 ±0.06	0.37-0.90	0.63 ±0.2	0.37

Sr generally shows a dichotomy, high (up to 2228 ppm, with a mean value of 1777 ppm) in the TLTF shoshonite samples, and relatively low for Group B (189 ppm) and Group C (198 ppm).

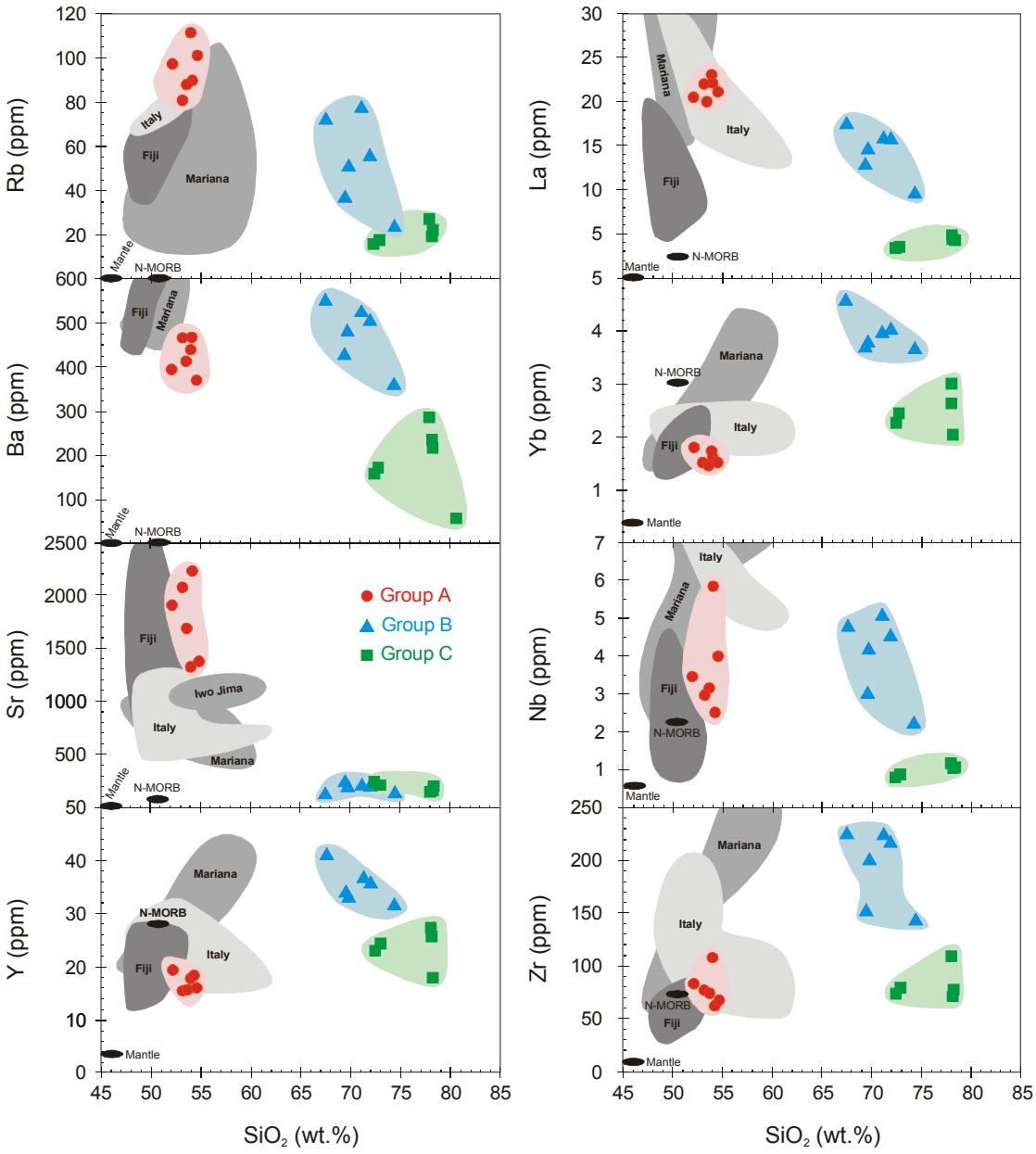

Figure 15: Trace element Haker diagrams for the distinct Group A (TLTF tephra), Group B (Rabaul tephra), and Group C (New Britain tephra). Data for Southern Italy (Roman province) are taken from Ellam et al. (1989); shoshonitic to tholeiitic Fiji basalts from Gill and Whelan (1989); for northern Mariana (Izu-Bonin) shoshonites from Sun and Stern (2001); and Iwo Jima from Lin et al. (1990), respectively. MORB values after Pearce and Peate (1995), primitive Mantle from McDonough and Sun (1995).

The Sr-enrichment in the TLTF shoshonites may also reflect storage during the active phase of sediment subduction as mentioned above. Rabaul and New Britain have lower Sr concentrations, although still twice as high as MORB which is caused by minor mantle enrichment of sediment and/or altered oceanic crust through recent subduction at the New Britain Trench (for comparison MORB 90 ppm). Nevertheless, the Sr values for Fiji and Mariana arcs show still greater enrichment than the TLTF shoshonites (Gill and Whelan, 1989; Sun and Stern, 2001). The overall trends of Zr, Y, and Yb are similar, despite of slight differences in concentration. Rabaul glasses are enriched in Zr (187 ppm), Y (36.4 ppm), and also in Yb (4.13 ppm) relative to MORB (74 ppm, 28.0 ppm, 3.05 ppm). TLTF glasses show approximately MORB characteristic in Zr (85 ppm) and a depletion of Y (17.4 ppm) and Yb (1.65 ppm). New Britain glass samples behave similar as the TLTF glasses at >70 wt.% SiO_2 with slight a enrichment in Zr (90 ppm) and a minor depletion of Y (22.3 ppm) and Yb (2.53 ppm) relative to MORB.

La and Nb reflects the clear distinction between all three Groups just like Rb and K_2O with increasing SiO_2 ($\rightarrow$ Figure 12). The TLTF glass shards contain abundant La (21.5 ppm) and Nb (21.3 ppm), Rabaul glass shards are less enriched in La (13.5 ppm), and Nb (18.2 ppm), and New Britain glass shards contain the lowest La (4.2 ppm), and Nb (8.0 ppm) concentration, which is still enriched relative to MORB (La 2.5 and Nb 2.2 ppm) but common in arc lavas.

More chemical characteristics of the TLTF shoshonites as well as Rabaul and New Britain glasses are summarized on N-MORB normalized spidergrams (Figure 16a and 17a) and C1-chondrite normalized rare-earth element (REE) patterns (Figure 16b and 17b).

All three Groups show elevated concentrations of large ion lithophile elements (LILE). A clear distinction can be emphasized for TLTF and Rabaul tephra showing greater enrichment than New Britain tephra. New Britain samples represent typical enriched arc lava composition compared to other global arcs, especially the Marianas (Figure 17a, Bloomer et al., 1989; Peate and Pearce, 1998; Taylor and Nesbitt, 1998; Sun and Stern, 2001). The TLTF and Rabaul samples share high level LILE pattern similarities.

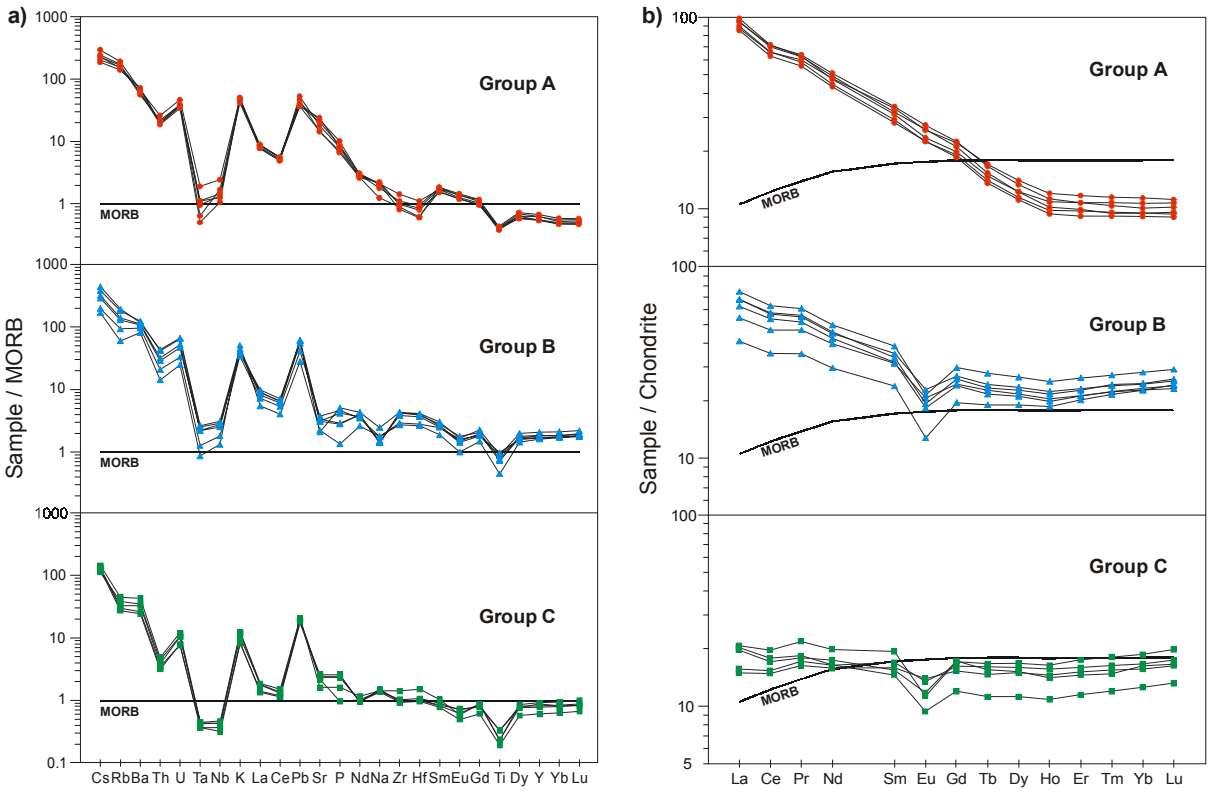

Figure 16: **a)** Multi-element spidergrams of representative glass samples of the distinct ash bed groups (MORB normalized after Pearce and Peate, 1995).**b)** Chondrite normalized REE patterns of representative glasses (C1-chondrite values from Sun and McDonough, 1989).

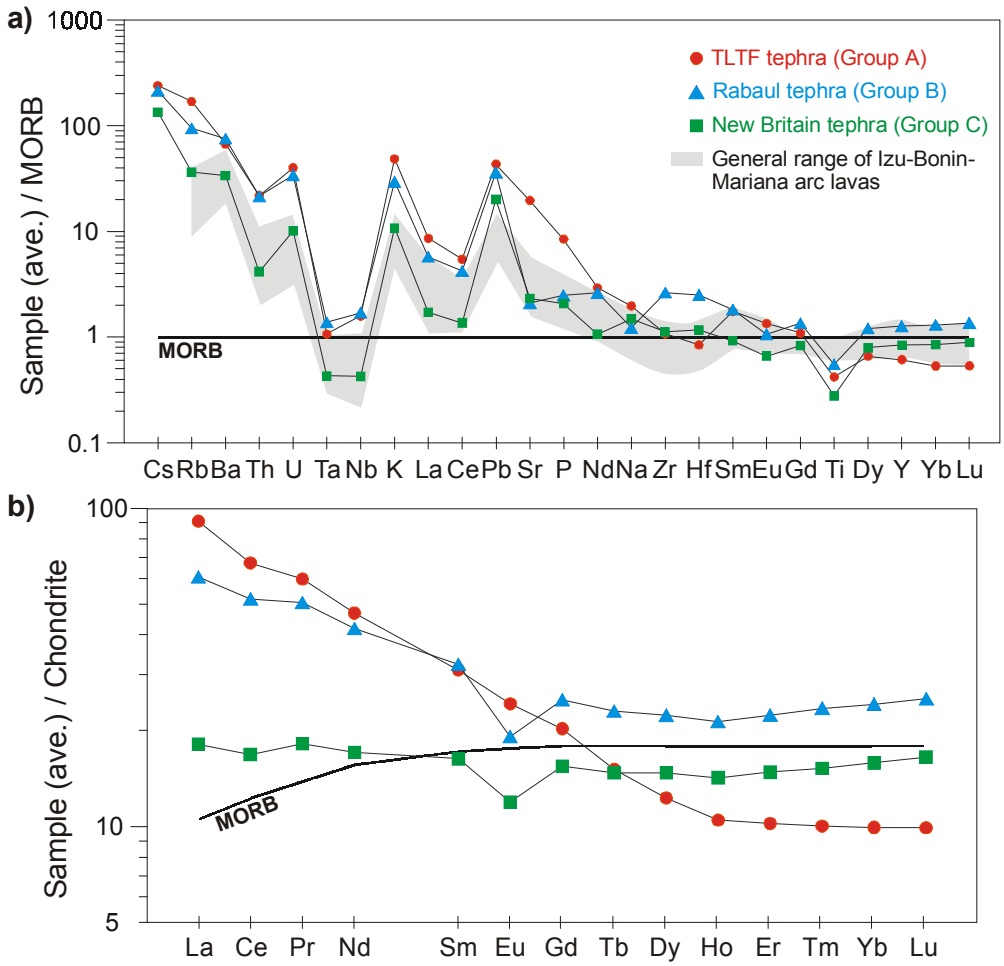

Figure 17: **a)** N-MORB normalized spidergram illustrating the element distinction among the individual tephra groups by the use of average values of Figure 16 compared with data of Izu-Bonin (Taylor and Nesbitt, 1998) and other Mariana arcs (e.g. Bloomer et al., 1989; Peate and Pearce, 1998; Sun and Stern, 2001). **b)** C1-Chondrite normalized average REE patterns of Figure 16.

Shoshonitic TLTF samples show thereby mostly the elevated concentrations of Cs (240 times MORB, Rabaul 214), Rb (170 times MORB, Rabaul 95), and Ba (67 times MORB, Rabaul 75). Sr clear without ambiguity the distinction among the three chemical Groups. The TLTF samples have values 20 times MORB, 17 times via average Mariana arc lavas (e.g. Bloomer et al., 1989; Peate and Pearce, 1998; Taylor and Nesbitt, 1998), and also 10 times of Izu-Bonin shoshonites (Alkalic Volcano Province shoshonites, Sun and Stern, 2001), whereas Rabaul and New Britain glass samples attend with 2 times MORB (Figure 17a) similar to global arc lavas.

Zr, Hf, Nb,Ti and Ta are typical high field strength elements (HFSE) and exhibit also differences in the TLTF shoshonitic, Rabaul, and New Britain tephra. The TLTF shoshonites show a mean Zr/Hf ratio of 47.2 which is significantly higher

than the mantle value of 36 (Sun and McDonough, 1989), and even higher (45.1) than the Alkalic Volcano Province shoshonites of the Izu-Bonin arc observed by Sun and Stern (2001). The Rabaul samples have 37.7 which is equal to global Mariana arc lavas (e.g. Elliot et al., 1997; Peate and Pearce, 1998) whereas New Britain have the lowest ratio of 34.7 pointing in general to a more depleted mantle source for the arc and the Manus Basin, respectively. Noticeable is the Nb–Ta trough which is a common characteristic of arc volcanoes. All three distinct Groups show such a trough, whereas the TLTF shoshonites and the Rabaul samples are more MORB like and the New Britain samples match with the more depleted Nb–Ta trough for arc volcanoes all over the world (e.g. Meen, 1987; Ellam et al., 1989; Gill and Whelan, 1989; Edwards et al., 1991). The mean Nb/Ta of 33.7±10 in the TLTF glasses and 23.3±3 in the Rabaul samples is above the mantle value of 17.8 (Sun and McDonough, 1989) and also above all other reported values for other volcanic arcs, including the special Alkalic Volcano Province shoshonites of the Izu-Bonin arc (22.3±2). New Britain glass shards show again mantle values (17.2±0.7). Figure 16b and 17b illustrate REE plots of representative glass samples. It is noticeable that there is a markedly different REE pattern for the TLTF samples in contrast to Rabaul and New Britain samples respectively. The TLTF volcanoes show enrichment in LREE with a steep continuous negative trend culminating in a flat HREE path that is depleted relative to MORB. Rabaul glass shards have similar LREE enrichments as the TLTF glasses, but differ with a negative Eu anomaly and a slight HREE enrichment relative to MORB. New Britain show barely a LREE enrichment, a stronger negative Eu anomaly, and the same HREE pattern as Rabaul but depleted relative to MORB.

6.3.3 Conclusion

The most distinctive chemical characteristics that distinguish the TLTF shoshonitic samples from the Rabaul and New Britain tephra on the one hand and from ordinary Izu-Bonin-Mariana arc lavas on the other is their strong enrichment in LILE, K, P, Sr, LREE, and the strongest depletion of HREE. Rabaul indicates with similar enrichment in LILE and LREE, but with average global arc lava values of P and Sr, a negative Eu anomaly, and a more enriched HREE pattern a more

complicated mantle source. In contrast thereto the New Britain arc have characteristics of typical arc lavas such as the ordinary Izu-Bonin-Mariana arc with larger depletion of MREE and HREE as N-MORB pointing to a more depleted mantle source.

7 DISCUSSION

7.1 Volcanic activity in the past 333 ka in the New Ireland Basin

With a combination of the established geochemical signature (→ chapter 6) of the TLTF samples (Group A), Rabaul samples (Group B), and New Britain samples (Group C), and the interpolation of their ash bed ages (→ chapter 4), it is now possible to establish a correlation of the ash beds.

As discussed earlier the ash beds at 2 ka (17675-12 cm, 17676-10 cm), at 4 ka (17675-22 cm, 17682-9 cm), at 18 ka (17677-52 cm, 17684-30 cm), at 20 ka (17675-138 cm, 17676-148 cm), and perhaps the 161 ka and 164 ka ash beds (17681-345 cm, 17682-713 cm) are those which appear to correlate with other (Figure 9). However, their geochemical differences illustrate that only GA beds 17681-345 cm and 17682-713 cm could really represent the same eruption and be truly correlative. Those air fall GA beds came from Rabaul, and represent two explosive high-volatile eruptions at 161 ka and 164 ka.

The ash beds at 2 ka, 4 ka, and 18/20 ka are all different in chemical composition. Sample 17675-12 cm is from New Britain, 17676-10 cm from TLTF at 2 ka, 17675-22 cm from New Britain, 17682-9 cm from Rabaul at 4 ka, and 17677-52 cm from the TLTF chain, 17684-30 cm from Rabaul at 18 ka. Also the 20 ka tephras 17675-138 cm is from Rabaul and 17676-148 cm is from New Britain. Furthermore, the discrete, prominent, homogeneous GA beds 17677-229 cm, and 17682-713 cm are from Rabaul whereas the GA beds 17677-117 cm, 17681-345 cm, -444 cm, and 17682-311 cm, -328 cm (Figure 12 and 13) have their origin at other New Britain arc volcanoes.

It is evident that the great majority of all ash beds in the New Ireland Basin are coming from Rabaul and New Britain, and not from the TLTF volcanoes. This result is not expected, because the TLTF volcanoes are known to be volatile-rich, and strongly alkalic and silica-undersaturated (e.g. Kennedy et al., 1990a; McInnes and Cameron, 1994). Additionally Edison, Conical, and TUBAF Seamounts feature highly vesicular lavas and abundant fragmental rocks (Herzig et al., 1994; Herzig et al., 1998).

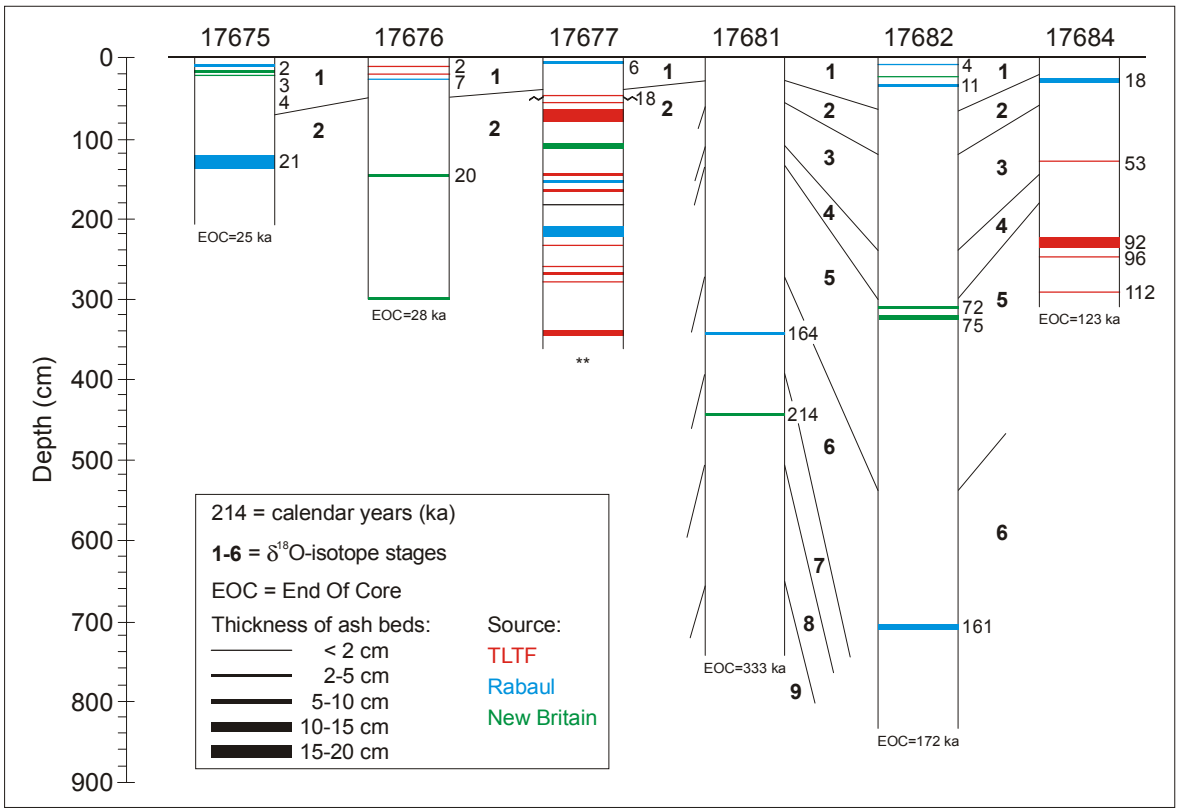

Figure 18: Correlation of the ash beds in the investigated sediment cores. Red color = TLTF, blue color = Rabaul, green color = New Britain arc.

Moreover, the TLTF islands have volumes of 500 km^3 (Wallace et al., 1983), suggesting a high likelihood of large volumes of TLTF sourced volcaniclastics and tephras filling the New Ireland Basin. None of these were found in the investigated cores. The thickest ash beds recovered in the cores were from Rabaul and New Britain respectively. Exceptions are two ash beds recovered by coring between Lihir and Tanga (17677-75 cm and 17684-239 cm; Table 2). All other ash beds from the TLTF volcanoes are less than < 5 cm thick. Thus, only small volume of tephra in the uppermost sediments of the New Ireland Basin originated at the TLTF volcanoes. Further evidence of a low input from the TLTF volcanoes is the background glass shard population analyzed in the sediment samples 17674-27 cm and -44 cm. Glass shards in sample 17674-27 cm have the geochemical signature of Rabaul, whereas those in sample 17674-44 cm represent a mix of Rabaul and TLTF derived shards.

7.1.1 Conclusion

Altogether it is evident that recent eruptions at the TLTF volcanoes are characterized by relatively small disruptive explosions, and not large highly explosive eruptions of the sort which occurred at Rabaul and all other volcanoes of the New Britain arc. Müller et al. (2001) concluded that part of the caldera (5.5 × 3.5 km in diameter) of the Luise volcano at Lihir collapsed due to normal erosional processes and was not accompanied by a large volume eruption. The Tanga Islands represent the eroded remnants of stratovolcanoes, the summits of which were largely destroyed by multiple caldera collapses during the Pleistocene and by later complex faulting. Bitlik and Bitbok are the remains of a trachyte dome built up on the caldera floor during a post-caldera phase of volcanism (Wallace et al., 1983). Similarly on the Feni Islands, Ambitle is a stratovolcano featuring remnants of small collapsed calderas (3 km in diameter) and later post-caldera trachyte domes (Wallace et al., 1983). Nevertheless, no large volume ash beds can be correlated with the formation of any of these calderas.

Another important aspect is that all recovered ash beds are younger than 333 ka. It is possible that the TLTF volcanoes have not been very active since 333 ka, or have only had small disruptive explosions (primarily at Tanga and Feni). However, plenty of passive degassing has occurred (and was observed at Lihir, Herzig et al., 1994; Herzig et al., 1998; Schmidt et al., in press.). The post-caldera lavas of Ambitle and Babase at the Feni Islands are 0.68 ka and 1.53 ka old, the Bitlik and Bitbok post-caldera lavas at the Tanga Islands have ages of 1.08 ka and 1.14 ka, whereas the Lihir hydrothermal system of the Luise stratovolcano (host of the giant Ladolam gold deposit) has an age of 0.95 ka. The ash beds in core 17684-239 cm (0.92 ka) and -248 cm (0.96 ka) might be related to the Luise event at 0.95 ka. Thus, all known volcanic events at the TLTF islands appear to be significantly older than the ash beds recovered in the sediment cores. This strongly suggests that the TLTF volcanoes have been relatively inactive since 333 ka and the most important input of volcanic ash since then is from the active volcanic New Britain arc.

7.2 Evolutionary model for the TLTF volcanic islands

About 15 million years ago the area of investigation constituted a normal island arc system including the New Ireland arc, the non-volcanic fore-arc (no TLTF volcanoes) and the Manus–Kilinailau Trench (Figure 19a). The island arc volcanism on New Ireland at that time reflects the SW-directed subduction of the cold, dense slab of the Pacific lithosphere. Melt generation then occurred at depths of > 100 km, as at normal volcanic arcs. At about 10 Ma the Ontong Java Plateau entered the Manus–Kilinailau Trench and blocked further subduction of the Pacific Plate (Figure 19b). After the collision, the cold dense Pacific slab probably break off and descended deeper into the mantle. Thereafter, melt generation in the mantle overlying the slab would have induced less volcanic activity at New Ireland. Also melt generation may have shifted in the fore-arc direction as the slab sank in the mantle (e.g., a reduction in subduction rate allowing enhanced metasomatism of the overlying mantle, or possibly greater vertical component of subduction). Figure 19c shows the inferred situation in the Pliocene. The original melt source for New Ireland disappears because the slab is now much deeper beneath this region (> 200 km).

But the mantle beneath the old fore-arc may fed by the last fluids leaving the descending, which would supply a LILE-enriched melt. Also, latter underlying mantle may flow around the edge of the broken off slab and rise into the lithosphere. After the slab has been totally subducted (Figure 19d), back-arc spreading and the opening of the Manus Basin at 3.5 Ma caused lithospheric extension in the now back-arc subduction metasomatized region. Decompressing and upwelling of this region would trigger partial melting of the mantle beneath the TLTF chain.

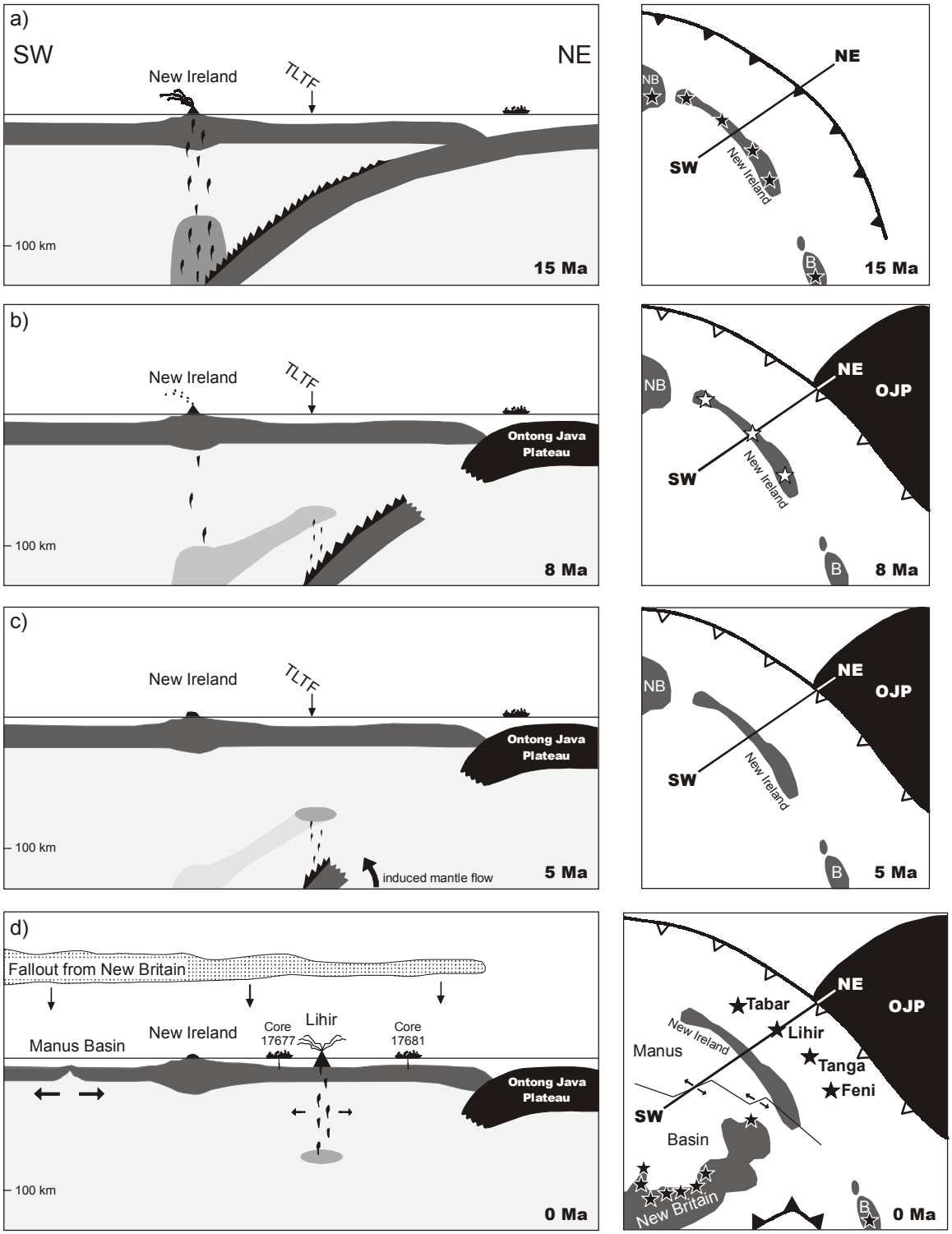

Figure 19: Cartoon illustrating the development of the TLTF volcanoes.

7.3 Evidence for the role of hydrous fluids

Mantle metasomatism by hydrous fluids released from the subducted lithosphere may modify the composition of the mantle and trigger melting (e.g. Tatsumi, 1989; McCulloch and Gamble, 1991). The argument is supported by inferences derived from flux melting models (Stolper and Newman, 1994). To examine the influence of fluid-induced mantle metasomatism on the TLTF, Rabaul, and New Britain samples, incompatible element ratios such as Ba/La (taken as indicator of fluid enrichment and plotted in Figure 20), Cs/Rb, Pb/Ce, and U/Th are used because of the higher fluid mobility of the numerator with respect to the less fluid-mobile denominator. Accordingly, lavas with higher ratios are likely to have sources that were strongly affected by fluid-induced enrichments.

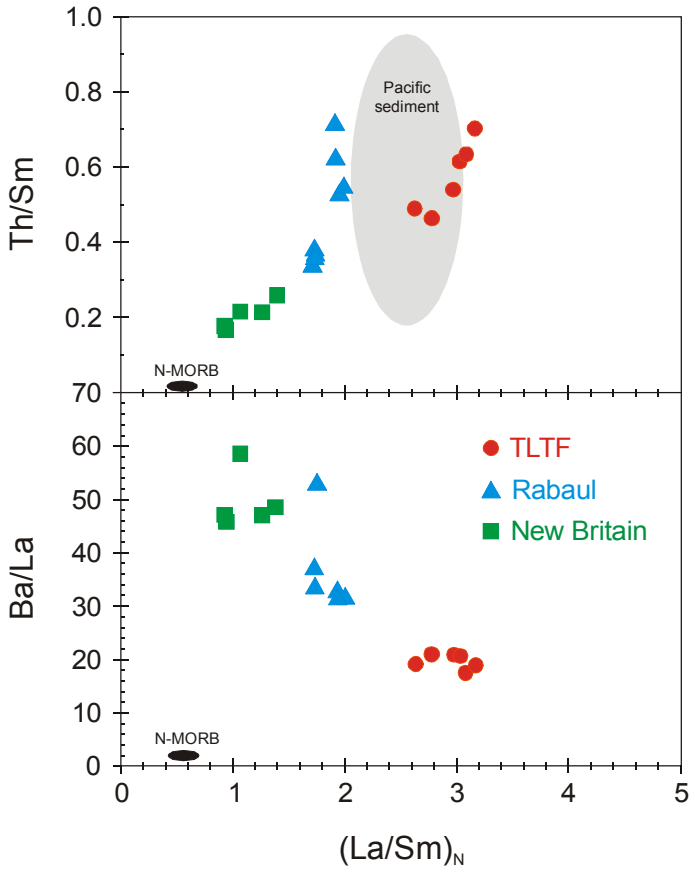

Figure 20: $(La/Sm)_N$ versus Ba/La taken as indicator of fluid enrichment, and $(La/Sm)_N$ versus Th/Sm as representative for sediment input. Data of Pacific sediment from (Ben Othman et al., 1989), N-MORB from (Pearce and Peate, 1995).

The ratio of Ba/La and Cs/Rb of the TLTF samples is 19 and 0.018, respectively (Table 5). Rabaul samples have 42 and 0.030 and the New Britain glasses show the highest ratios of 52 and 0.047. Pb/Ce and U/Th also distinguish between TLTF (0.35 – 0.61) and New Britain (0.7 – 0.96), whereas Rabaul suggests more TLTF affinities (0.35 – 0.65) which point to a more varied mantle source beneath Rabaul. The U/Th in the tephra further constrains the contribution of fluid metasomatism. Under normal redox conditions in the mantle, both U and Th are tetravalent and have similar chemical behaviors. In a hydrous subduction environment, U may be oxidized to U^{6+} and form uranyl complexes that are mobilized in hydrous fluids (Brenan et al., 1995). Interaction between a high U/Th fluid and the sub arc mantle should enrich U and all other fluid-mobile LILE elements. U/Th ratios are well above MORB values (0.39) for all samples analyzed in this study. The highest here again were New Britain tephras (0.95) followed by similar ratios for Rabaul and the TLTF glasses (0.65, res. 0.70). Nevertheless, elevated U and other incompatible elements can be attributed to other causes, for example enriched mantle orsedimentary component. Similar geochemical features found in other enriched arcs, e.g. the Aeolian islands (Ellam et al., 1989), the Philippines (McDermott et al., 1993), and are interpreted to indicate involvement of a sedimentary component rather than a hydrous fluid (Hawkesworth et al., 1997).

7.4 Evidence for a greater sedimentary component

To recognize the involvement of pelagic sediments in the mantle source, incompatible elements with limited fluid mobility are preferred since their concentration and ratios should not be affected by hydrous fluids. The Th/Sm ratio is taken as indicator of possible sediment enrichment and plotted in Figure 20. For the TLTF glasses, Th/Sm is positively correlated with $(La/Sm)_N$ indicating that LREE enrichment and the relative contribution of subducted sediment may be directly related. Rabaul samples can be subdivided into three samples that show New Britain tephra characteristics with higher abundances, and the remaining samples with a) higher sediment input to the mantle source or more likely b) a mixing of TLTF mantle source and the depleted New Britain mantle source. New Britain glasses show a slight sediment component in their source. Taken together,

the trace element compositions support the involvement of subducted sediment and archived incompatible elements in the mantle beneath the TLTF volcanoes, whereas the New Britain mantle source is fed by active sediment-poor subduction at the New Britain Trench. Rabaul seems to be a mix of TLTF and New Britain-type mantle.

7.5 Fractionation of incompatible elements in the TLTF tephra

One distinctive chemical characteristic that distinguishes the TLTF tephra from New Britain and Rabaul on the one hand and ordinary Izu-Bonin-Mariana arc lavas on the other is their strong enrichment in the LREE (Figure 17b). Strong fractionation of LREE relative to HREE in melts can be due to the involvement of certain refractory phases. Melting with residual garnet for example should cause not only greater LREE enrichment but also steeper HREE patterns at a smaller extent of partial melting because of the extremely high HREE partitioning coefficient (*D*) of garnet (Hanson, 1980; Green, 1994). HREE fractionation through garnet in shoshonites are explained from continental arcs such as Sunda (Edwards et al., 1991), but the flat HREE pattern of the TLTF glasses are inconsistent with residual garnet. The absence of garnet and the presence of numerous spinel inclusions in olivine from mantle xenoliths of the TUBAF seamount suggests that melt generation for the TLTF tephras was far above the garnet stability field, and took place at shallow depths of < 80 km (Franz and Wirth, 2000; McInnes et al., 2001). This excludes garnet as a residual phase causing HREE depletion in the TLTF tephras. But what kind of other refractory phase/phases could have caused that? As mentioned earlier (→ section 3.4.2) a n elevated proportion of feldspar, clinopyroxene, phlogopite, amphibole, and titanomagnetite were found in the TLTF ash beds. Clinopyroxene and amphibole are known to have mineral/silicate liquid *D* values that could lead to flat overall HREE patterns in the TLTF tephra (Green, 1994). The D_{REE} of phlogopite appears also sufficient to fractionate HREE from melt and produce a relatively flat pattern (Green, 1994). Apatite *D´*s for REE increase with decreasing temperature and increasing SiO_2 but not enough to produce marked depletion of HREE (Green, 1994). It is most likely that a combination of clinopyroxene, phlogopite, and

amphibole are responsible for the flat HREE pattern. However, Apatite may play a greater role in the P_2O_5 enrichment of the TLTF tephra relative to other island arcs (e.g., New Britain).

Neither source signature nor crystallization of common phases alone can account for the highly fractionated LILE/HFSE in the TLTF and Rabaul tephra. Crystallization of titanomagnetite or other Ti-phases during magmatic processes may be responsible for HFSE depletions. Rabaul samples show an enrichment in Zr and Hf which suggests a greater role for rutile or another Ti-rich phase. Sun and Stern (2001) proposed for the decoupling of LILE/HFSE in shoshonitic lavas from the Izu-Bonin-Mariana arc a source enrichment in incompatible elements and depletion in HFSE caused by low-pressure fractionation of minor Ti-rich phases.

7.6 Implications for the mantle source of the TLTF volcanoes and Rabaul related to New Britain

Shedding light on the question what kind of mantle underlies the observed chemically distinct provinces is limited by a lack of Pb, Sr, and Nd isotope data. Nevertheless, trace element concentrations in the investigated samples provide some clues. A useful projection is the Nb/Yb plot. Yb is used as a denominator to minimize the effects of fractional crystallization subduction-related metasomatism and hence “see through” to the mantle source composition (Pearce and Peate, 1995). As shown in Figure 21, there is a clear distinction between the mantle source of the TLTF volcanoes and the Rabaul and New Britain volcanoes.

On the $(Ce/Yb)_N$ versus $(Nb/Yb)_N$ diagram (Figure 21), the TLTF tephra plot parallel to MORB array but they represent an enriched source with Nb/Yb considerably greater than that of MORB. Even more enriched are basalts from the Solomon Sea. It is unusual for back-arc basin lavas (such as those from the Solomon Sea) to have such high Nb/Yb values. This suggests that there is a widespread province of high Nb/Yb mantle that extends under the Solomon Sea and under the TLTF volcanoes (e.g., New Ireland Basin).

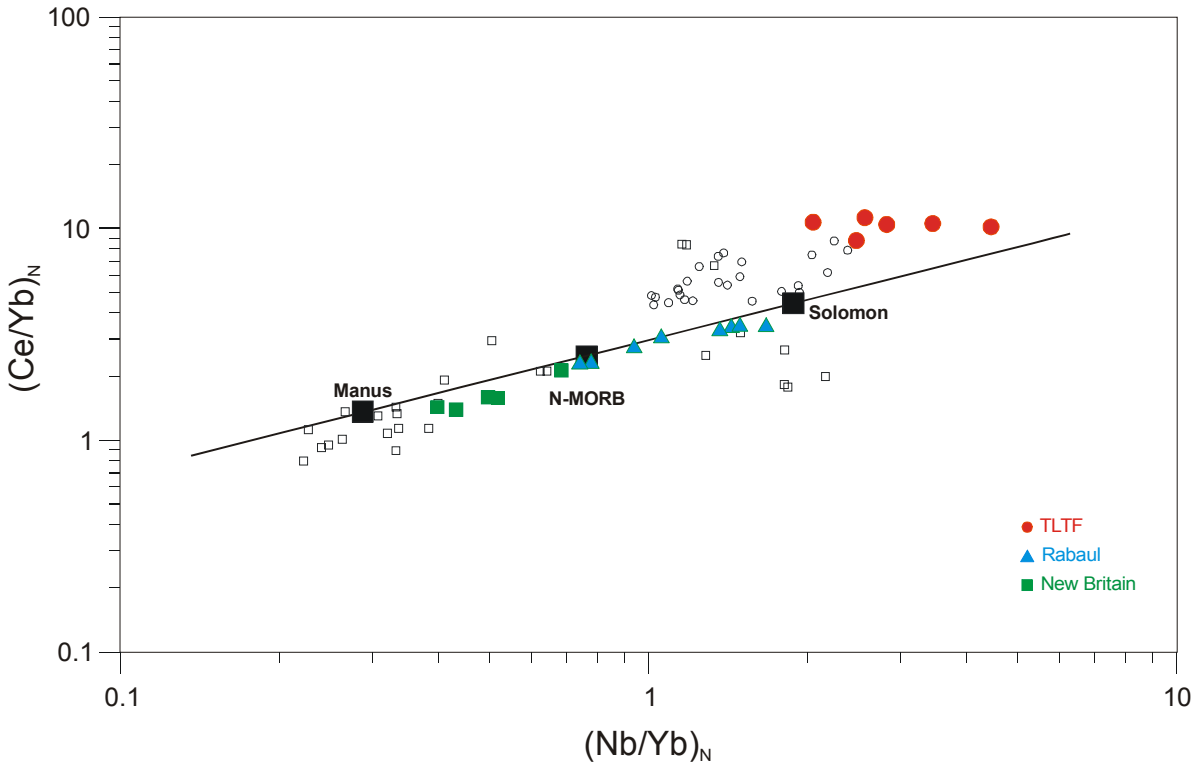

Figure 21: $(Ce/Yb)_N$ versus $(Nb/Yb)_N$ diagram. Open circles = Müller et al. (2001), open cubes = Wallace et al. (1983), Manus data after Woodhead et al. (1998), Solomon basalts from Davis and Price (1987), N-MORB after Hofmann (1988) and Pearce and Peate (1995).

Rabaul glasses are more N-MORB like, but still enriched. They might reflect mixing between N-MORB and enriched Solomon mantle. This is not unlikely because of their geographical proximity to the TLTF volcanoes. In contrast, New Britain glasses are highly depleted relative to N-MORB which suggest highly depleted mantle underlies the Manus Basin. Samples from Wallace et al. (1983) support the idea that the boundary between Solomon and Manus mantle occurs near Rabaul (Figure 21).

7.6.1 Conclusion

A possible mantle distribution beneath the TLTF islands, Rabaul and New Britain is illustrated in Figure 22. Based on the distinct major and trace element concentrations it is very likely that the TLTF volcanoes overly enriched Solomon mantle rather than N- MORB mantle.

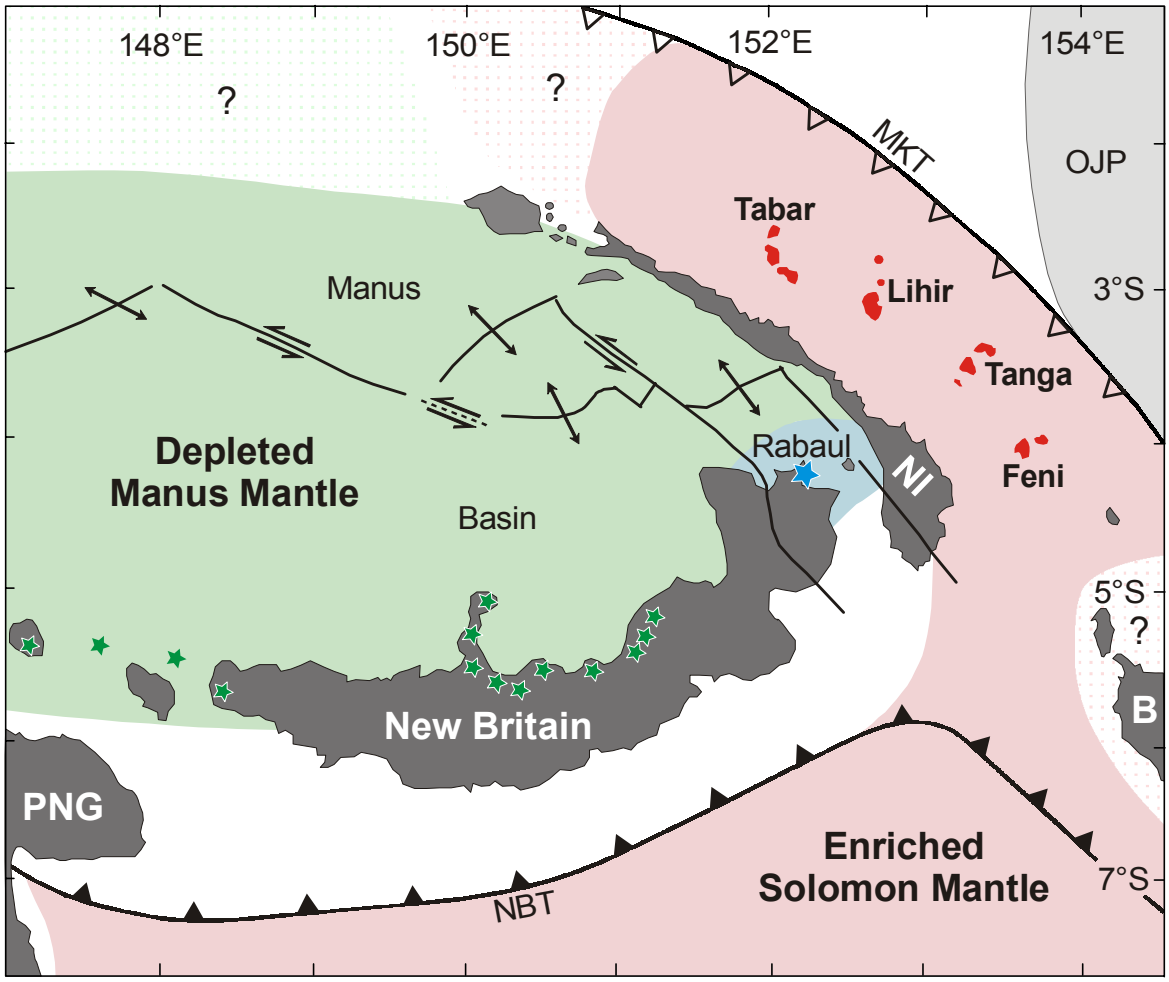

Figure 22: Assumed Solomon mantle distribution under the TLTF volcanic chain in contrast to a more depleted mantle source beneath the Manus Basin. Rabaul displays a enriched mantle between New Britain and the TLTF volcanoes. NBT = active New Britain Trench, MKT = stalled Manus–Kilinailau Trench. For tectonic units see → Figure 2.

The New Britain mantle was additionally enriched through active subduction at the Manus–Kilinailau Trench before the subduction stalled 10 Ma ago. This explains the overall higher Sr, Pb, LILE, and LREE values in the TLTF samples compared to Solomon basalts.

The samples attributed to the New Britain arc display, on the basis of the observed geochemistry, a highly depleted mantle source similar to that beneath the Manus back-arc basin.

The Rabaul volcanoes in the far northeast of New Britain have a much more complicated mantle source. It is obvious that samples attributed to Rabaul contain chemical signatures of both mantle types (enriched Solomon and depleted Manus) and possibly greater fractional crystallization of Ti-rich phases. On the one hand

high LILE, K, Pb, and LREE relative to HREE are like the TLTF shoshonites, and on the other hand their negative Eu anomaly, P, Sr, and HREE (slightly enriched) pattern more closely resembles New Britain glasses.

8 REFERENCES

Baker P. E. (1982). Evolution and classification of orogenic volcanic rocks. In *Andesites* (ed. R. S. Thorpe), pp. 11-23. John Wiley, UK.

Bassinot F. C., Labeyrie L. D., Vincent E., Quidelleur X., Shackleton N. J., and Lancelot Y. (1994). The astronomical theory of climate and the age of the Brunhes-Matuyama magnetic reversal. *Earth & Planetary Science Letters* **126**(3-5), 91-108.

Ben Othman D., White W. M., and Patchett J. (1989). The geochemistry of marine sediments, island arc magma genesis, and crust-mantle recycling. *Earth & Planetary Science Letters* **94**, 1-21.

Berger W. H. and Killingley J. S. (1977). Glacial-Holocene transition in deep-sea carbonates: Selective dissolution and the deep-sea carbonate signal. *Science* **197**, 563-566.

Bloomer S. H., Stern R. J., Fisk E., and Geschwind C. H. (1989). Shoshonitic volcanism in the Mariana Arc: Mineralogic and major and trace element characteristics. *Journal of Geophysical Research* **94**, 4,469-4,496.

Bouma A. H. (1969). Methods for the study of sediment structures. In *John Wiley & Sons*, pp. 458.

Brenan J. M., Shaw H. F., Ryerson F. J., and Phinney D. L. (1995). Mineral-aqueous fluid partitioning of trace elements at 900 °C and 2.0 GPa: Constraints on the trace element chemistry of mantle and deep crustal fluids. *Geochimica et Cosmochimica Acta* **59**, 3331-3350.

Coleman P. J. and Kroenke L. W. (1981). Subduction without volcanism in the Solomon island arc. *Geo-Marine Letters* **1**(2), 129-123.

Coleman P. J. and Packham G. H. (1976). The Melanesian borderlands and India-Pacific plate boundary. *Earth Science Review* **12**, 197-233.

Curtis J. W. (1973). Plate tectonics of the Papua New Guinea Solomon region. *Journal of the Geololgical Society of Australia* **20**, 21-36.

Davis H. L. and Price R. C. (1987). Basalts from the Solomon and Bismarck Seas. *Geo-Marine Letters* **6**, 193-202.

Edwards C., Menzies M. A., and Thirlwall. (1991). Evidence from Muriah, Indonesia, for the interplay of supra-subduction zone and intraplate processes in the genesis of potassic alkaline magmas. *Journal of Petrology* **32**, 555-592.

Ellam R. M., Hawkesworth C. J., Menzies M. A., and Rogers N. W. (1989). The volcanism of Southern Italy: role of subduction and the relationship between potassic and sodic alkaline magmatism. *Journal of Geophysical Research* **94**(B4), 4589-4601.

Elliot T., Plank T., Zindler A., White W., and Bourdon B. (1997). Element transport from slab to volcanic front at the Mariana arc. *Journal of Geophysical Research* **102**, 14,991-15,019.

Ewart A. (1963). Petrology and petrogenesis of the Quarternary pumice ash in the Taupo area, New Zealand. *Journal of Petrology* **4**, 392-431.

Exon N. F., Stewart W. D., Sandy M. J., and Tiffin D. L. (1986). Geology and offshore petroleum prospects of the eastern New Ireland Basin, northeastern Papua New Guinea. *BMR Journal of Australian Geology and Geophysics* **10**, 39-51.

Exon N. F. and Tiffin D. L. (1984). Geology and petroleum prospects of offshore New Ireland Basin in northern Papua New Guinea. In *Transactions of the Third Circum-Pacific Energy and Mineral Resources Conference* (ed. S. T. Watson), pp. 623-630.

Fisher R. V. and Schmincke H.-U. (1984). Pyroclastic Rocks, pp. 472. Springer-Verlag.

Fisher R. V. and Smith G. A. (1991). Volcanism, tectonocs and sedimentation. In *Sedimentation in volcanic settings*, Vol. 45 (ed. R. V. Fischer and G. A. Smith), pp. 1-5. SEPM (Society for Sedimentary Geology), Special Publication.

Franz L., Becker K.-P., Kramer W., and Herzig P. (2002). Metasomatic mantle xenoliths from the Bismarck Microplate (Papua New Guinea) - Thermal evolution, geochemistry and extent of slab-induced metasomatism. *Journal of Petrology* **43**, 315-343.

Franz L. and Wirth R. (2000). Spinel inclusions in olivine of peridotite xenoliths from TUBAF seamount (Bismarck Archipelago/Papua New Guinea): evidence for the thermal and tectonic evolution of the oceanic lithosphere. *Contribution of Mineralogy and Petrology* **140**, 283-295.

Garbe-Schönberg C.-D. (1993). Simultaneous determination of thirty-seven trace elements in twenty-eight international rock standards by ICP-MS. *Geostandard Newsletter* **17**, 81-97.

Gill J. B., Morris J. D., and Johnson R. W. (1993). Timescale for producing the geochemical signature of island arc magmas: U-Th-Po and Be-B systematics in recent Papua New Guinea lavas. *Geochimica et Cosmochimica Acta* **57**, 4269-4283.

Gill J. B. and Whelan P. (1989). Early rifting of an Oceanic Island Arc (Fiji) produced shoshonitic to tholeiitic basalts. *Journal of Geophysical Research* **94**(B4), 4561-4578.

Govindaraju K. (1994). 1994 compilation of working values and sample description for 383 geostandards. *Geostandard Newsletter* **18**, 1-158.

Green T. H. (1994). Experimental studies of trace-element partitioning appicable to igneous petrogenesis - Sedona 16 years later. *Chemical Geology* **117**, 1-36.

Hanson G. N. (1980). Rare earth elements in petrogenetic studies of igneous systems. *Annual Review of Earth and Planetary Science* **8**, 371-406.

Hawkesworth C. J., Turner S., Peate D. W., McDermott F., and van Carlsten P. (1997). Elemental U and TH variations in island arc rocks: Implications for U-series isotopes. *Chemical Geology* **139**, 207-221.

Heiken G. and Wohletz K. (1985). Volcanic ash, pp. 246. University of California Press.

Heiken G. and Wohletz K. (1991). Fragmentation processes in explosive volcanic eruptions. In *Sedimentation in Volcanic Settings*, Vol. 45 (ed. R. V. Fischer and G. A. Smith), pp. 19-36. SEPM (Society for Sedimentary Geology), Special Publication.

Herguera J. C., Jansen E., and Berger W. H. (1992). Evidence for a bathyal front at 2000 m depth in the Glacial Pacific, based on a depth transact on Ontong Java Plateau. *Paleoceanography* **7**, 273-288.

Herzig P. M., Hannington M. D., Stoffers P., Arribas A., Becker K.-P., Binns R., Brown P., Gennerich H. H., Hartmann M., Heesemann B., Hefter J., Jonasson I., Kila R., Lange S., McInnes B. I. M., Meyers J., Percival J., Petersen S., Pichler P., Rosenberger A., Ruggieri G., Schott T., Schwarz U., Seifert H., Villinger H., and Winn K. (1994). Tectonics, petrology and hydrothermal processes in areas of alkaline island arc volcanoes in the

Southwest Pacific. In *Cruise Report SONNE-94*, pp. 273. Freiberg University of Mining and Technology.

Herzig P. M., Hannington M. D., Stoffers P., Becker K.-P., Drischel M., Franz L., Gemmell B., Höppner B., Horn C., Horz K., Franklin J., Jellineck T., Jonasson I., Kia P., Mühlhan N., Nickelsen S., Percival J., Perfit M., Petersen S., Schmidt M., Seifert T., Thiessen O., Türkay M., Tunnicliffe V., and Winn K. (1998). Volcanism, hydrothermal processes and biological communities at shallow submarine volcanoes of the New Ireland fore-arc (Papua New Guinea). In *Cruise Report SONNE-133*, pp. 146. Freiberg University of Mining and Technology.

Herzig P. M., Petersen S., and Hannington M. D. (1999). Epithermal-type gold mineralization at Conical Seamount: a shallow submarine volcano sou th of Lihir Island, Papua New Guinea. In *Mineral Deposits: Processes to Processing, Proceedings of the fifth biennial SGA meeting and the tenth Quadrennial IAGOD symposium London* (ed. C. J. Stanley), pp. 527-530.

Hofmann A. W. (1988). Chemical differentiation of the Earth: the relationship between mantle, continental crust, and oceanic crust. *Earth & Planetary Science Letters* **90**, 297-314.

Izett G. A. (1981). Volcanic ash beds: recorders of Upper Cenozoic silicic pyroclastic volcanism in the western United States. *Journal of Geophysical Research* **86**, 10200-10222.

Jenner G. A., Longerich H. P., Jackson S. E., and Fryer B. J. (1990). ICP-MS - A powerful tool for high-precision trace-element analysis in Earth sciences: Evidence from analysis of selected USGS reference samples. *Chemical Geology* **83**, 133-148.

Jochum K. P., Dingwell D. B., Rocholl A., Stoll B., and Hofmann A. W. (2000). The preparation and preliminary characterization of eight Geological MPI-DING Reference Glasses for in-situ microanalysis. *Geostandard Newsletter* **24**(1), 87-113.

Johnson R. W. (1979). Geotectonics and volcanism in Papua New Guinea: a review of the late Cenozoic. *BMR Journal of Australian Geology and Geophysics* **4**, 181-207.

Johnson R. W., Perft M. R., Chappell B. W., Jaques A. L., Shuster R. D., and Ridley W. I. (1988). Volcanism in the New Ireland basin and Manus Island region: Notes on the geochemistry and petrology of some dredged volcanic rocks from a rifted-arc region. *Geology and offshore resources of Pacific island area - New Irland and Manus region, Papua New Guinea*, 111-128.

Kearey P. and Vine F. J. (1990). Global Tectonics, pp. 302. Blackwell Science.

Kennedy A. K., Grove T. L., and Johnson R. W. (1990a). Experimental and major element constraints on the evolution of lavas from Lihir Island, Papua New Guinea. *Contribution of Mineralogy and Petrology* **104**, 722-734.

Kennedy A. K., Hart S. R., and Frey F. A. (1990b). Composition and isotopic constraints on the petrogenesis of alkaline arc lavas: Lihir, Papua New Guinea. *Journal of Geophysical Research* **95**(5), 6929-6942.

Kroenke L. W. (1972). Geology of the Ontong Java Plateau. *Rept. Hawaii Institute Geophys. HIG* **72**(5), 119.

Kroenke L. W. (1984). Cenozoic tectonic development of the SW Pacific. *United Nations Escap, Ccop/Sopac Technical Bulletin* **6**, 122.

Le Bas M. J., Le Maitre R. W., Streckeisen A., and Zanettin B. (1986). A chemical classification of volcanic rocks based on the total alkali-silica diagram. *Journal of Petrology* **27**, 745-750.

Licence P. S., Terril J. E., and Fergusson L. J. (1987). Epithermal gold mineralisation, Ambitle Island, Papua New Guinea. *In: Proceedings of the Pacific Rim Congress, The Australian Institute of Mining and Metallurgy, Melbourne.* **87**, 273-278.

Lin P. N., Stern R. J., and Bloomer S. H. (1989). Shoshonitic volcanism in the northern Mariana Arc: 2. Large ion lithophile and rare earth element abundances: Evidence for the source of incompatible element enrichments in intraoceanic arcs. *Journal of Geophysical Research* **94**, 4497-4514.

Lin P. N., Stern R. J., Morris J., and Bloomer S. H. (1990). Nd- and Sr-isotopic compositions of lavas from the northern Mariana and southern Volcano arcs: implications for the origin of island arc melts. *Contribution of Mineralogy and Petrology* **105**(381-392).

Marlow M. S., Exon N. F., and Dadisman S. V. (1991). Hydrocarbon potential and gold mineralisation in the New Ireland Basin, Papua new Guinea. In *Geology and Geophysics of continental margins*, Vol. 53, pp. 119-137. AAPG Memoir.

McCulloch M. T. and Gamble J. A. (1991). Geochemical and geodynamical constraints on subduction zone magmatism. *Earth Planetary Science Letters* **102**, 358-374.

McDermott F., Defant M. J., Hawkesworth C. J., and Maury R. C. (1993). Isotope and trace element evidence for three component mixing in the genesis of the North Luzon arc lavas (Philippines). *Contribution of Mineralogy and Petrology* **113**, 9-23.

McDonough W. F. and Sun S.-S. (1995). The composition of the Earth. *Chemical Geology* **120**, 223-252.

McInnes B. I. A. (1992). A glimpse of epithermal subduction zone processes from Simberi Island, Papua New Guinea. Ph. D. Thesis, University of Ottawa.

McInnes B. I. A. and Cameron E. M. (1994). Carbonated, alkaline hybridizing melts from a sub-arc environment: Mantle wedge samples from the Tabar-Lihir-Tanga-Feni arc, Papua New Guinea. *Earth & Planetary Science Letters* **122**, 125-141.

McInnes B. I. A., Gregoire M., Binns R. A., Herzig P. M., and Hannington M. D. (2001). Hydrous metasomatism of oceanic sub-arc mantle, Lihir, Papua New Guinea: petrology and geochemistry of fluid-metasomatised mantle wedge xenoliths. *Earth & Planetary Science Letters* **188**, 169-183.

Meen J. K. (1987). Formation of shoshonites from calcalkaline basalt magma: geochemical and experimental constraints from the type locality. *Contribution of Mineralogy and Petrology* **97**, 333-351.

Middelmost E. A. K. (1989). Iron oxidation ratios, norms and the classification of volcanic rocks. *Chemical Geololgy* **77**, 19-26.

Moberly R. j. (1972). Origin of lithosphere behind island arcs, with reference to the western Pacific. *Geological Society of America Memoirs* **132**, 25-32.

Morimoto N., Fabries J., Ferguson A. K., Ginzburg I. V., Ross M., Seifert F. A., Zussman J., Aoki K., and Gottardi G. (1988). Nomenclature of pyroxenes. *Mineralogy and Petrology* **39**, 55-76.

Müller D., Franz L., Herzig P. M., and Hunt S. (2001). Potassic igneous rocks from the vicinity of epithermal gold mineralization, Lihir Island, Papua New Guinea. *Lithos* **57**, 163-186.

Nadeau M.-J., Grootes P. M., Schleicher M., Hasselberg P., Rieck A., and Bitterling M. (1998). Sample throughput and data quality at the Leibniz-Labor AMS facility. *Radiocarbon* **40**(1), 239-245.

Pearce J. A. and Peate D. W. (1995). Tectonic implcations of the composition of volcanic arc magmas. *Annual Review of Earth and Planetary Science* **23**, 251-285.

Peate D. W. and Pearce J. A. (1998). Causes of spatial compositional variations in Mariana arc lavas: Trace element evidence. *The Island Arc* **7**, 479-495.

Rickwood P. C. (1989). Boundary lines within petrologic diagrams which use oxides of major and minor elements. *Lithos* **22**, 247-263.

Ringwood A. E. (1974). The petrological evolution of island arc systems. *Journal of the Geololgical Society of London* **130**, 183-204.

Rytuba J. J., McKee E. H., and Cox D. P. (1993). Geochronology and geochemistry of the Ladolam gold deposite, Lihir Island, and gold deposites and volcanoes of Tabar and Tatau, Papua Ne wGuinea. *U.S.G.S. Bulletin* **2039**, 119-126.

Schmidt M., Botz R., Winn K., Stoffers P., Thiessen O., and Herzig P. (in press.). Seeping hydrocarbons and related carbonate mineralisations in sediments south of Lihir Island (New Ireland fore arc basin, Papua New Guinea). *Chemical Geology*.

Schmincke H.-U. and Sumita M. (1998). Volcanic evolution of Gran Canaria reconstructed from apron sediments: Synthesis of VICAP Project Drilling. In *Proceedings of the Ocean Drilling Program, Scientific Results*, Vol. 157 (ed. P. P. E. Weaver, H.-U. Schmincke, J. V. Firth, and W. Duffield), pp. 443-469.

Silver E. A. and Reed D. L. (1988). Backthrusting in accretionary wedges. *Journal of Geophysical Research* **93**, 3116-3126.

Stewart W. D. and Sandy M. J. (1988). Geology of New Ireland and Djaul islands, northeastern Papua New Guinea. In *Geology and Off-shore Resources of Pacific Island Arcs - New Ireland and Manus region, Papua New Guinea.*, Vol. 9 (ed. M. S. Marlow, S. V. Dadisman, and N. F. Exon), pp. 13-30. Circum-Pacific Council for Energy and Mineral Resources, Earth and Science Series.

Stoffers P., Hartmann M., Schott T., and Winn K. (1994). Sedimentology. In *Tectonics, petrology and hydrothermal processes in areas of alkaline island arc volcanoes in the Southwest Pacific* (ed. P. Herzig, M. D. Hannington, and P. Stoffers), pp. 151-180. Cruise Report SONNE-94. Freiberg University of Mining and Technology.

Stolper E. and Newman S. (1994). The role of water in the petrogenesis of Mariana trough magmas. *Earth & Planetary Science Letters* **121**, 293-325.

Stracke A. and Hegener E. (1998). Rifting-related volcanism in an ocean post-collisional setting: the Tabar-Lihir-Tanga-Feni (TLTF) island chain, Papua New Guinea. *Lithos* **45**, 545-560.

Stuiver M., Reimer P. J., Bard E., Beck J. W., Burr G. S., Hughes K. A., Cromer B., McCormac B., van der Plicht J., and M. S. (1998). INTCAL 98 Radiocarbon age calibration, 24,000-0 cal. BP. *Radiocarbon* **40**(1041-1083).

Sun C.-H. and Stern R. J. (2001). Genesis of Mariana shoshonites: Contribution of the subduction component. *Jounal of Geophysical Research* **106**(1), 589-608.

Sun S.-s. and McDonough W. F. (1989). Chemical and isotopic systematics of oceanic basalts: implications for mantle composition and processes. In *Magmatism in the ocean basins*, Vol. 42 (ed. A. D. Saunders and M. J. Norry), pp. 313-345. Geological Society Special Publications.

Tatsumi Y. (1989). Migration of fluid phases and genesis of basalt magmas in subduction zones. *Journal of Geophysical Research* **94**, 4697-4707.

Taylor B. (1979). Bismarck Sea: Evolution of a back-arc basin. *Geology* **7**, 171-174.

Taylor R. N. and Nesbitt R. W. (1998). Isotopic characteristics of subduction fluids in an intra-oceanic setting, Izu-Bonin Arc, Japan. *Earth & Planetary Science Letters* **164**, 79-98.

Thorarinsson S. (1974). The terms tephra and tephrachronology. In *World bibliography and index of Quarternary tephrochronology* (ed. J. A. Westgate and C. M. Gold), pp. 1-528. Printing Services Dept., University of Alberta, Canada.

Tregoning P., Lambeck K., Stolz A., Morgan P., McClusky S. C., van der Beek P., McQueen H., Jackson R. J., Little R. P., Laing A., and Murphy B. (1998). Estimation of current plate motions in Papua New Guinea from Global Positioning System observations. *Geophysical Research* **103**(6), 12.181-12.203.

Wallace D. A., Johnson R. W., Chappel B. W., Arculus R. J., Perfit M. R., and Crick I. H. (1983). Cainozoic volcanism of the Tabar, Lihir, Tanga, and Feni islands, Papua New Guinea: Geology, whole-rock analyses, and rock-forming minerals. *BMR Report* **243**, 62.

Weissel J. K. (1981). Magnetic lineations in marginal basins of the western Pacific. *Philosophical Transactions of the Royal Society of London* **A300**, 217-442.

Winn K., Horz K., and Stoffers P. (1998). Sedimentology. In *Volcanism, hydrothermal processes and biological communities at shallow submarine volcanoes of the New Ireland fore-arc (Papua New Guinea)* (ed. P. Herzig,

M. D. Hannington, and P. Stoffers), pp. 83-101. Cruise Report SONNE-133. Freiberg University of Mining and Technology.

Winn K., Sarnthein M., and Erlenkeuser H. (1991). $\delta^{18}O$ stratigraphy and chronology of Kiel sediment cores from the East Atlantic. In *Berichte-Reports*, Vol. 45, pp. 99. Geologisch-Paläontologisches Institut.

Wood C. P., Nairn I. A., McKee C. O., and Talai B. (1995). Petrology of the Rabaul Caldera area, Papua New Guinea. *Journal of Volcanology and Geothermal Research* **69**, 285-302.

Woodhead J. D., Eggins S. M., and Johnson R. W. (1998). Magma genesis in the New Britain Island arc: Further insights into melting and mass transfer processes. *Journal of Petrology* **39**(9), 1641-1668.

Woodhead J. D. and Johnson R. W. (1993). Isotopic and trace-element profiles across the New Britain island arc, Papua New Guinea. *Contributions to Mineralogy and Petrollogy* **113**, 479-491.

9 APPENDICES

9.1 Core descriptions

Figure 23: Core 17674

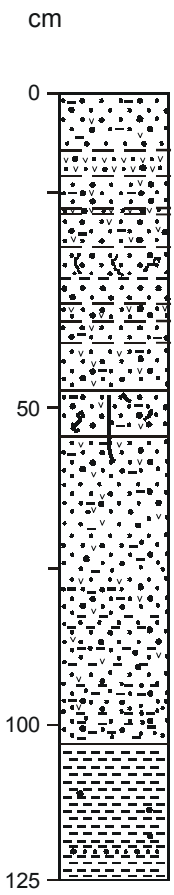

Color	Depth	Lithological description
10YR 7/4	0- 9 cm	Grayish orange, loosely consolidated, fine to medium grained foraminiferal sand speckled with larger forams, passing into dark yellowish brown foram sand as above, with darker hues from ash.
10YR 4/2	9- 13 cm	Grayish orange foram sand as above, compacter.
10YR 7/4	13- 18 cm	Dark yellowish brown foram sand with irregular dark stains, as above.
10YR 4/2	18- 19 cm	Grayish orange, compact, foram sand, speckled with larger forams, as above.
10YR 7/4	19- 24 cm	Foram sand as above, mottled, with open worm burrows.
10YR 7/2-4/2	24- 29 cm	Dark yellowish brown foraminiferal sand as above, coarser.
10YR 4/2	29- 33 cm	Sand as above, with irregular darker flecks from ash.
10YR 4/2	33- 35 cm	Grayish orange, compact, fine to medium grained foram sand, speckled.
10YR 7/4	35- 39 cm	Dark yellowish brown foram sand as above, with darker streaks (ash).
10YR 4/2	39- 47 cm	Grayish orange to pale yellowish brown foraminiferal sand as above,
10YR 7/4-6/2	47- 54 cm	Coarser with open worm tubes. Vertical burrow 48-65 cm.
10Y 4/2	54-101 cm	Lighter grayish olive, sandy foraminiferal ooze speckled with larger forams, brown mottled (bioturbation) 85-87 cm, from 87 cm to base more clayey layers.
10Y 4/2 to 5YR 4/1	101- 125 cm	Grayish orange to brownish gray plastic clays, without larger forams, foram sand at 111.8-112.2 cm with larger forms.

Legend for Cores 17674 - 17684

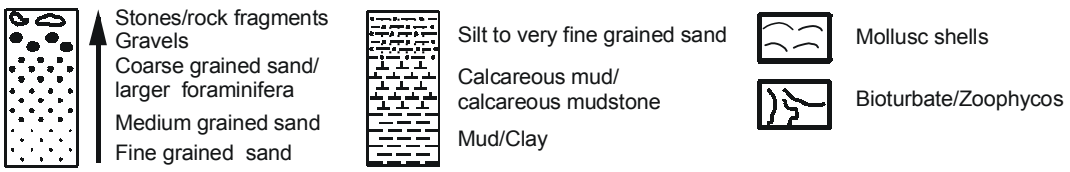

Figure 24: Core 17675

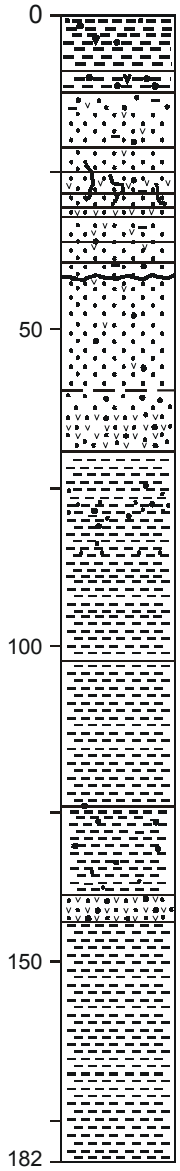

Colour	Depth	Lithological description
10YR 7/4	0-9 cm	Grayish orange, soft, poorly consolidated foraminiferal mud, passing into
10YR 7/4-6/2	9-12 cm	grayish orange to pale yellowish brown compact clays with brown streaks and layers, floating larger foraminifera.
10YR 7/4	12-18 cm	Grayish orange foram sand as above, compacter.
10YR 4/2	18-21 cm	Light brown sand, with black stains.
10YR 4/2	21-25 cm	Darker than above, occasional enrichment of forams in nests.
10YR 7/4-4/2	25-28 cm	Browner hues than above, coarser with larger forams, higher ash content.
10YR 4/2	28-30.5 cm	Dark grayish olive foram sand, with lighter streaks, bioturbated.
10YR 2/2	30.5-32 cm	Dusky yellowish brown foram and ash layer.
10YR 4/2	32-36 cm	Brown sand as above with black streaks and layers.
10YR 4/2	36-39 cm	Brown sand, mottled, with larger forams, as above.
10YR 5/4	39-42 cm	Darker brown foram sand, speckled with larger forams, irreg. low. boundary.
5Y 3/2-5/6	42-59 cm	Olive gray to light olive brown sand, darker and compacter esp. between 57-67 cm. Transitional boundary to
5Y 3/2	59-69 cm	olive gray volcanic sand, darker below 75 cm. Sharp boundary to
5Y 3/2	69-102 cm	olive gray clays, coarser at 84-90 cm, greenish layer at 92.5-93 cm.
5Y 3/2	102-125 cm	As above, lighter.
5Y 3/2	125-139 cm	Light olive gray clays with a few floating larger forams. Bioturbated, mottling >1cm diameter to 140 cm. Bioturbation not observed below 140 cm.
5Y 3/2	139-143 cm	Olive grey, fine to medium grained, volcanic sand.
5Y 3/2	143-182 cm	Dark olive gray clays with coarse grains below 162 cm, mottling frequent to 180 cm, less coarse particles to base.

Figure 25: Core 17676

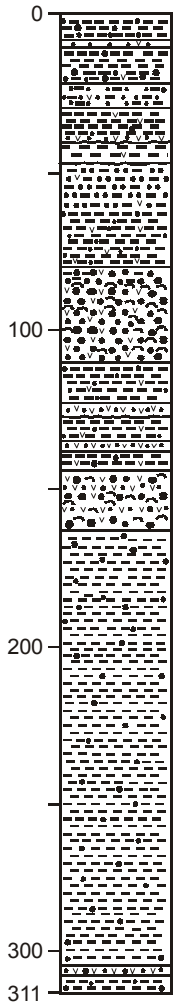

cm	Colour	Depth	Lithological description
	10YR 5/4	0-8 cm	Moderate yellowish brown, slightly sandy foraminiferal ooze.
	10YR 4/2	8-10 cm	Dark yellowish brown, fine grained, foram sand with dark stains.
	10YR 6/6-5/4	10-18 cm	Light yellowish brown to dark yellow clays with olive tint.
	10YR 4/2	18-21 cm	Clay as above, darker, speckled with larger forams.
	10YR 6/6	21-29 cm	Dark yellowish orange, fine grained, foram sand, with grayish olive green hue.
	5Y 5/2	29-40 cm	Light olive gray, silty clays with small pelecypod, coarser at 35.5-36.5 cm with more ash, forming irregular layer.
	5 Y 2/1-4/2	40-47 cm	Olive black to light olive gray, mottled clays, irregular lower boundary.
	5Y 4/2-5/6	47-80 cm	Olive gray to light olive brown volcanic sands with ash pockets at 64.5-65, 74-75, and 77.5-78.5 cm and irregular layers 4-5 mm in thickness. Darker and compacter between 62 and 72 cm.
	5Y 3/2		
	5Y 7/2 to 10Y 8/2	80-110 cm	Whitish gray to yellowish gray, medium to coarse grained volcanic and shell debris with two 1-2 cm olive gray, silty layers as above, near the top.
	5Y 4/4-5/2	110-123 cm	Light olive gray to moderate olive brown clays with greenish streaks and occassional larger forams.
	10YR 6/2	123-127 cm	Dark yellowish brown, very fine grained ash, with irregular lower boundary.
	5Y 3/2	127-135 cm	Olive gray clays, slightly silty, large greenish streaks at 131.7-132.1 cm.
	10YR 6/2	135-138 cm	Dark yellowish brown, very fine grained ash, as above.
	5Y 3/2	138-144 cm	Clay as above, with larger foraminifera.
	5Y 7/2 to 10Y 8/2	144-164 cm	Medium to coarse grained debris with dark yellowish brown, fine grained ash, coarser grained at 146-148 cm, large black grains at 156-156.5 cm.
	5Y 3/2	164-301 cm	Olive gray clays, monotonous, hard and compact with greenish streaks and thin dark brown layers, speckled. Dark brown streaks at 188-188.5 cm, 203.5-204 cm, 224,5 cm (1 mm), 244-246 cm, 267-268 cm. Two nests with material from 148-164 cm at 255.5 cm (6 mm Ø) and 281 cm (2 mm Ø).
	10YR 2/2	301-304 cm	Dusky yell. brown fine grained ash layer (core catcher).
	5Y 3/2	304-311 cm	Olive gray clays with larger forams.

Figure 26: Core 17677

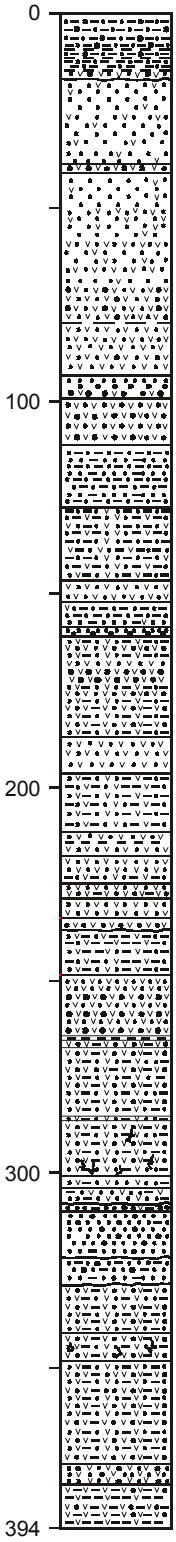

Colour	Depth	Lithological description
10YR 4/2-5/4	0-9 cm	Dark yell. brown, silty clay and very fine grained sand, speckled with forams.
+ 5YR 3/4	9-11 cm	Dark yellowish brown, fine sandy clay.
5Y 5/6	11-14 cm	Light olive brown silty clay, as above.
5Y 5/2	14-16 cm	Light olive gray, fine grained ash, speckled with larger forams. Irr. boundary to
10YR 5/4-4/2	16-38 cm	Moderate to dark yellowish brown, very fine grained to fine grained sand, bioturbated.
5Y 3/2	38-39 cm	Dark yellowish brown to olive gray, peppery fine to medium grained volc. ash.
10YR 5/4	39-70 cm	Dark yellowish brown, peppery fine grained sand with thin ash layers at 50.1 to 50.3 cm and 67 to 67.9 cm and at the base. Occasional brownish-black nests of volcanic ash
10YR 5/4	70-79 cm	Dark yellowish brown foraminifera sand as above, coarser.
10YR 5/4	79-92 cm	Moderate to dark yellowish brown, very fine grained, silty ash with thin fine to medium grained layers.
5Y 6/1-5/6	92-98 cm	Light olive gray to light olive brown turbidite, very coarse grained at base to fine grained at top, core recovery about 40% 92-96 cm.
N1+10YR 5/2	98-110 cm	Black, medium grained, volcanic ash, with coarse grained parts, bedded with moderate yellowish brown layers 98-105 cm, occassional white specks (forams).
5Y 5/6	110-127 cm	Light olive brown, fine silt, and very fine grained, clayey sand, with greenish streaks and floating larger forams 200-500 µm.
5Y 3/2	127-145 cm	Olive gray, fine grained clayey sand and ash, almost homogeneous without distinct layering, speckled with larger forams, especially near the base.
5Y 6/1-4/1	145-151 cm	Olive gray, fine grained clayey sand and ash, almost homogeneous with no distinct layering, speckled with larger forams, especially near the base.
5Y 4/1	151-157 cm	Olive gray, sandy clays, white speckled with forams, darker towards the base. Moderate dark gray (N5), fine grained, volcanic ash in pockets.
N5	157-159 cm	Dark gray, ash, graded, medium grained at base to very fine grained at top.
N5	159-186 cm	Medium gray, fine to medium grained ash with clayey component, speckled with forams. 5 mm thick alternations of fine & medium layers at 163-168 cm. Coarser at 168-171 cm, finer at 171-176 cm. Clay content higher at 176-186 cm
N1 to 5Y 2/1	186-195 cm	Black to olive black, fine grained ash. Two thin "pearly" layers of individual larger pl. & ben. foraminifera separated by 2 mm black ash at 190.1 & 190.3 cm.
5Y 3/2	195-210 cm	Olive gray, fine grained clayey sand and ash, almost homogenous, larger forams enriched in nests, and also floating in matrix, more clayey 204-207 cm.
N1	210-217 cm	Black, very fine grained to silty ash, with clayey intercalation 211-214 cm.
5Y 2/1	217-225 cm	Olive black, very fine grained ash, very fine silty with clayey nests 192-196 cm.
N2	225-228 cm	Grayish black ash, with fine to medium grained ash lenses, speckled with forams.
5Y 4/1	228-233 cm	Olive gray very fine grained ash, occassional large forams.
5GY 4/1	233-236 cm	Dark greenish grey fine to medium grained ash, salt und pepper texture.
N3	236-247 cm	Medium dark gray silty clay with ash streaks, some larger forams, and thin (1-2 mm) fine grained ash layers especially towards the base.
5YR 4/1 to 5Y 4/1	219-263 cm	Brownish to olive gray, medium grained to fine silty, graded ash. Upper 4 cm almost homogeneous, silty ash. 223-235 cm with at least 7 cycles, 1.5 cm thick.
N3	235-264 cm	Medium dark gray clay with ash streaks.
5Y 3/2	264-266 cm	Olive gray, medium to coarse grained ash, speckled with forams.
5GY 4/1	266-284 cm	Dark greenish gray, fine silty sand, speckled with forams, enriched in nests. Grayish bluish green (5BG 5/2) streaks and thin mm-thick layers.
5Y 2/1	284-285 cm	Olive black, very fine grained silty ash.
5GY 4/1	285-299 cm	Dark greenish gray, fine silty sand, speckled with forams, greenish streaks. More bioturbate in basal 2 cm with ash pockets
5Y 2/1	299-302 cm	Olive black, very fine grained silty ash, darker als above, fine grained ash pockets.
5Y 2/1 N1	302-306 cm	Olive black to black, very fine grained silty ash. Two graded layers each 2 cm thick. Darker at base.
5YR 2/1	306-308 cm	Brownish black, almost homogeneous, very fine silty ash.
5Y 4/1	308-321 cm	Olive gray, very fine grained sand with coarser parts and greenish streaks.
N3	321-328 cm	Dark gray clayey sand with coarser lenses > 1 cm, speckled with larger forams.
N3-N2	328-340 cm	Dark gray to grayish black, very fine silty ash with floating larger forams.
N4 5YR 5/1	340-347 cm	Moderate dark gray to brownish gray very fine silty ash with few floating larger forams, enrichment of foraminifera in nests.
5YR 4/1	347-374 cm	Brownish gray, fine silty ash rich clay. Speckled with larger forams, more frequent by 358-363 cm, frequent streaks and lenses below 363 cm.
N1	374-379 cm	Black, fine grained ash, with medium grained parts. Lighter layer in the middle.
5YR 4/1	379-394 cm	Dark brownish gray, ash rich clay, speckled with forams.

Figure 27: Core 17681

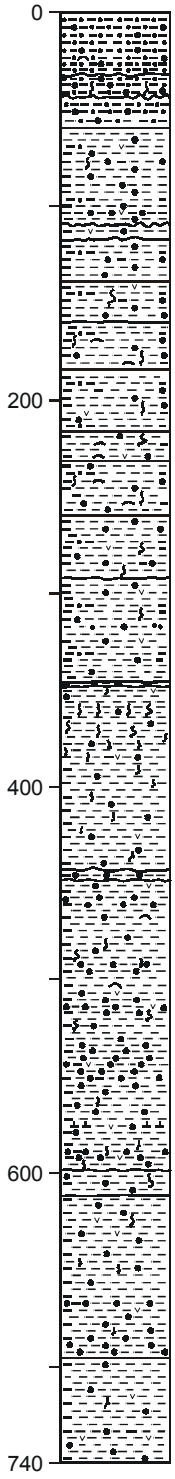

Color	Depth	Lithological description
10YR 8/4 -6/6	0-31 cm	Pale yell. brown to dark yell. orange, very fine silty mud, almost homogeneous, lightly speckled with floating foraminifera. Sporadic darker stains 14-20 cm, lighter from 20-25 cm, darker to 31 cm. Molluscan shell fragments bet. 18-30 cm.
10YR 6/2 -7/4	31- 42 cm	Pale yell. brown to grayish orange, silty foram sand, coarser downwards. Two thin mm-thick dark yell. orange sandy mud with larger forams and shell fragments.
10YR 6/6 -7/4	42- 57 cm	Dark yell. to grayish orange, silty clay with floating forams, compacter and coarser + frequent larger tests, and 1-2 mm dark yell. brown (10YR 4/2) layers below 50 cm.
5Y 5/2	57 - 107 cm	Light olive gray clay with floating coarser forams, blackish to greenish mottled 59-70 cm, bioturbate with disturbed layering, foram enrichment in nests. Basal 3 cm grayish olive clay with dark streaks and specks.
N7 to 5GY 6/1	107- 115 cm	Very light gray to greenish gray, soft clay with brown flecks and streaks (vol. ash?). Basal part almost homogeneous without distinct layering, speckled with larger forams.
5Y 5/2	115- 138 cm	Light olive gray clay, less compact, speckled with larger forams. Dark yell. green layers (5GY 5/2) up to 0.5 cm thick, frequent between 124-134 cm.
5Y 4/2	138-156 cm	Olive gray, compacter clay with larger forams, bioturbate, lightly mottled, vol. ash in darker nests (Ø 5 mm).
10Y 6/2 to 5GY 6/1	156-182 cm	Pale olive to lighter greenish gray, mod. hard, clay with floating larger forams, also enriched in nests (incl. ash?). Bioturbated, mottled, more heavily towards the base. Isolated molluscan fragments.
5GY 6/1	182-215 cm	Clay as above, darker, with olive gray streaks and flecks (5Y 4/1).
N 5-6	215-232 cm	Med. light gray to med. gray clay with pale yell. brown tinted lenses 1 cm thick. Molluscan fragments and forams as above. Darker stained layer at 228-229 cm.
N 6 to 10YR 6/2	232-257 cm	Med. dark gray clay with pale yell. brown streaks and lenses. Frequent foram nests, molluscan fragments and dark streaks (Corg?).
N 4 to 5Y 6/4	257-289 cm	Med. dark gray clay with dusky yell. streaks and lenses, basal part darker. Bioturbate, abundant larger forams, and dark streaks and stains.
5Y 5/2 to 5Y 4/4	289-344 cm	Light olive gray clay with darker mod. olive brown layers (1-3 mm) and streaks with foram and ash enrichment. 1x1,5 cm wood at 292-293 cm. Irregular basal boundary.
5Y 3/2	344-346 cm	Olive gray, very hard compact clay, with larger forams. Corg (?) rich.
5Y 7/2 to10Y 6/2	346-440 cm	Yell. gray to pale olive, hard clay, with larger forams, molluscan fragments. Lightly mottled, bioturbate. Darker streaks due Corg/wood throughout. Darker intercalations between 357-365 cm, and 372-390 cm, strongly bioturbate.
5Y 5/2 to 5Y 5/6	440-446 cm	Light olive gray to light olive brown, very hard, compact, clay, coarser through abundant larger forams. Upper 3 cm lighter with strongly irregular intrastratal and lower boundaries.
5Y 5/2, 5/6 to 10YR 6/2	446-595 cm	Light olive brown/gray to pale yell. brown, compact clay. 5 broad units at 448-462 cm, 462- 494 cm, 494-517 cm, 517-560 cm and 560-596 cm. Lighter hues with fewer forams in the upper segment, darker and speckled with frequent forams below. Bioturbate and lightly mottled. Nests enriched with forams and volcanic ash. Sporadic organic material (terrestrial?) and isolated small molluscan fragments, and hard calcareous concretions at 574-576 cm. Basal boundary very irregular, erosive.
10Y 6/2	595-609 cm	Pale olive, compact clay with coarser lenses > 1 cm, speckled with larger forams. Enrichment of org. matter at irregular basal boundary.
5Y 7/2 to 5Y 5/2	609-693 cm	Yell. gray to light olive gray, very fine, compact clay with dark streaks/flecks, and single floating larger forams, numerous towards the base. Darker bet. 652-673 cm with frequent streaks, and more organic matter. Sediment bioturbate, mottled. Ash enrichment in pockets.
5Y 5/2	693-740 cm	Clay, as above, silty, salt and pepper texture through floating larger forams and ash? particles.

Figure 28: Core 17682

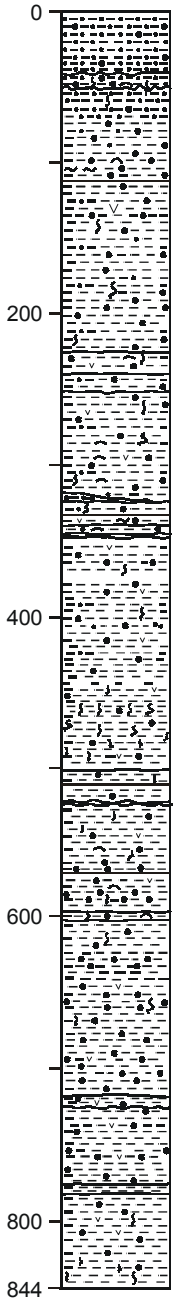

Colour	Depth	Lithological description
10YR 7/6 10YR 3/4, N 8	0- 41.5 cm	Yellow, very silty mud, soft, speckled white with abundant larger forams near , surface and around 38cm, also enriched in lenses and pockets. Dark brown irregular and banded stains at 15-19 cm and 32-41 cm. Bioturbate, mottled, vertical burrows. Color change to -
5Y 5/2	41.5- 112 cm	olive gray, soft clay with floating coarser forams, frequent bet. 72-97 cm. Scattered mollusc fragments, enriched at irregular layer bet. 50-51 cm, ubiquitous black streaks (wavilly), flecks and stains esp. bet. 45-50 cm and 105-107 cm. Bioturbate, mottled, vertical stains. Lighter hues (5Y6/3) bet. 64 cm (gradational) to 97 cm (sharp change).
5Y 5/2	112- 227 cm	Clay as above, with brown streaks, compacter downwards. Darker and lighter layering to 1 cm thickness. Speckled with larger forams and volcanic ash enriched in pockets. Sporadic molluscan fragments, lightly bioturbate. Dark gray (N2) medium to coarse grained sandstone block (vol. bomb?) at 129-134 cm (5 cm Ø).
5Y 3/2 to 5/2	227-239 cm	Dark olive gray, rel. soft clay as above with floating larger forams, also locally enriched. Bioturbated, mottled. Darker irregular layering towards the base.
5Y 6/1 5YR 6/1	239-252 cm	Clay as above, lighter, with brownish layers/streaks and brown mottling/tints. Scoured lower boundary.
5Y 5/2	252-323 cm	Light olive gray clay, with organic streaks as above, speckled with larger forams enriched in pockets (vol. ash?) and some nannofossils. Bioturbate, with light and dark mottling. Basal sandy lense at 318-323 cm, irregular boundaries.
5Y 5/2	323-333 cm	Light olive gray clay with streaks as above, some bioturbation.
5Y 4/1	333-340 cm	Brownish gray, hard compact, sandy clay with higher organic/volcanic ash content (check). Upper 2 cm with dark organic (??) strings. Irregular basal boundary.
10Y6/2 to N5	340-345 cm	Pale olive to medium gray, compact sandy clay, with frequent forams and a few molluscan fragments.
10Y6/2 to10Y 4/1	345-347 cm	Pale olive to dark greenish gray, sandy clay, speckled with forams and mottled with sporadic brown-black ash pockets. Irregular boundaries.
5Y 5/2 to 5Y 7/2	347-502 cm	Light olive gray to yell. gray, silty clay, banded (2-3 cm) bet. 427-453 cm with greenish layers. Forams, organic matter and ash enriched in lenses, layers, nests and pockets. Sandy foram enrichment bet. 417-445 cm, foram layers bet. 481-492 cm, wood (1-2 cm) bet. 461-472 cm. Mottled, bioturbate throughout.
5Y 5/2	502-512 cm	Light olive gray, silty, compact clay with yell. brown (5Y 8/1) intense mottling, bioturbate.
5Y 4/1	512-569 cm	Olive gray compact clay with darker greenish (5G 3/1) streaks, foram pockets/layers, esp. bet. 522-524 cm and 541-542 cm, giving impression of irregular boundaries. Light color banding. Scattered molluscan fragments and organic matter, bioturbate.
5Y 5/2	569-595 cm	Light olive gray, silty, compact clay with greenish streaks, more forams in pockets. Vertical yell. (5Y 7/6) taint 2.5 cm broad tapering to bottom at 571-593 cm. Some molluscan fragments
5Y 4/4 to 5Y 5/2	595-601 cm	Moderate olive brown, silty, compact clay and ash with light and dark brown flecks (1-2 cm). Some larger floating forams and molluscan fragments, bioturbate.
5Y 5/2 to10Y 4/2	601-717 cm	Light olive gray to grayish olive, silty, medium to hard clay with floating forams throughout, enriched in olive brown pockets to 626 cm. Greenish streaks/mm layers, esp. bet. 607-621 cm and 690-710 cm. Vertical yell. taint as above bet. 672-682 cm. Lightly bioturbate. Some organic matter. Lightly irregular lower boundary.
5YR 4/2	717-725 cm	Brownish gray,silty to fine grained (vol.?) sand, coarser to base, enriched in forams. Very dark gray (N3), fine to medium grained sand. Irregular lower boundary.
5Y 5/2	725-776 cm	Light olive gray, compact clay, speckled with larger forams. Greenish streaks at 4-6 cm intervals, frequent (1-2 cm) spacing bet. 738-745 cm. Brownish carbon. streaks.
5Y 5/3	776-782 cm	Clay, as above, darker, with almost vertical yell. tint. 4-5mm lighter bands (5Y 6/3).
5Y 5/2 to 5Y 4/1	782-844 cm	Light olive gray to olive gray, fine silty, compact clay with darker streaks, stains and layers (mm-cm). Organic/volcanic? material in small mm-lenses. Bioturbate, mottled. Irregular contacts with coarser grains (2-3 mm layers) at 787 cm, 797 cm, 807 cm, and at 828-829 cm.

Figure 29: Core 17684

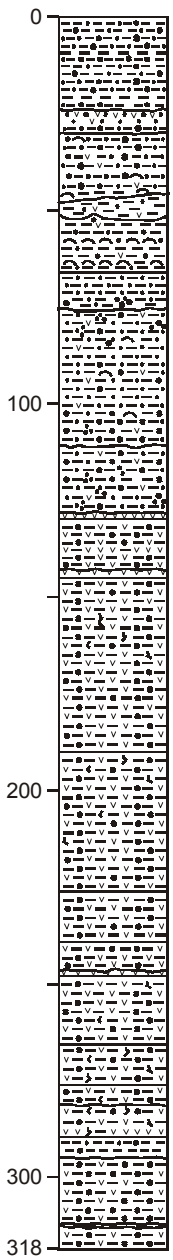

Colour	Depth	Lithological description
10YR 5/4	0- 24 cm	Mod. yell. brown, silty sand, clayey at top, speckled with black grains. Foram enrichment in nests and at irregular base.
N1 - N2	24- 30 cm	Black to grayish-black, fine grained ash, lighter 5 mm layers bet. 27 and 29 cm . Lower boundary lightly irregular.
10YR 7/4	30- 48 cm	Grayish orange, foram sand speckled with black ash grains. Molluscan fragm.
10YR 5/6	48- 51 cm	Yell. brown, silty clay, ash stains.
10YR 5/4 -6/2	51- 66 cm	Pale to yell. brown clay as above, coarser at foram layers, mollusc shell fragments, dispersed and in layers (<2 mm at 58 cm and 63 cm).
5Y 5/2	66- 76 cm	Olive gray, fine silty clay with larger forams, speckled and in pockets.
10YR 4/2 -6/2	76-111 cm	Dark grayish brown to light brownish gray, clay, streaky-rough with larger forams and ash, concretions to 3 mm ø, mollusc fragments. Compacter towards the base. Irregular upper and lower boundaries.
5Y 3/2	111-128 cm	Dark olive gray, compact sandy clays with abundant floating forams, especially towards the base.
N1	128-129.5 cm	Black, fine to medium grained volcanic ash, erosional upper boundary.
N2 - N1	129.5-145 cm	Dark gray to black, fine grained volcanic ash rich clay with floating forams. Black ash layers at 137 cm (5 mm) and 144-145 cm (erosional upper surface).
N2	145-190 cm	Dark grayish black, fine grained, compact volcanic ash rich clay, streaky with floating forams as above, with lighter and darker flecks through bioturbation.
N2	190-226 cm	Darker grayish black, fine grained, compact volcanic ash rich clay, rougher and streaky with floating forams, also in nest. Lightly bioturbate. Lower boundary transitional to
N1	226-239 cm	black, fine grained, compact volcanic ash rich clay as above. Transitional colour change to
5Y 8/1-N2	239-246 cm	Light greenish gray clay with black, fine grained, volcanic ash, as above.
N1	246-248 cm	Black, medium grained, volcanic ash, finely layered (1-2 mm).
N2	248-266 cm	Dark grayish black, volcanic ash rich clay as above. Lightly bioturbate. Transitional colour change to
N2	266-276 cm	darker grayish black, volcanic ash rich clay as above. Bioturbate.
N2	276-281 cm	Dark grayish black, lighter coloured, volcanic ash rich clay as above.
N2	281-291 cm	Darker grayish black, volcanic ash rich clay with a 5 mm ash layer at base. Strongly bioturbate. 1-2 mm layers at 285 cm and 288 cm.
5Y 8/0-8/1	291-295 cm	White to light greenish gray , compact clay. Irregular lower boundary.
N2- 5Y 3/2	295-311 cm	Dark olive gray to black, volcanic ash rich, compact clay with larger forams.
5Y 8/0-8/1	311-312 cm	White to light greenish gray , compact clay as above. Irregular boundaries.
N2- 5Y 3/2	312-318 cm	Dark olive gray to black, volcanic ash rich, compact clay, enriched with larger forams.

9.2 Parasound profiles

Figure 30: Core 17674

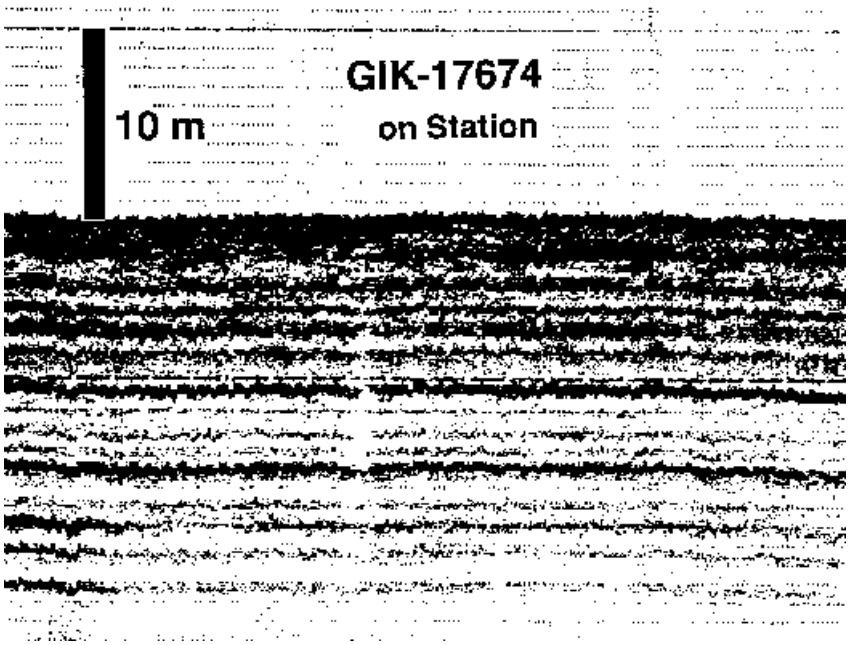

Figure 31: Core 17675

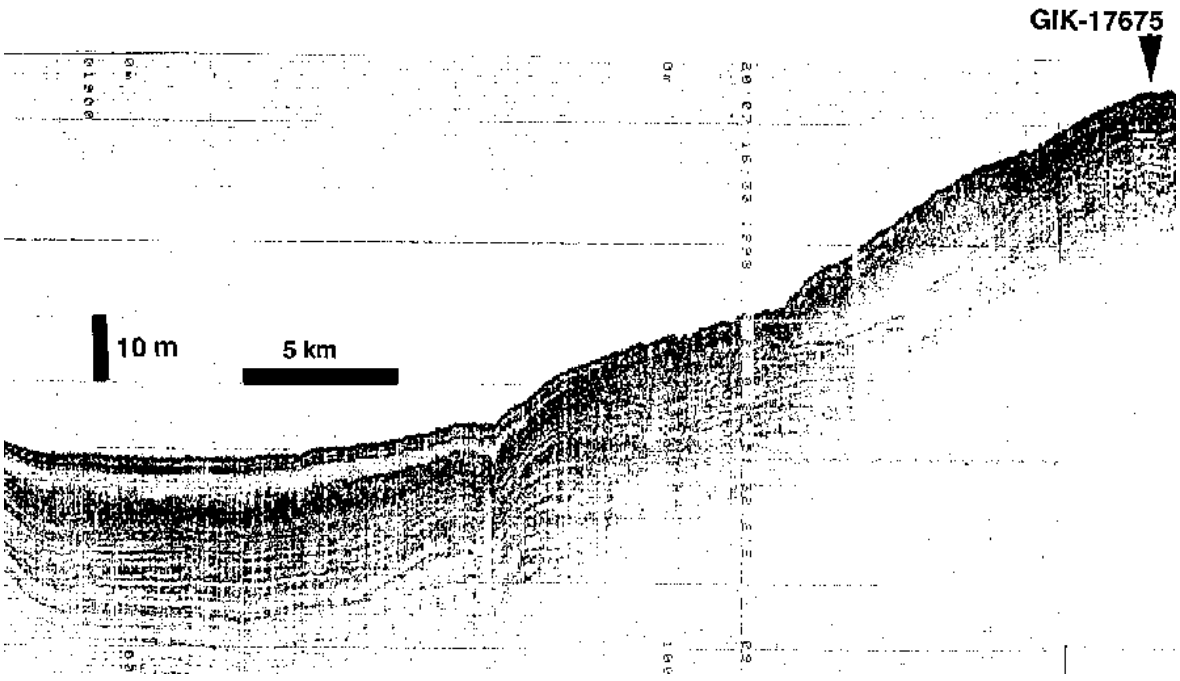

Figure 32: Core 17676

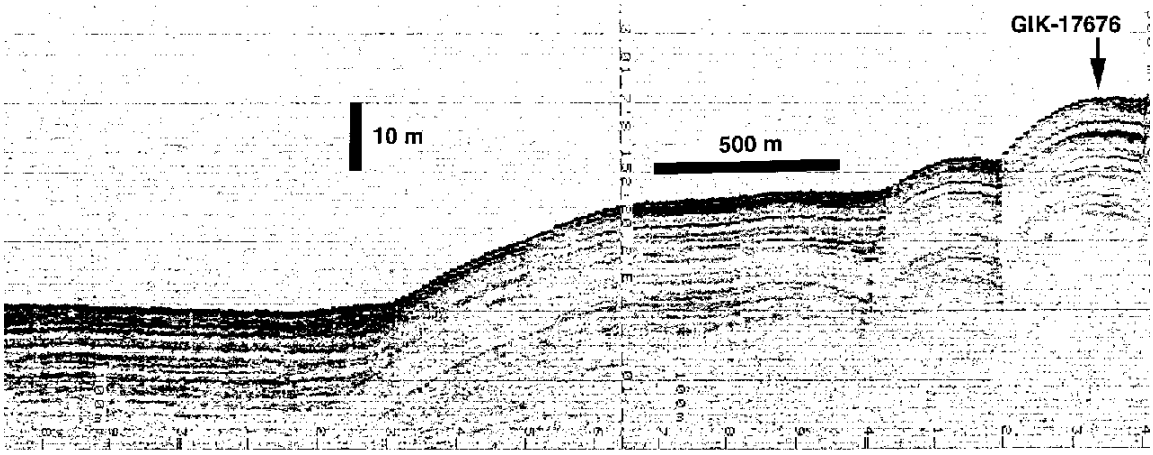

Figure 33: Core 17677

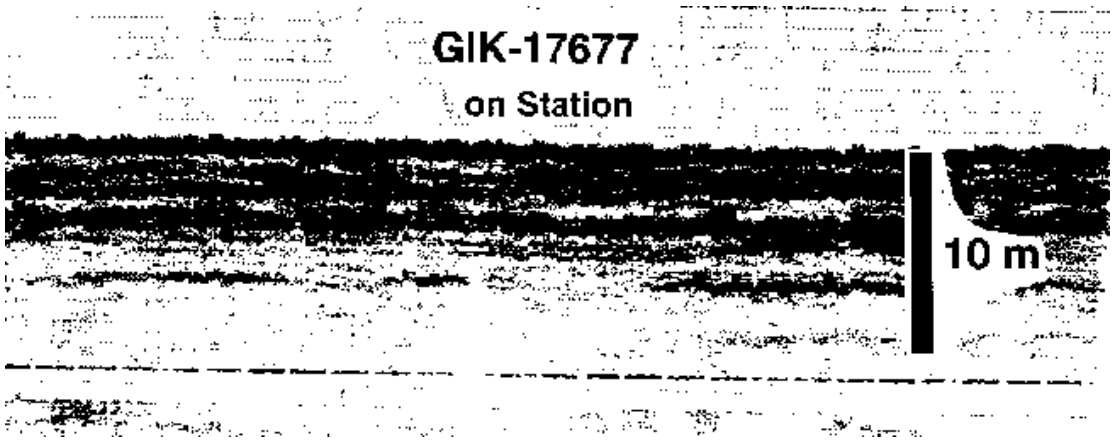

Figure 34: Core 17681

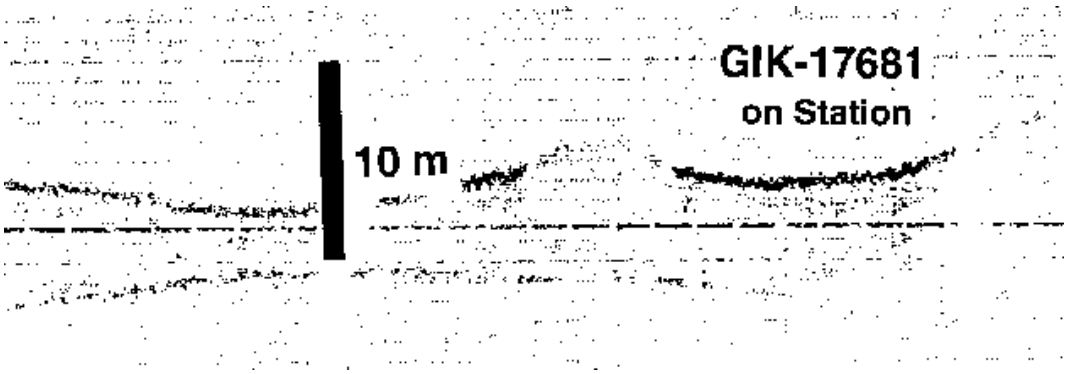

Figure 35: Core 17682

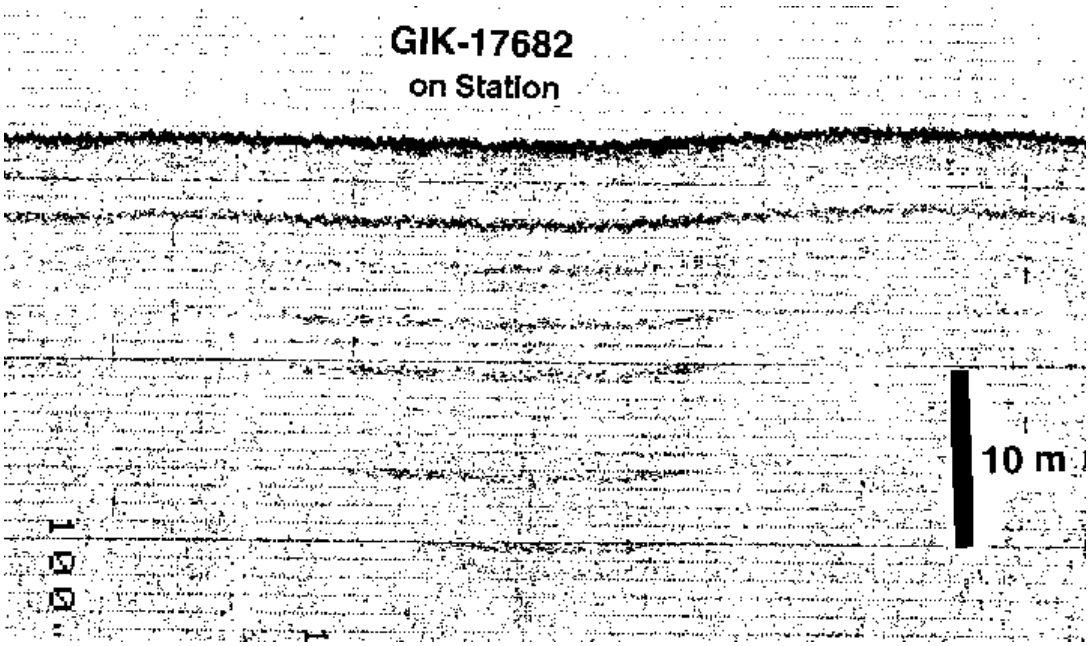

Figure 36: Core 17684

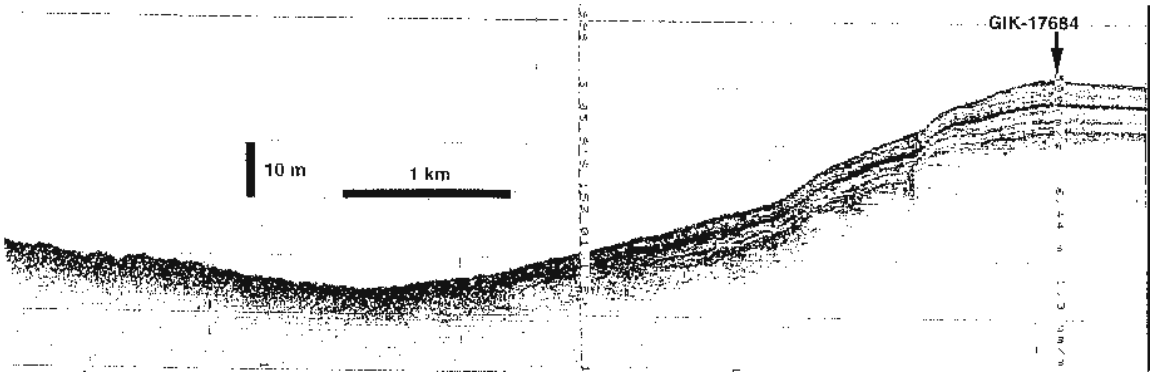

9.3 Magnetic susceptibility measurements

Magnetic susceptibility is used as a tool for the identification of volcanic ash layers and in core to core correlation. It has no dimension and reflects the amount of magnetic minerals in the sediment. For uniformity, measurements were made at 1 cm intervals and report in cgs units, with the zero value equal to the measurement in the air. The magnetic susceptibility was measured on the whole core on all gravity cores. In the case of the big box cores, the measurements were made on the 12 cm core liners pushed through the sediment layers. Correlation with the gravity core from the same station then showed the amount of surface sediment missing in the gravity core.

9.3.1 Magnetic susceptibility profiles

Figure 37: Core 17674

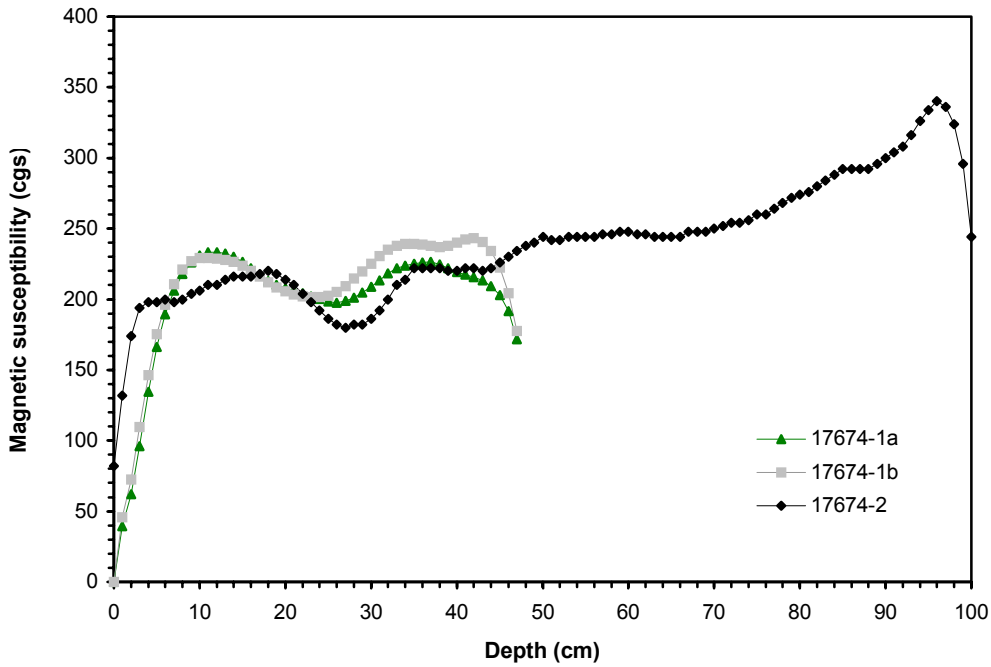

Figure 38: Core 17675

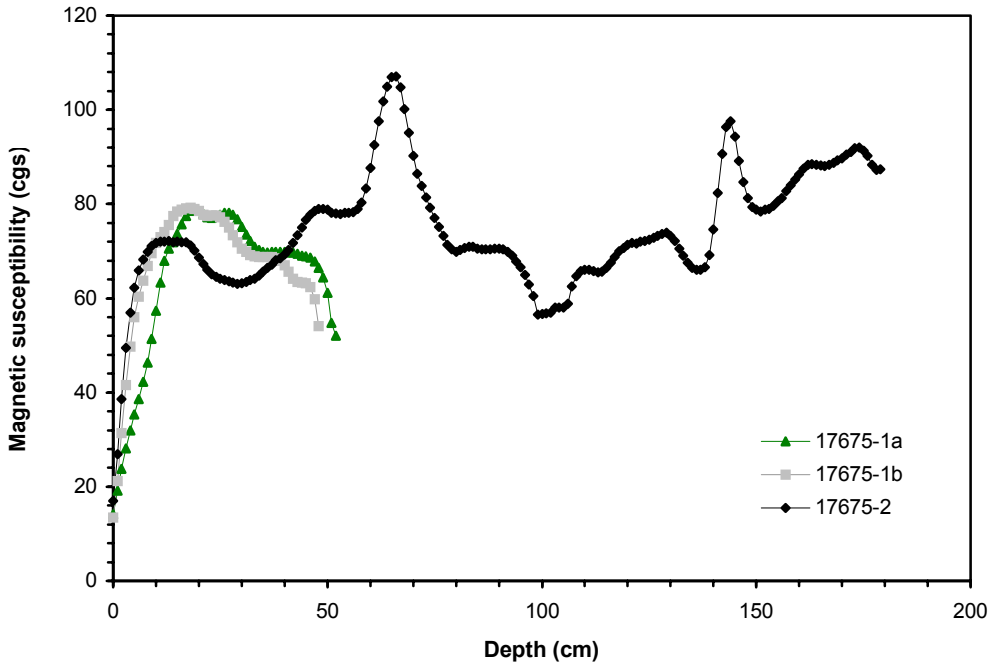

Figure 39: Core 17676

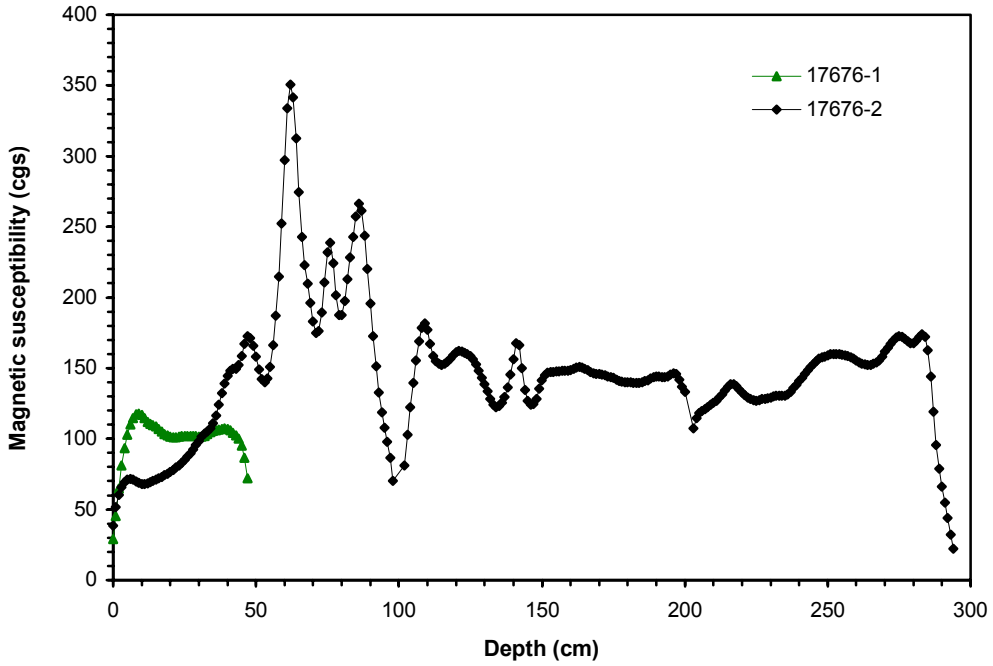

Figure 40: Core 17677

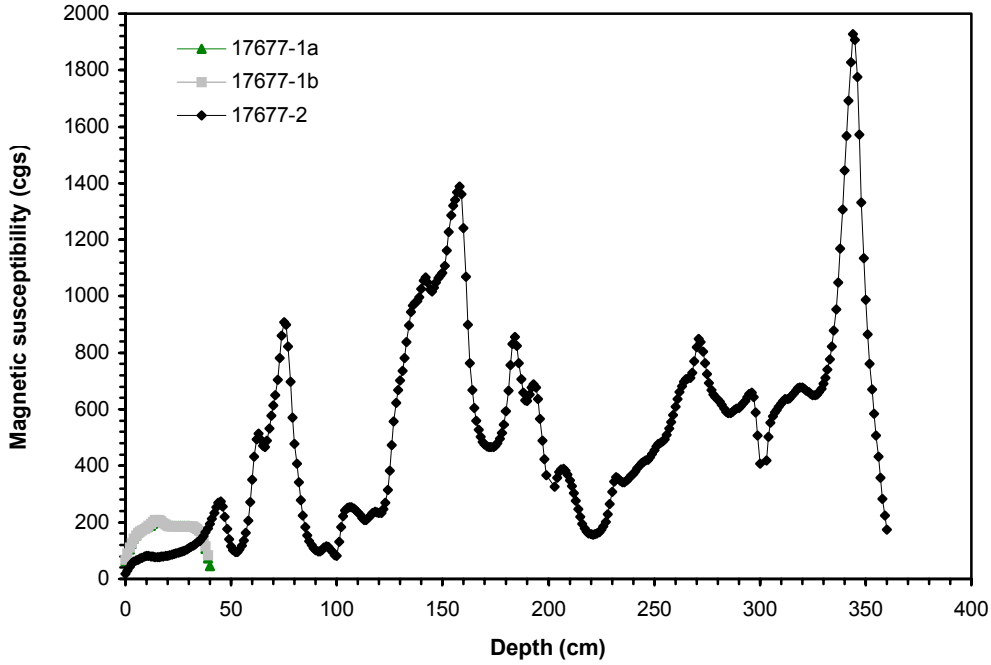

Figure 41: Core 17681

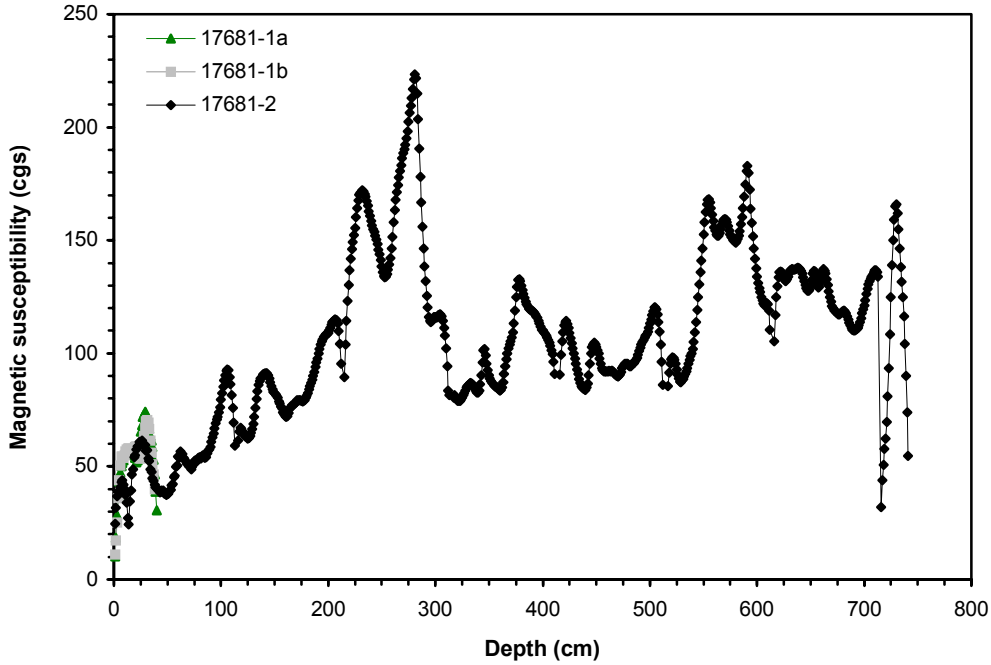

Figure 42: Core 17682

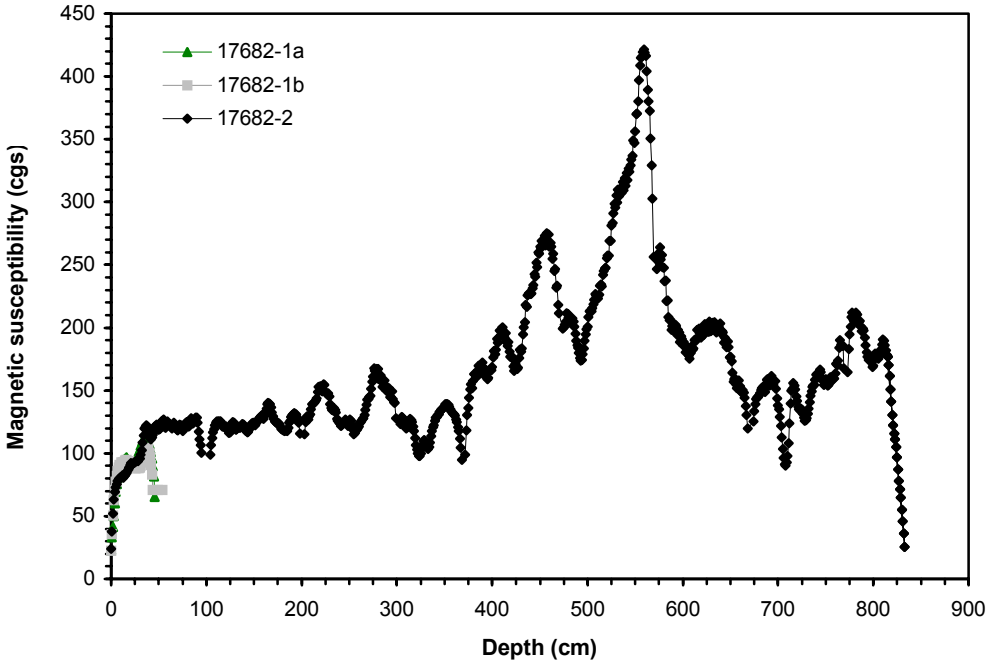

Figure 43: Core 17684

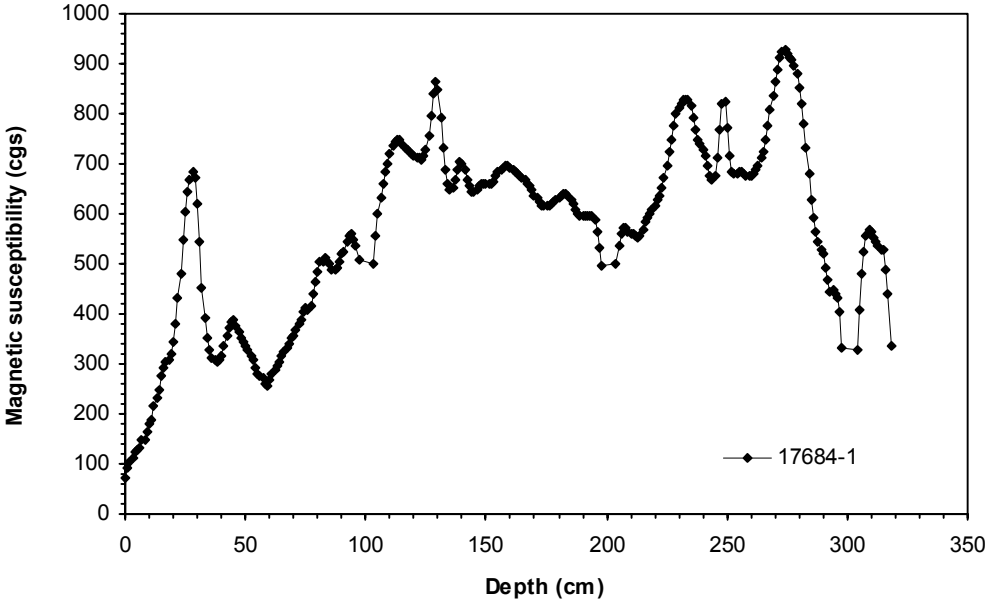

9.4 $\delta^{18}O$-isotope analysis of *Globigerinoides ruber* (white)

Table 6: Core 17675

Core 17675-1

Depth (cm)	Composite depth (cm)	$\delta^{13}C$	2σ	$\delta^{18}O$	2σ	Calibrated age BP (ka)	Remarks
0		1.43	0.01	-2.79	0.02	0.00	undisturbed surface
1		1.31	0.02	-2.94	0.02	0.16	
4		1.05	0.02	-2.80	0.03	0.48	
7		1.33	0.02	-2.85	0.03	0.64	
10		1.47	0.01	-2.64	0.02	1.12	
14		1.62	0.01	-2.63	0.02	1.12	
17		1.50	0.02	-2.54	0.03	1.60	
20		1.68	0.02	-2.72	0.01	1.93	
25		1.54	0.01	-2.72	0.03	2.25	
30		1.49	0.02	-2.62	0.03	2.73	
35		1.25	0.01	-0.99	0.03	2.73	
40		1.26	0.01	-2.43	0.04	3.21	
45		1.44	0.01	-2.56	0.03	3.53	
49		1.53	0.01	-2.36	0.04	4.01	AMS ^{14}C-dating

Core 17675-2

Depth (cm)	Composite depth (cm)	$\delta^{13}C$	2σ	$\delta^{18}O$	2σ	Calibrated age BP (ka)	Remarks
1	3	1.45	0.01	-2.75	0.04	0.48	Core fit: 3 cm in the box core (-1)
5	7	1.36	0.02	-2.82	0.03	1.12	= 1 cm in the gravity core (-2)
10	12	1.54	0.02	-2.62	0.03	1.92	
15	17	1.57	0.01	-2.58	0.02	2.73	
20	22	1.37	0.01	-2.73	0.04	3.53	
25	27	1.44	0.02	-2.58	0.02	4.33	
30	32	1.29	0.02	-2.52	0.03	5.13	
35	37	1.54	0.02	-2.45	0.03	5.94	
40	42	1.27	0.02	-2.34	0.02	6.74	
45	47	1.27	0.02	-2.23	0.02	7.54	
50	52	1.05	0.01	-2.20	0.03	8.38	
55	57	1.32	0.02	-2.20	0.02	9.24	after $\delta^{18}O$ stack of Bassinot et al. (1994)
60	62	0.95	0.02	-1.97	0.03	10.10	
65	67	1.19	0.02	-2.10	0.03	10.97	
70	72	0.92	0.02	-1.72	0.04	12.08	
80	82	1.08	0.07	-1.75	0.10	14.30	
90	92	0.74	0.01	-1.53	0.03	16.52	
98	100	1.06	0.03	-1.05	0.04	18.30	after $\delta^{18}O$ stack of Winn et al. (1991)
110	112	1.17	0.01	-1.06	0.03	19.28	
120	122	1.17	0.02	-1.02	0.01	20.10	
130	132	1.09	0.02	-1.18	0.01	20.91	
140	142	1.18	0.01	-1.13	0.02	21.73	
150	152	1.16	0.02	-1.19	0.05	22.55	
160	162	1.32	0.01	-1.18	0.03	23.37	
170	172	1.00	0.01	-1.17	0.03	24.18	
180	182	1.22	0.01	-1.23	0.02	25.00	

Table 7: Core 17676

Core 17676-1

Depth (cm)	Composite depth (cm)	$\delta^{13}C$	2σ	$\delta^{18}O$	2σ	Calibrated age BP (ka)	Remarks
0		1.33	0.02	-2.87	0.03	0.00	undisturbed surface
1		1.29	0.01	-2.86	0.03	0.18	
4		1.71	0.01	-2.68	0.01	0.73	
5		1.64	0.02	-2.65	0.03	0.92	
7		1.65	0.02	-2.65	0.02	1.28	
10		1.58	0.02	-2.70	0.02	1.83	
14		1.63	0.01	-2.63	0.03	2.57	
15		1.55	0.02	-2.61	0.01	2.75	
17		1.33	0.01	-2.56	0.02	3.12	
20		1.56	0.02	-2.49	0.02	3.67	
23		1.53	0.02	-1.02	0.03	4.22	
25		1.77	0.03	-2.39	0.01	4.59	
28		1.35	0.02	-2.43	0.02	5.04	
30		1.27	0.01	-2.43	0.04	5.50	
35		1.29	0.01	-2.30	0.03	6.42	
40		1.54	0.01	-2.23	0.02	7.34	
43		1.13	0.02	-2.25	0.03	7.89	
45		1.01	0.02	-2.19	0.04	8.25	

Core 17676-2

Depth (cm)	Composite depth (cm)	$\delta^{13}C$	2σ	$\delta^{18}O$	2σ	Calibrated age BP (ka)	Remarks
1	19	1.49	0.01	-2.51	0.03	3.49	Core fit: 19 cm in the box core (-1)
4	22	1.54	0.04	-2.69	0.03	4.04	= 1 cm in the gravity core (-2)
7	25	1.74	0.01	-2.58	0.02	4.59	
10	28	1.56	0.02	-2.63	0.02	5.14	
15	33	1.44	0.02	-2.47	0.03	6.05	
20	38	1.31	0.01	-2.35	0.02	6.97	
25	43	1.07	0.02	-2.37	0.03	7.89	
30	48	1.49	0.02	-2.31	0.02	8.81	
37	53	1.28	0.01	-1.92	0.03	10.44	after $\delta^{18}O$ stack of Bassinot et al. (1994)
41	59	1.02	0.01	-1.87	0.02	12.41	
44	62	1.25	0.02	-1.74	0.01	13.39	
50	68	0.84	0.01	-1.61	0.02	15.36	
55	73	0.75	0.02	-1.32	0.03	17.00	
60	78	0.97	0.02	-1.47	0.04	17.00	
61	79	1.46	0.02	-1.28	0.01	17.00	
93	111	0.94	0.02	-1.19	0.02	18.30	after $\delta^{18}O$ stack of Winn et al. (1991)
98	116	1.09	0.01	-1.16	0.02	18.63	
155	165	1.27	0.02	-1.35	0.02	21.05	
170	188	1.29	0.02	-1.27	0.02	22.56	
180	198	1.60	0.01	-1.40	0.02	23.21	
190	208	1.50	0.02	-1.54	0.03	23.87	
199	217	1.57	0.01	-1.53	0.02	24.46	
207	225	1.41	0.04	-1.46	0.07	24.98	
215	233	1.22	0.02	-1.19	0.03	25.50	
222	240	1.43	0.02	-1.42	0.03	25.96	
230	248	1.60	0.02	-1.35	0.02	26.49	
240	258	1.45	0.01	-1.62	0.03	27.14	
250	268	1.35	0.02	-1.34	0.02	27.80	
260	278	1.49	0.02	-1.47	0.03	28.45	
270	288	1.47	0.01	-1.46	0.03	29.11	
276	294	1.11	0.02	-1.70	0.03	29.50	
287	305	1.26	0.01	-1.50	0.03	30.02	
293	311	1.38	0.02	-1.50	0.03	30.42	

Table 8: Core 17677

Core 17677-1

Depth (cm)	Composite depth (cm)	$\delta^{13}C$	2σ	$\delta^{18}O$	2σ	Calibrated age BP (ka)	Remarks
1		1.54	0.02	-2.83	0.02	0.16	undisturbed surface
4						0.63	
7		1.75	0.01	-2.63	0.03	1.09	
10		1.79	0.02	-2.81	0.03	1.56	
13		1.38	0.02	-2.51	0.02	2.03	
17		1.65	0.02	-2.54	0.02	2.66	
20		1.51	0.02	-2.51	0.02	3.13	
25		1.50	0.02	-2.47	0.02	3.91	
30		1.87	0.02	-2.49	0.02	4.69	
35		1.67	0.01	-2.49	0.02	5.47	
39		1.54	0.02	-2.49	0.02	6.02	

Core 17677-2

Depth (cm)	Composite depth (cm)	$\delta^{13}C$	2σ	$\delta^{18}O$	2σ	Calibrated age BP (ka)	Remarks
1	35	1.62	0.02	-2.64	0.03	5.47	Core fit: 35 cm in the box core (-1)
4	38	1.53	0.02	-2.62	0.02	5.94	= 1 cm in the gravity core (-2)
7	41	1.35	0.01	-2.72	0.03	6.41	
10	44	1.27	0.02	-2.56	0.03	6.88	
15	49	1.21	0.02	-2.59	0.03	7.66	
20	54	1.59	0.02	-2.66	0.03	8.44	
25	59	1.69	0.02	-2.51	0.02	9.22	
30	64	1.27	0.02	-2.35	0.03	10.00	
35	69	0.60	0.01	-2.13	0.03	12.23	
40	74	0.80	0.01	-1.59	0.02	15.26	
45	79	1.13	0.02	-1.43	0.03	18.00	
51	85	1.24	0.02	-1.10	0.02	18.00	The δ^{18} O level for the interglacial
56	90	1.10	0.02	-1.17	0.02	18.00	is around -2.6 per mill and the
65	99	1.33	0.02	-1.91	0.02	18.00	glacial level is at about -1.1 per mill.
77	111	1.40	0.01	-1.84	0.03	18.00	
80	114	0.70	0.01	-1.82	0.02	18.00	The δ^{18}O values below 45 cm show that
87	121	1.27	0.01	-1.94	0.02	18.00	the older and younger foraminifera are
91	125	0.70	0.02	-1.87	0.03	18.00	mixed.
95	129	0.93	0.02	-1.82	0.06	18.00	
104	138	1.24	0.02	-1.91	0.02	18.00	Therefore, the δ^{18}O stratigraphy
109	143	1.70	0.03	-1.87	0.03	18.00	could not be applied to this
118	152	1.76	0.02	-2.02	0.01	18.00	sediment section.
126	160	1.50	0.02	-1.93	0.04	18.00	
133	167	1.55	0.01	-1.95	0.02	18.00	
138	172	1.57	0.01	-2.10	0.02	18.00	
139	173	1.26	0.01	-2.01	0.03	18.00	
145	179	1.34	0.03	-1.94	0.02	18.00	
161	195	1.61	0.02	-1.83	0.02	18.00	
168	202	1.36	0.02	-1.79	0.02	18.00	
175	209	1.61	0.02	-1.87	0.03	18.00	
187	221	1.16	0.02	-2.04	0.04	18.00	
190	224	1.49	0.02	-1.82	0.03	18.00	
205	239	1.27	0.02	-2.02	0.02	18.00	
211	245	1.35	0.02	-2.01	0.03	18.00	
216	250	1.35	0.01	-2.05	0.02	18.00	
229	263	1.35	0.02	-1.91	0.02	18.00	
234	268	1.27	0.02	-2.04	0.02	18.00	
239	273	1.32	0.02	-1.89	0.03	18.00	
244	278	1.36	0.02	-1.90	0.03	18.00	
249	283	1.42	0.03	-1.86	0.02	18.00	
253	287	1.45	0.03	-1.85	0.02	18.00	
266	300	1.37	0.06	-1.92	0.06	18.00	

Table 9: Core 17681

Core 17681-1

Depth (cm)	Composite depth (cm)	$\delta^{13}C$	2σ	$\delta^{18}O$	2σ	Calibrated age BP (ka)	Remarks
0		1.67	0.01	-2.71	0.03	0.00	undisturbed surface
5		1.46	0.02	-2.74	0.03	2.27	
10		1.60	0.01	-2.65	0.02	4.55	
15		1.43	0.02	-2.55	0.03	6.82	
20		1.54	0.01	-2.44	0.02	9.09	
25		1.12	0.01	-2.14	0.03	11.25	
30		1.27	0.01	-1.89	0.02	13.32	
35		1.05	0.02	-1.50	0.02	15.40	
39		1.00	0.04	-1.88	0.06	17.06	

Core 17681-2

Depth (cm)	Composite depth (cm)	$\delta^{13}C$	2σ	$\delta^{18}O$	2σ	Calibrated age BP (ka)	Remarks
13	15	1.41	0.02	-2.41	0.02	6.82	Core fit: 15 cm in the box core (-1)
15	17	1.34	0.01	-2.45	0.03	7.73	= 13 cm in the gravity core (-2)
20	22	1.45	0.02	-2.19	0.02	10.00	
25	27	1.39	0.02	-2.05	0.04	12.77	
30	32	1.33	0.02	-1.67	0.02	15.53	
35	37	1.06	0.02	-1.11	0.01	18.30	
40	42	1.16	0.01	-1.00	0.02	20.95	
45	47	0.88	0.02	-1.23	0.03	23.61	
50	52	1.27	0.01	-1.22	0.03	26.26	
55	57	1.46	0.01	-1.11	0.02	28.91	
60	62	1.29	0.01	-1.21	0.03	31.57	
65	67	1.16	0.02	-1.38	0.02	34.22	
70	72	1.46	0.02	-1.40	0.03	36.88	
75	77	1.34	0.02	-1.39	0.02	39.53	
80	82	1.26	0.03	-1.31	0.05	42.18	
85	87	1.37	0.03	-1.29	0.04	44.84	
90	92	1.15	0.06	-1.50	0.06	47.49	
95	97	1.31	0.02	-1.56	0.03	50.14	
100	102	1.41	0.01	-1.60	0.03	52.80	
105	107	1.45	0.01	-1.88	0.02	55.45	
110	112	1.17	0.02	-1.70	0.02	58.05	
113	115	1.28	0.02	-1.67	0.03	59.61	
123	125	1.24	0.01	-1.60	0.02	64.81	
133	135	1.62	0.01	-1.40	0.02	70.01	
143	145	1.57	0.01	-2.01	0.03	75.21	
153	155	1.95	0.02	-1.96	0.02	80.41	
163	165	1.52	0.01	-2.10	0.01	85.61	
173	175	1.48	0.02	-1.96	0.05	90.80	
183	185	1.49	0.02	-2.16	0.03	96.00	
193	195	1.33	0.01	-2.02	0.03	101.20	
202	204	1.69	0.02	-2.11	0.03	105.88	
213	215	1.31	0.02	-2.09	0.03	111.60	
222	224	1.23	0.02	-2.03	0.03	116.28	
233	235	1.13	0.01	-2.55	0.02	122.00	
243	245	1.30	0.01	-2.40	0.02	124.60	
253	255	0.92	0.02	-2.37	0.02	127.20	
263	265	0.74	0.01	-2.02	0.02	129.80	
273	275	0.88	0.02	-1.19	0.04	132.40	
283	285	0.76	0.01	-0.95	0.02	135.00	
293	295	0.89	0.01	-1.43	0.02	139.83	
303	305	1.11	0.01	-1.27	0.02	144.67	
313	315	1.04	0.01	-1.31	0.02	149.50	
323	325	0.97	0.01	-1.13	0.02	154.33	
333	335	0.76	0.03	-1.45	0.03	159.17	

Core 17681-2 (continued)

Depth (cm)	Composite depth (cm)	$\delta^{13}C$	2σ	$\delta^{18}O$	2σ	Calibrated age BP (ka)	Remarks
340	342	0.98	0.02	-1.40	0.05	162.55	
353	355	1.52	0.02	-1.59	0.04	168.83	
363	365	0.81	0.05	-1.50	0.06	173.67	
373	375	1.18	0.02	-1.52	0.03	178.50	
383	385	1.27	0.01	-1.63	0.04	183.33	
393	395	1.54	0.01	-1.95	0.03	188.17	
403	405	1.60	0.04	-2.28	0.07	193.00	
413	415	1.29	0.02	-1.94	0.03	198.33	
423	425	1.51	0.01	-2.15	0.02	203.67	
433	435	1.40	0.01	-2.19	0.02	209.00	
446	448	1.04	0.01	-2.03	0.02	215.93	
453	455	0.82	0.02	-1.80	0.02	219.67	
463	465	0.90	0.02	-1.68	0.03	225.00	
473	475	1.05	0.02	-1.79	0.03	229.00	
483	485	1.29	0.02	-2.20	0.02	233.00	
493	495	1.27	0.01	-2.13	0.03	237.00	
503	505	0.65	0.01	-2.16	0.04	241.00	
513	515	0.97	0.01	-1.65	0.03	247.00	
523	525	0.89	0.02	-1.48	0.04	253.00	
533	535	0.98	0.01	-1.64	0.02	258.15	
543	545	0.95	0.02	-1.58	0.02	263.29	
553	555	0.45	0.02	-1.54	0.01	268.44	
563	565	1.00	0.02	-1.84	0.03	273.59	
573	575	1.17	0.01	-1.74	0.03	278.74	
583	585	1.53	0.02	-1.85	0.04	283.88	
591	593	1.21	0.02	-1.93	0.02	288.00	
603	605	1.37	0.02	-1.65	0.03	292.40	
613	615	0.58	0.01	-1.50	0.03	296.07	
620	622	1.24	0.02	-1.74	0.02	298.64	
630	632	1.31	0.03	-1.78	0.01	302.31	
640	642	1.55	0.01	-1.78	0.02	305.98	
650	652	1.34	0.02	-1.86	0.02	309.65	
660	662	1.16	0.01	-2.26	0.03	313.32	
670	672	1.03	0.01	-1.97	0.04	316.99	
680	682	1.31	0.01	-2.26	0.03	320.66	
690	692	1.04	0.02	-2.24	0.02	324.33	
700	702	1.11	0.05	-2.25	0.06	328.00	
710	712	0.32	0.01	-1.58	0.04	331.67	
713	715	1.52	0.04	-1.52	0.05	332.77	

Table 10: Core 17682

Core 17682-1

Depth (cm)	Composite depth (cm)	$\delta^{13}C$	2σ	$\delta^{18}O$	2σ	Calibrated age BP (ka)	Remarks
0		1.12	0.01	-2.90	0.01	0.00	undisturbed surface
5		1.56	0.01	-2.69	0.02	1.19	
10		1.78	0.01	-2.54	0.01	2.38	
13		1.55	0.01	-2.63	0.01	3.10	
15		1.69	0.01	-2.47	0.01	3.57	
21		1.52	0.02	-2.53	0.02	5.00	
27		1.53	0.01	-2.62	0.02	6.43	
30		1.55	0.01	-2.44	0.01	7.14	
35		1.51	0.01	-2.34	0.01	8.33	
40		1.47	0.06	-2.42	0.08	9.52	
42		1.08	0.01	-2.06	0.01	10.00	after $\delta^{18}O$ stack of Bassinot et al. (1994)
46		1.15	0.01	-1.73	0.02	10.55	

Core 17682-2

Depth (cm)	Composite depth (cm)	$\delta^{13}C$	2σ	$\delta^{18}O$	2σ	Calibrated age BP (ka)	Remarks
1	13	1.62	0.02	-2.50	0.02	3.10	Core fit: 13 cm in the box core (-1)
5	17	1.31	0.02	-2.68	0.03	4.05	= 1 cm in the gravity core (-2)
10	22	1.51	0.01	-2.49	0.01	5.24	
15	27	1.64	0.01	-2.45	0.01	6.43	
20	32	1.55	0.01	-2.13	0.04	7.62	
25	37	1.51	0.01	-2.28	0.04	8.81	
30	42	1.53	0.07	-1.95	0.08	10.00	after $\delta^{18}O$ stack of Bassinot et al. (1994)
35	47	0.85	0.09	-2.08	0.11	10.69	
40	52	1.38	0.01	-1.77	0.01	11.38	
45	57	0.98	0.02	-1.70	0.02	12.08	
50	62	1.07	0.01	-1.47	0.02	12.77	
54	66	1.00	0.01	-1.24	0.03	13.32	
59	71	1.10	0.01	-1.23	0.01	14.01	
65	77	1.20	0.01	-1.30	0.01	14.84	
70	82	1.34	0.01	-1.16	0.01	15.53	
75	87	1.42	0.01	-1.08	0.02	16.23	
80	92	0.92	0.01	-1.19	0.02	16.92	
85	97	1.39	0.01	-1.36	0.02	17.61	
90	102	1.43	0.01	-1.15	0.02	18.30	after $\delta^{18}O$ stack of Winn et al. (1991)
95	107	1.55	0.10	-1.29	0.10	19.70	
100	112	1.29	0.02	-1.29	0.02	21.10	
110	122	1.34	0.02	-1.28	0.02	23.90	
123	135	1.44	0.01	-1.49	0.02	27.54	
130	142	1.44	0.01	-1.67	0.01	29.50	$\delta^{18}O$ event 3.0
140	152	1.64	0.00	-1.58	0.02	32.10	
150	162	1.27	0.01	-1.50	0.03	34.69	
160	172	1.66	0.10	-1.20	0.12	37.29	
168	180	1.26	0.01	-1.49	0.04	39.36	
182	194	1.41	0.01	-1.52	0.02	42.99	
193	205	1.52	0.08	-1.67	0.09	45.85	
199	211	1.57	0.01	-1.42	0.01	47.41	
200	212	1.64	0.01	-1.53	0.02	47.67	
210	222	1.65	0.01	-1.65	0.02	50.26	
220	232	1.17	0.01	-1.81	0.01	52.86	
230	242	1.24	0.02	-1.87	0.02	55.45	$\delta^{18}O$ event 3.31
241	253	1.32	0.02	-1.83	0.02	58.14	
250	262	1.04	0.02	-1.75	0.03	60.34	
260	272	1.39	0.01	-1.32	0.02	62.78	
270	282	1.43	0.00	-1.25	0.02	65.22	$\delta^{18}O$ event 4.22
280	292	1.42	0.01	-1.43	0.01	66.95	

Core 17682-2 (continued)

Depth (cm)	Composite depth (cm)	$\delta^{13}C$	2σ	$\delta^{18}O$	2σ	Calibrated age BP (ka)	Remarks
440	452	1.45	0.01	-1.88	0.02	106.74	
450	462	1.22	0.02	-2.16	0.03	109.83	
460	472	1.04	0.02	-2.23	0.02	112.92	
470	482	1.14	0.01	-2.47	0.02	116.01	
470	482	1.63	0.01	-2.33	0.01	116.01	
480	492	1.25	0.01	-2.35	0.01	119.10	
490	502	1.31	0.01	-2.48	0.01	122.19	
500	512	1.32	0.01	-2.28	0.03	124.03	
510	522	1.13	0.01	-2.35	0.04	125.86	
520	532	0.64	0.01	-1.57	0.02	127.70	
530	542	0.87	0.02	-1.43	0.03	129.54	
540	552	0.75	0.07	-1.13	0.08	131.38	
550	562	0.76	0.01	-1.01	0.03	133.21	
560	572	0.87	0.01	-1.13	0.02	135.05	
570	582	1.48	0.10	-0.83	0.11	136.89	
570	582	1.07	0.01	-1.14	0.01	136.89	
580	592	1.11	0.02	-1.16	0.02	138.73	
590	602	1.32	0.02	-1.19	0.02	140.56	
600	612	1.12	0.01	-1.20	0.02	142.40	
610	622	1.09	0.01	-1.16	0.01	144.24	
620	632	0.92	0.01	-1.25	0.01	146.08	
630	642	0.95	0.01	-1.18	0.02	147.91	
640	652	1.08	0.01	-1.07	0.03	149.75	
650	662	1.24	0.01	-0.96	0.02	151.59	
660	672	1.06	0.01	-1.03	0.02	153.43	
670	682	1.00	0.01	-1.23	0.02	155.26	
680	692	1.27	0.05	-1.05	0.07	157.10	$\delta^{18}O$ event 6.41
690	702	1.34	0.01	-1.35	0.03	158.20	
700	712	0.96	0.01	-1.34	0.02	159.30	
707	719	1.41	0.01	-1.63	0.02	160.06	
720	732	1.15	0.01	-1.34	0.01	161.49	
730	742	1.29	0.01	-1.40	0.02	162.59	
742	754	1.27	0.01	-1.32	0.02	163.91	
750	762	1.05	0.02	-1.50	0.02	164.78	
760	772	1.10	0.01	-1.48	0.02	165.88	
770	782	0.97	0.02	-1.37	0.03	166.98	
779	791	1.01	0.01	-1.21	0.01	167.97	
790	802	1.27	0.01	-1.40	0.01	169.17	
799	811	1.04	0.02	-1.70	0.03	170.16	
810	822	1.35	0.01	-1.86	0.02	171.37	$\delta^{18}O$ event 6.5
816	828	1.56	0.02	-1.72	0.02	172.03	

Table 11: Core 17684

Core 17684-1

Depth (cm)	Composite depth (cm)	$\delta^{13}C$	2σ	$\delta^{18}O$	2σ	Calibrated age BP (ka)	Remarks
0		1.54	0.02	-2.62	0.03	0.00	undisturbed surface
5		1.40	0.02	-2.62	0.05	2.50	
10		1.67	0.01	-2.48	0.03	5.00	
15		1.42	0.02	-2.33	0.02	7.50	
20		1.36	0.01	-2.33	0.01	10.00	after $\delta^{18}O$ stack of Bassinot et al. (1994)
25		0.93	0.01	-1.43	0.03	18.30	after $\delta^{18}O$ stack of Winn et al. (1991)
30		1.48	0.02	-1.74	0.02	19.70	
35		1.68	0.02	-1.84	0.02	21.10	
40		1.52	0.01	-1.79	0.04	22.50	
45		1.40	0.02	-1.80	0.02	23.90	
50		1.43	0.02	-1.93	0.03	25.30	
55		1.54	0.02	-1.83	0.03	26.70	
60		1.49	0.02	-1.89	0.03	28.10	
65		1.60	0.01	-1.93	0.04	29.50	
70		1.36	0.02	-1.91	0.04	31.30	
80		1.43	0.02	-1.89	0.04	34.91	
90		1.34	0.01	-1.84	0.02	38.52	
95		1.54	0.02	-1.68	0.03	40.33	
100		1.67	0.01	-1.88	0.03	42.13	
110		1.43	0.07	-1.72	0.10	45.74	
120		1.52	0.02	-1.76	0.03	49.35	
130		1.28	0.02	-1.64	0.03	52.96	
140		1.39	0.01	-1.71	0.04	56.57	
150		1.33	0.01	-1.94	0.04	60.17	
160		1.17	0.02	-1.78	0.03	63.78	
170		0.96	0.01	-1.97	0.03	67.39	
180		1.29	0.02	-1.82	0.04	71.00	
190		1.22	0.02	-1.93	0.02	74.83	
200		1.23	0.02	-2.24	0.03	78.67	
210		1.29	0.02	-2.32	0.04	82.50	
220		1.12	0.02	-2.25	0.03	86.34	
230		1.25	0.01	-2.19	0.04	90.17	
240		1.29	0.01	-2.46	0.03	94.01	
250		1.06	0.01	-2.41	0.03	97.84	
260		1.03	0.01	-2.39	0.03	101.68	
270		0.82	0.01	-2.47	0.03	105.51	
280		1.14	0.01	-2.40	0.02	109.35	
293		1.07	0.02	-2.43	0.03	114.33	
302		1.06	0.02	-2.29	0.02	117.78	
306		1.02	0.02	-2.36	0.02	119.32	
310		0.87	0.02	-2.34	0.02	120.85	
313		0.84	0.02	-2.41	0.02	122.00	
315		0.89	0.01	-2.27	0.02	122.77	

9.5 Major element statistics

Table 12: Electron microbrobe analyses of MPI-DING glass standards (Jochum et al., 2000)

	GOR132-G Mainz	GOR132-G Kiel (n=9)	Ti-G Mainz	Ti-G Kiel (n=40)	ATHO Mainz	ATHO Kiel (n=5)
SiO_2	45.50	45.58	58.40	59.49	75.90	75.44
TiO_2	0.30	0.30	0.74	0.75	0.24	0.25
Al_2O_3	10.90	10.88	17.10	16.85	11.60	12.27
FeO^T	10.20	10.29	6.46	6.42	3.11	3.05
MnO	0.15	0.15	0.13	0.13	0.10	0.12
MgO	22.40	22.48	3.73	3.70	0.11	0.09
CaO	8.49	8.67	7.07	7.15	1.64	1.64
Na_2O	0.80	0.81	3.13	3.07	4.05	3.94
K_2O	0.03	0.03	1.91	2.06	2.66	2.75
P_2O_5	0.04	0.10	0.18	0.26	0.03	0.09
Total	98.81	99.30	98.85	99.88	99.44	99.66

9.6 Major element analyses

Table 13: Major element analyses of glass shards in wt.% of core 17674

Core	Depth (cm)	SiO_2	TiO_2	Al_2O_3	FeO^T	MnO	MgO	CaO	Na_2O	K_2O	P_2O_5	Total	Mg#
17674	27.2	68.45	0.82	15.08	4.03	0.14	0.90	2.77	2.64	3.22	0.24	98.30	35.9
17674	27.2	69.22	0.99	14.60	4.74	0.16	1.01	2.75	2.97	3.50	0.29	100.23	34.7
17674	27.2	68.43	0.83	15.40	4.15	0.18	1.00	2.80	2.87	3.08	0.24	98.96	37.5
stdev		0.45	0.09	0.40	0.38	0.02	0.06	0.02	0.17	0.21	0.03	0.98	
av (n=3)		**68.70**	**0.88**	**15.03**	**4.31**	**0.16**	**0.97**	**2.77**	**2.83**	**3.27**	**0.26**	**99.17**	**36.0**
17674	44.4	56.09	0.54	21.22	4.98	0.19	1.33	3.18	5.32	7.10	0.39	100.32	40.0
17674	44.4	56.44	0.46	21.19	5.15	0.21	1.36	3.11	5.07	7.18	0.41	100.56	39.7
17674	44.4	55.19	0.54	20.49	5.81	0.19	1.43	3.77	5.39	6.64	0.57	100.03	38.1
stdev		0.64	0.04	0.41	0.44	0.01	0.05	0.36	0.17	0.29	0.10	0.27	
av (n=3)		**55.91**	**0.51**	**20.96**	**5.31**	**0.20**	**1.37**	**3.35**	**5.26**	**6.97**	**0.46**	**100.31**	**39.2**
17674	44.4	69.10	0.84	15.02	3.57	0.12	0.90	2.57	2.89	3.29	0.21	98.52	38.7
17674	44.4	68.77	0.84	15.51	3.65	0.10	0.88	2.48	2.90	3.56	0.22	98.92	37.7
17674	44.4	69.52	0.88	14.41	3.67	0.17	0.82	2.47	2.99	3.96	0.20	99.09	36.0
17674	44.4	69.11	0.91	15.61	3.68	0.16	0.89	2.55	2.87	3.90	0.22	99.90	37.7
stdev		0.31	0.04	0.55	0.05	0.03	0.04	0.05	0.05	0.31	0.01	0.58	
av (n=4)		**69.13**	**0.87**	**15.14**	**3.64**	**0.14**	**0.88**	**2.52**	**2.91**	**3.68**	**0.21**	**99.10**	**37.5**

Table 14: Major element analyses of glass shards in wt.% of core 17675

Core	Depth (cm)	SiO_2	TiO_2	Al_2O_3	FeO^T	MnO	MgO	CaO	Na_2O	K_2O	P_2O_5	Total	Mg#
17675	12.1	69.24	0.77	14.81	4.10	0.13	0.92	2.67	3.39	3.13	0.22	99.37	36.0
17675	12.1	69.04	0.77	14.51	4.08	0.18	0.90	2.66	3.10	3.13	0.22	98.60	35.7
17675	12.1	69.11	0.76	15.13	3.96	0.17	0.92	2.69	3.67	3.23	0.23	99.88	36.7
17675	12.1	68.02	0.77	14.83	4.19	0.13	0.94	2.72	3.68	3.17	0.23	98.69	36.0
17675	12.1	68.09	0.79	14.85	4.25	0.14	1.01	2.81	3.09	3.05	0.28	98.36	37.3
stdev		0.59	0.01	0.22	0.11	0.03	0.04	0.06	0.29	0.06	0.02	0.63	
av (n=5)		**68.70**	**0.77**	**14.83**	**4.12**	**0.15**	**0.94**	**2.71**	**3.39**	**3.14**	**0.24**	**98.98**	**36.3**
17675	18.3	78.49	0.22	11.62	1.35	0.06	0.23	1.17	2.27	1.83	0.05	97.29	30.1
17675	18.3	78.21	0.23	11.65	1.35	0.07	0.23	1.29	2.23	1.75	0.04	97.04	29.6
17675	18.3	79.18	0.25	11.68	1.28	0.05	0.23	1.30	1.52	1.73	0.06	97.28	31.1
17675	18.3	78.16	0.26	12.12	1.39	0.04	0.24	1.32	2.08	1.84	0.03	97.49	30.2
stdev		0.47	0.02	0.24	0.04	0.01	0.00	0.07	0.35	0.05	0.02	0.18	
av (n=5)		**78.51**	**0.24**	**11.77**	**1.34**	**0.05**	**0.23**	**1.27**	**2.03**	**1.79**	**0.04**	**97.28**	**30.2**
17675	21.5	80.08	0.24	11.91	1.33	0.05	0.23	1.38	1.90	1.79	0.05	98.95	30.3
17675	21.5	78.79	0.22	11.68	1.33	0.05	0.22	1.32	1.78	1.76	0.03	97.18	29.1
17675	21.5	79.69	0.25	12.06	1.29	0.10	0.24	1.37	1.97	1.83	0.03	98.82	32.1
17675	21.5	80.11	0.27	11.99	1.29	0.04	0.22	1.36	1.98	1.86	0.04	99.15	30.3
17675	21.5	77.71	0.22	11.60	1.28	0.06	0.21	1.29	1.67	1.69	0.03	95.75	28.8
17675	21.5	78.68	0.26	12.38	1.35	0.04	0.25	1.32	1.86	1.86	0.00	98.00	31.4
stdev		0.95	0.02	0.28	0.03	0.02	0.02	0.04	0.12	0.06	0.02	1.31	
av (n=6)		**79.18**	**0.24**	**11.94**	**1.31**	**0.06**	**0.23**	**1.34**	**1.86**	**1.80**	**0.03**	**97.98**	**30.4**
17675	138.4	69.89	0.56	13.67	2.40	0.07	0.42	1.49	2.48	3.94	0.07	94.98	30.3
17675	138.4	69.31	0.53	13.88	2.49	0.06	0.42	1.45	2.74	3.95	0.12	94.95	29.9
17675	138.4	68.77	0.74	14.90	3.85	0.09	0.92	3.10	2.82	3.27	0.23	98.68	37.5
17675	138.4	68.77	0.66	14.12	2.97	0.10	0.66	2.56	2.38	3.66	0.14	96.03	35.7
stdev		0.53	0.09	0.54	0.66	0.02	0.24	0.82	0.21	0.32	0.07	1.76	
av (n=4)		**69.19**	**0.62**	**14.14**	**2.93**	**0.08**	**0.61**	**2.15**	**2.60**	**3.71**	**0.14**	**96.16**	**34.1**

Table 15: Major element analyses of glass shards in wt.% of core 17676

Core	Depth (cm)	SiO_2	TiO_2	Al_2O_3	FeO^T	MnO	MgO	CaO	Na_2O	K_2O	P_2O_5	Total	Mg#
17676	10.3	54.87	0.59	21.56	4.48	0.17	1.26	3.47	4.93	6.31	0.41	98.25	41.3
17676	10.3	54.82	0.47	21.34	4.36	0.14	1.08	3.15	5.43	6.50	0.35	97.82	38.3
stdev		0.04	0.09	0.15	0.09	0.02	0.13	0.23	0.36	0.14	0.04	0.30	
av (n=2)		**54.85**	**0.53**	**21.45**	**4.42**	**0.15**	**1.17**	**3.31**	**5.18**	**6.41**	**0.38**	**97.85**	**39.9**
17676	20.3	52.68	0.51	19.74	7.30	0.19	2.18	5.10	5.41	6.38	0.79	100.56	42.7
17676	20.3	52.75	0.55	19.54	7.06	0.21	1.94	4.83	5.99	6.73	0.75	100.65	40.7
17676	20.3	54.74	0.50	20.64	5.95	0.19	1.85	4.15	6.63	5.67	0.60	101.19	43.7
17676	20.3	53.86	0.51	20.69	6.13	0.19	1.80	4.47	5.85	6.82	0.58	101.16	42.3
17676	20.3	53.62	0.49	19.93	6.89	0.22	1.93	4.24	6.66	5.79	0.78	100.82	41.1
stdev		0.85	0.02	0.53	0.59	0.01	0.14	0.40	0.54	0.53	0.10	0.29	
av (n=5)		**53.53**	**0.51**	**20.11**	**6.67**	**0.20**	**1.94**	**4.56**	**6.11**	**6.28**	**0.70**	**100.60**	**42.1**
17676	22.2	75.00	0.40	13.91	2.02	0.12	0.24	0.88	3.39	4.65	0.06	100.65	23.1
17676	22.2	74.25	0.41	13.84	1.93	0.09	0.23	0.89	3.54	4.73	0.07	99.98	23.1
stdev		0.53	0.01	0.05	0.06	0.02	0.01	0.01	0.11	0.06	0.01	0.48	
av (n=2)		**74.62**	**0.40**	**13.87**	**1.97**	**0.10**	**0.24**	**0.88**	**3.46**	**4.69**	**0.07**	**100.32**	**23.1**
17676	147.5	59.10	0.71	14.48	10.11	0.14	2.36	6.95	2.52	0.84	0.19	97.40	36.8
17676	147.5	59.60	0.63	15.20	9.18	0.12	2.40	7.08	2.37	0.79	0.20	97.58	39.5
17676	147.5	58.29	0.65	14.45	10.12	0.15	2.52	7.25	2.45	0.74	0.18	96.81	38.3
stdev		0.66	0.04	0.42	0.54	0.01	0.08	0.15	0.08	0.05	0.01	0.40	
av (n=3)		**59.00**	**0.66**	**14.71**	**9.80**	**0.14**	**2.43**	**7.09**	**2.45**	**0.79**	**0.19**	**97.26**	**38.2**
17676	300.0	78.33	0.26	11.66	1.32	0.09	0.22	1.32	2.44	1.83	0.04	97.51	29.3
17676	300.0	77.07	0.24	11.55	1.43	0.07	0.22	1.29	2.00	1.74	0.02	95.62	27.5
17676	300.0	75.94	0.26	11.46	1.35	0.07	0.23	1.30	1.74	1.77	0.03	94.15	29.6
17676	300.0	78.13	0.23	11.35	1.40	0.05	0.20	1.21	2.49	1.84	0.04	96.95	26.4
17676	300.0	77.33	0.23	11.37	1.38	0.07	0.22	1.30	1.80	1.77	0.06	95.53	28.2
stdev		0.95	0.01	0.13	0.04	0.01	0.01	0.04	0.35	0.04	0.01	1.32	
av (n=5)		**77.36**	**0.24**	**11.48**	**1.38**	**0.07**	**0.22**	**1.28**	**2.09**	**1.79**	**0.04**	**95.95**	**28.2**

Table 16: Major element analyses of glass shards in wt.% of core 17677

Core	Depth (cm)	SiO_2	TiO_2	Al_2O_3	FeO^T	MnO	MgO	CaO	Na_2O	K_2O	P_2O_5	Cr	F	Cl	SO_2	Total	Mg#
17677	6.8	69.32	0.85	15.04	4.14	0.16	0.97	2.68	3.63	3.03	0.27					100.07	36.8
17677	6.8	67.47	0.75	14.49	4.03	0.15	0.90	2.72	2.67	3.05	0.25					96.47	35.8
17677	6.8	68.20	0.77	14.51	3.87	0.15	0.88	2.61	3.47	3.08	0.24					97.78	36.1
17677	6.8	68.92	0.74	14.60	3.91	0.11	0.88	2.57	3.08	3.12	0.21					98.15	36.1
17677	6.8	67.82	0.77	14.34	3.99	0.13	0.91	2.66	2.78	3.05	0.22					96.68	36.3
stdev		0.77	0.04	0.26	0.10	0.02	0.04	0.06	0.42	0.03	0.02					1.44	
av (n=5)		**68.34**	**0.78**	**14.60**	**3.99**	**0.14**	**0.91**	**2.65**	**3.13**	**3.06**	**0.24**					**97.83**	**36.2**
17677	51.5	61.71	0.45	19.00	2.46	0.13	0.41	1.52	5.58	6.36	0.11					97.73	29.2
17677	51.5	62.00	0.43	19.13	2.52	0.11	0.39	1.51	6.58	6.32	0.10					99.10	28.1
17677	51.5	62.29	0.46	19.26	2.50	0.11	0.42	1.51	6.49	6.35	0.12					99.50	29.5
17677	51.5	61.61	0.44	18.99	2.54	0.13	0.39	1.54	6.37	6.41	0.10					98.52	27.6
17677	51.5	62.15	0.45	19.02	2.56	0.14	0.43	1.64	6.50	6.52	0.10					99.51	29.8
17677	51.5	62.33	0.43	19.09	2.57	0.12	0.41	1.56	6.72	6.46	0.11					99.79	28.3
17677	51.5	62.78	0.43	18.82	2.41	0.15	0.43	1.55	4.98	6.41	0.09					98.06	31.0
17677	51.5	62.43	0.47	19.55	2.58	0.11	0.44	1.54	5.60	6.31	0.09					99.11	29.9
17677	51.5	62.14	0.46	18.64	2.51	0.12	0.44	1.56	4.96	6.46	0.10					97.38	30.3
stdev		0.36	0.01	0.26	0.05	0.02	0.02	0.04	0.70	0.07	0.01					0.86	
av (n=9)		**62.16**	**0.45**	**19.05**	**2.52**	**0.12**	**0.42**	**1.55**	**5.98**	**6.40**	**0.10**					**98.75**	**29.3**
17677	56.8	63.40	0.45	19.68	2.59	0.14	0.45	1.51	5.14	6.39	0.12					99.87	30.1
17677	56.8	63.98	0.46	19.73	2.66	0.14	0.44	1.55	5.41	6.04	0.13					100.55	29.1
17677	56.8	63.94	0.46	19.55	2.53	0.12	0.43	1.61	5.30	6.22	0.10					100.26	29.9
17677	56.8	63.31	0.47	19.56	2.52	0.14	0.43	1.62	5.14	6.10	0.09					99.40	30.1
17677	56.8	64.12	0.46	19.54	2.48	0.10	0.42	1.52	5.71	6.31	0.10					100.77	29.9
17677	56.8	63.99	0.46	19.48	2.56	0.11	0.43	1.53	5.71	6.39	0.09					100.76	29.7
stdev		0.34	0.01	0.09	0.06	0.02	0.01	0.05	0.26	0.15	0.02					0.55	
av (n=6)		**63.79**	**0.46**	**19.59**	**2.56**	**0.12**	**0.43**	**1.56**	**5.40**	**6.24**	**0.11**					**100.27**	**29.8**
17677	75.0	53.72	0.52	20.94	5.42	0.21	1.50	4.38	5.35	6.83	0.50					99.36	40.9
17677	75.0	53.09	0.50	20.54	5.55	0.17	1.53	3.87	5.25	7.09	0.51					98.09	40.8
17677	75.0	53.19	0.52	20.40	5.73	0.20	1.60	4.17	5.45	6.92	0.53					98.70	41.1
stdev		0.34	0.01	0.28	0.16	0.02	0.05	0.25	0.10	0.13	0.01					0.64	
av (n=3)		**53.33**	**0.51**	**20.62**	**5.57**	**0.19**	**1.54**	**4.14**	**5.35**	**6.95**	**0.51**					**98.72**	**41.0**
17677	116.6	69.02	0.46	13.35	3.59	0.16	0.71	2.92	4.04	1.18	0.16	0.03	0.06	0.15	0.07	95.91	33.1
17677	116.6	69.75	0.41	13.35	3.35	0.13	0.64	2.97	4.11	1.15	0.16	0.02	0.02	0.15	0.01	96.20	32.2
17677	116.6	71.03	0.36	13.50	3.24	0.14	0.60	2.87	4.21	1.17	0.16	0.05	0.07	0.18	0.11	97.68	31.7
17677	116.6	69.23	0.42	13.22	3.34	0.13	0.63	3.20	4.47	1.11	0.14	0.01	0.06	0.18	0.13	96.26	32.1
17677	116.6	68.69	0.46	13.27	3.38	0.13	0.68	3.10	4.32	1.11	0.19	0.00	0.05	0.19	0.06	95.63	33.4
17677	116.6	68.65	0.44	13.24	3.44	0.14	0.66	3.02	4.38	1.13	0.17	0.01	0.05	0.14	0.11	95.57	32.4
17677	116.6	71.44	0.42	13.44	3.37	0.17	0.67	2.95	4.28	1.10	0.19	0.04	0.06	0.16	0.01	98.30	33.0
17677	116.6	70.78	0.40	13.27	3.30	0.14	0.60	2.86	4.29	1.09	0.18	0.01	0.03	0.17	0.00	97.13	31.2
17677	116.6	71.20	0.44	13.30	3.28	0.15	0.66	2.90	4.21	1.15	0.18	0.02	0.04	0.14	0.04	97.68	33.4
17677	116.6	69.25	0.42	13.54	3.70	0.14	0.78	3.20	4.40	1.01	0.17	0.04	0.05	0.17	0.06	96.91	34.6
17677	116.6	70.43	0.43	13.35	3.36	0.16	0.69	3.09	4.20	1.10	0.18	0.03	0.03	0.13	0.02	97.21	33.9
17677	116.6	70.49	0.47	13.49	3.41	0.18	0.64	3.03	4.25	1.09	0.14	0.00	0.03	0.15	0.06	97.43	32.0
17677	116.6	68.75	0.46	13.64	4.10	0.19	0.87	3.59	3.39	1.10	0.22	0.00	0.07	0.17	0.09	96.62	34.6
17677	116.6	69.93	0.40	13.97	3.75	0.17	0.82	3.48	4.29	1.08	0.19	0.01	0.07	0.15	0.01	98.31	35.3
17677	116.6	70.99	0.43	13.35	3.38	0.13	0.64	2.83	4.22	1.08	0.17	0.04	0.05	0.18	0.02	97.51	32.2
17677	116.6	71.17	0.42	13.51	3.29	0.14	0.70	2.90	4.15	1.05	0.21	0.03	0.03	0.15	0.06	97.81	34.7
17677	116.6	68.99	0.47	13.51	3.73	0.11	0.82	3.46	4.17	1.04	0.19	0.04	0.08	0.15	0.13	96.89	35.5
17677	116.6	70.58	0.41	13.22	3.38	0.13	0.65	2.85	4.31	1.06	0.17	0.01	0.06	0.14	0.08	97.04	32.6
17677	116.6	70.74	0.38	14.49	3.44	0.18	0.73	3.44	4.19	0.98	0.21	0.04	0.04	0.14	0.01	99.01	34.8
stdev		0.97	0.03	0.30	0.22	0.02	0.08	0.24	0.22	0.05	0.02	0.02	0.02	0.02	0.04	0.94	
av (n=19)		**70.06**	**0.43**	**13.47**	**3.46**	**0.15**	**0.69**	**3.09**	**4.20**	**1.09**	**0.18**	**0.02**	**0.05**	**0.16**	**0.06**	**97.11**	**33.4**

Table 9.16: 17677 (continued)

Core	Depth (cm)	SiO_2	TiO_2	Al_2O_3	FeO^T	MnO	MgO	CaO	Na_2O	K_2O	P_2O_5	Cr	F	Cl	SO_2	Total	Mg#
17677	154.3	67.71	0.71	14.36	3.40	0.17	0.75	2.21	4.14	3.57	0.17					97.18	35.4
17677	154.3	68.79	0.72	14.79	3.49	0.14	0.75	2.19	4.05	3.58	0.19					98.70	35.0
17677	154.3	68.80	0.74	14.79	3.40	0.13	0.76	2.13	4.30	3.39	0.19					98.63	35.9
17677	154.3	67.05	0.71	14.39	3.33	0.14	0.71	2.12	4.18	3.56	0.18					96.37	34.9
17677	154.3	67.33	0.72	14.69	3.38	0.10	0.74	2.14	4.18	3.57	0.16					97.01	35.2
stdev		0.82	0.01	0.22	0.06	0.02	0.02	0.04	0.09	0.08	0.01					1.04	
av (n=5)		**67.94**	**0.72**	**14.60**	**3.40**	**0.14**	**0.74**	**2.16**	**4.17**	**3.53**	**0.18**					**97.58**	**35.3**
17677	157.6	56.91	0.44	20.03	3.77	0.16	0.97	2.74	6.05	6.68	0.25					97.99	39.2
17677	157.6	57.10	0.40	20.05	3.79	0.15	0.95	2.58	6.12	6.80	0.27					98.20	38.5
17677	157.6	57.07	0.40	19.78	3.72	0.19	0.93	2.43	5.74	6.78	0.25					97.29	38.6
17677	157.6	57.33	0.40	20.09	3.64	0.16	0.95	2.43	6.07	6.85	0.26					98.19	39.4
17677	157.6	56.67	0.35	20.23	3.43	0.16	0.84	2.30	6.56	6.75	0.26					97.55	38.0
stdev		0.25	0.03	0.16	0.15	0.01	0.05	0.17	0.29	0.06	0.01					0.41	
av (n=5)		**57.02**	**0.40**	**20.03**	**3.67**	**0.16**	**0.93**	**2.50**	**6.11**	**6.77**	**0.26**					**97.84**	**38.7**
17677	160.2	60.49	0.41	20.18	2.88	0.11	0.42	1.56	7.18	6.04	0.10					99.37	26.7
17677	160.2	60.84	0.38	19.22	2.64	0.09	0.46	1.45	6.24	5.08	0.11					96.51	30.2
17677	160.2	61.44	0.35	19.49	2.53	0.07	0.42	1.64	6.16	4.94	0.11					97.16	29.4
17677	160.2	61.42	0.37	19.06	2.55	0.08	0.48	1.55	5.79	5.04	0.12					96.45	32.0
17677	160.2	60.87	0.36	18.96	2.44	0.08	0.43	1.34	6.46	5.61	0.10					96.66	30.5
stdev		0.41	0.02	0.49	0.17	0.02	0.03	0.12	0.51	0.47	0.01					1.23	
av (n=5)		**61.01**	**0.37**	**19.38**	**2.61**	**0.09**	**0.44**	**1.51**	**6.37**	**5.34**	**0.11**					**97.23**	**29.7**
17677	183.3	56.57	0.52	20.43	4.97	0.18	1.35	2.63	6.07	6.59	0.41					99.71	40.4
17677	183.3	55.35	0.42	22.42	3.96	0.13	0.95	4.87	5.42	5.54	0.37					99.44	37.5
17677	183.3	55.36	0.53	20.04	5.56	0.15	1.45	2.88	5.45	7.12	0.46					99.01	39.5
17677	183.3	56.02	0.49	20.41	4.42	0.14	1.21	2.74	6.29	6.57	0.40					98.68	40.7
stdev		0.59	0.05	1.08	0.69	0.02	0.22	1.06	0.44	0.66	0.04					0.45	
av (n=4)		**55.83**	**0.49**	**20.82**	**4.73**	**0.15**	**1.24**	**3.28**	**5.81**	**6.45**	**0.41**					**99.21**	**39.6**
17677	228.9	66.05	0.79	14.88	3.38	0.16	0.80	2.39	5.07	3.53	0.22	0.01	0.05	0.20	0.09	97.40	37.1
17677	228.9	66.38	0.76	15.07	3.62	0.17	0.90	2.39	4.66	3.41	0.24	0.05	0.08	0.23	0.01	97.74	38.2
17677	228.9	65.71	0.75	14.91	3.67	0.22	0.86	2.37	5.01	3.57	0.25	0.01	0.06	0.20	0.04	97.50	37.0
17677	228.9	65.26	0.81	14.96	3.92	0.21	0.97	2.63	4.69	3.35	0.25	0.02	0.09	0.20	0.05	97.21	38.3
17677	228.9	65.16	0.78	14.91	4.16	0.22	0.98	2.57	4.83	3.33	0.29	0.02	0.03	0.20	0.08	97.40	37.0
17677	228.9	66.29	0.78	15.06	3.84	0.17	0.90	2.47	4.88	3.55	0.23	0.02	0.07	0.22	0.02	98.32	36.9
17677	228.9	67.53	0.77	15.17	3.66	0.18	0.82	2.35	4.81	3.65	0.26	0.02	0.08	0.22	0.00	99.35	35.9
17677	228.9	66.49	0.76	15.04	3.70	0.16	0.86	2.35	4.98	3.63	0.25	0.03	0.10	0.22	0.06	98.37	36.7
17677	228.9	65.57	0.84	15.06	3.98	0.18	0.96	2.55	4.80	3.35	0.26	0.00	0.11	0.17	0.00	97.72	37.6
17677	228.9	66.68	0.83	15.13	4.00	0.20	0.97	2.56	5.05	3.45	0.26	0.02	0.08	0.22	0.11	99.30	37.7
17677	228.9	67.16	0.78	14.98	3.34	0.20	0.77	2.07	4.76	3.58	0.24	0.02	0.06	0.18	0.01	98.01	36.5
17677	228.9	65.21	0.80	15.07	3.83	0.22	0.96	2.62	4.83	3.43	0.26	0.00	0.09	0.19	0.18	97.39	38.5
17677	228.9	65.33	0.81	15.12	3.83	0.17	0.90	2.47	4.86	3.48	0.30	0.03	0.13	0.21	0.10	97.41	37.0
17677	228.9	65.17	0.81	15.10	4.20	0.20	1.04	2.81	4.92	3.30	0.31	0.00	0.07	0.23	0.08	98.06	38.2
17677	228.9	67.27	0.83	15.54	4.29	0.22	1.17	3.01	3.68	3.28	0.27	0.02	0.07	0.19	0.01	99.74	40.5
17677	228.9	66.80	0.79	15.52	4.67	0.17	1.22	3.27	4.44	3.44	0.22	0.05	0.10	0.14	0.14	100.72	39.5
17677	228.9	65.21	0.80	15.07	3.83	0.22	0.96	2.62	4.83	3.43	0.26	0.00	0.09	0.19	0.18	97.39	38.5
17677	228.9	65.33	0.81	15.12	3.83	0.17	0.90	2.47	4.86	3.48	0.30	0.03	0.13	0.21	0.10	97.41	37.0
17677	228.9	65.17	0.81	15.10	4.20	0.20	1.04	2.81	4.92	3.30	0.31	0.00	0.07	0.23	0.08	98.06	38.2
17677	228.9	67.27	0.83	15.54	4.29	0.22	1.17	3.01	3.68	3.28	0.27	0.02	0.07	0.19	0.01	99.74	40.5
17677	228.9	66.80	0.79	15.52	4.67	0.17	1.22	3.27	4.44	3.44	0.22	0.05	0.10	0.14	0.14	100.72	39.5
17677	228.9	67.24	0.77	15.05	3.51	0.14	0.81	2.28	4.88	3.43	0.24	0.02	0.13	0.20	0.03	98.49	36.5
17677	228.9	67.97	0.76	15.36	3.85	0.21	0.93	2.43	4.83	3.34	0.27	0.01	0.08	0.18	0.11	100.10	37.6
17677	228.9	67.70	0.79	15.48	4.02	0.17	0.97	2.65	4.01	3.32	0.28	0.01	0.09	0.20	0.01	99.56	37.7
17677	228.9	67.74	0.80	15.46	4.02	0.18	1.02	2.62	4.71	3.40	0.25	0.05	0.05	0.17	0.00	100.36	38.7
17677	228.9	67.44	0.71	14.81	3.55	0.18	0.84	2.25	4.98	3.57	0.21	0.00	0.06	0.20	0.08	98.70	37.2
17677	228.9	66.04	0.65	14.59	2.78	0.11	0.66	2.20	4.73	3.60	0.16	0.02	0.08	0.39	0.05	95.64	37.1
stdev		0.96	0.04	0.25	0.40	0.03	0.14	0.30	0.37	0.11	0.03	0.02	0.02	0.04	0.05	1.26	
av (n=27)		**66.37**	**0.79**	**15.14**	**3.88**	**0.19**	**0.95**	**2.57**	**4.71**	**3.44**	**0.25**	**0.02**	**0.08**	**0.20**	**0.07**	**98.65**	**37.9**

Table 9.16: 17677 (continued)

Core	Depth (cm)	SiO_2	TiO_2	Al_2O_3	FeO^T	MnO	MgO	CaO	Na_2O	K_2O	P_2O_5	Cr	F	Cl	SO_2	Total	Mg#
17677	231.1	51.12	0.56	18.16	8.12	0.23	2.86	6.56	4.72	5.38	0.71					98.41	46.8
17677	231.1	51.76	0.56	18.77	8.29	0.20	2.28	6.46	5.23	5.74	0.59					99.88	40.7
stdev		0.45	0.00	0.43	0.12	0.02	0.41	0.07	0.36	0.26	0.09					1.04	
av (n=2)		**51.44**	**0.56**	**18.46**	**8.20**	**0.21**	**2.57**	**6.51**	**4.97**	**5.56**	**0.65**					**99.14**	**43.9**
17677	264.8	53.58	0.48	22.39	6.11	0.24	1.76	3.80	3.55	6.79	0.49					99.20	41.8
17677	264.8	54.70	0.51	21.81	6.11	0.17	2.11	4.72	3.86	6.88	0.50					101.37	46.4
17677	264.8	55.48	0.52	21.41	6.37	0.19	1.59	3.66	3.11	6.55	0.49					99.37	38.4
stdev		0.95	0.02	0.50	0.15	0.04	0.27	0.57	0.38	0.17	0.00					1.21	
av (n=3)		**54.58**	**0.50**	**21.87**	**6.20**	**0.20**	**1.82**	**4.06**	**3.51**	**6.74**	**0.49**					**99.98**	**42.3**
17677	270.0	54.89	0.57	20.31	5.58	0.14	1.79	4.02	6.35	6.60	0.59					100.85	44.5
17677	270.0	54.22	0.55	20.66	6.03	0.18	1.75	4.07	6.43	5.80	0.61					100.31	42.1
17677	270.0	52.56	0.53	20.52	6.48	0.18	2.17	4.73	5.73	6.60	0.67					100.17	45.6
17677	270.0	53.32	0.53	20.48	6.06	0.16	1.89	4.21	6.00	6.96	0.61					100.20	43.8
17677	270.0	53.10	0.50	20.81	5.94	0.13	1.79	4.04	6.39	5.77	0.56					99.05	43.0
17677	270.0	54.17	0.57	20.27	5.94	0.17	1.64	3.74	6.83	6.79	0.60					100.71	40.9
stdev		0.86	0.03	0.20	0.29	0.02	0.18	0.33	0.38	0.51	0.03					0.64	
av (n=6)		**53.71**	**0.54**	**20.51**	**6.00**	**0.16**	**1.84**	**4.13**	**6.29**	**6.42**	**0.61**					**100.22**	**43.4**
17677	272.4	54.38	0.50	21.55	5.23	0.24	1.54	3.68	6.40	6.88	0.43					100.84	42.4
17677	272.4	54.78	0.51	20.49	5.73	0.19	1.52	2.96	7.00	6.46	0.48					100.11	39.9
17677	272.4	53.85	0.51	21.05	5.77	0.21	1.68	4.18	5.60	6.87	0.54					100.25	42.1
17677	272.4	53.41	0.51	20.29	6.52	0.20	1.68	3.93	5.83	6.56	0.55					99.49	39.2
17677	272.4	52.41	0.58	19.79	6.42	0.21	1.96	3.68	4.75	6.63	0.55					96.98	43.3
17677	272.4	53.72	0.51	20.44	5.59	0.16	1.60	3.77	6.29	6.41	0.49					98.99	41.7
17677	272.4	53.94	0.55	20.37	5.79	0.17	1.62	4.99	6.14	5.03	0.56					99.17	41.2
17677	272.4	53.40	0.54	20.46	6.00	0.20	1.84	4.33	4.45	6.30	0.56					98.08	43.3
17677	272.4	51.31	0.54	20.35	6.15	0.20	1.64	4.56	5.76	6.06	0.56					97.13	40.1
17677	272.4	54.03	0.52	20.72	5.41	0.19	1.52	3.70	6.34	6.44	0.48					99.35	41.2
17677	272.4	52.47	0.54	20.48	6.04	0.18	1.73	4.08	5.39	6.33	0.51					97.75	41.7
17677	272.4	53.20	0.52	20.53	5.81	0.20	1.65	3.73	5.99	6.49	0.55					98.67	41.5
stdev		0.96	0.02	0.43	0.38	0.02	0.13	0.52	0.71	0.48	0.04					1.23	
av (n=13)		**53.41**	**0.53**	**20.54**	**5.87**	**0.20**	**1.66**	**3.97**	**5.83**	**6.37**	**0.52**					**98.90**	**41.5**
17677	345.5	53.55	0.49	19.00	7.03	0.17	2.06	5.00	5.56	6.40	0.74					100.01	42.3
17677	345.5	53.25	0.49	19.60	6.25	0.18	1.81	4.47	5.64	6.56	0.58					98.84	42.0
17677	345.5	53.42	0.55	19.14	6.59	0.20	1.95	4.64	5.68	6.06	0.72					98.94	42.5
17677	345.5	53.55	0.49	19.00	7.03	0.17	2.06	5.00	5.56	6.40	0.74					100.01	42.3
17677	345.5	52.25	0.49	19.60	6.25	0.18	1.81	4.47	5.64	6.56	0.58					97.84	42.0
17677	345.5	53.42	0.55	19.14	6.59	0.20	1.95	4.64	5.68	6.06	0.72					98.94	42.5
17677	345.5	54.92	0.44	20.87	5.92	0.15	1.35	3.68	6.29	6.24	0.42					100.28	36.3
17677	345.5	54.35	0.56	20.13	5.75	0.21	1.52	3.18	6.58	6.42	0.57					99.28	39.7
17677	345.5	53.24	0.55	19.89	6.34	0.19	1.89	4.52	5.52	6.52	0.61					99.28	42.6
17677	345.5	54.83	0.50	20.43	5.42	0.20	1.37	4.98	6.10	6.89	0.46					101.19	38.8
17677	345.5	54.14	0.55	19.60	6.44	0.21	1.61	3.96	5.85	6.55	0.61					99.52	38.5
stdev		0.78	0.04	0.61	0.50	0.02	0.26	0.58	0.35	0.24	0.11					0.89	
av (n=13)		**53.72**	**0.52**	**19.67**	**6.33**	**0.19**	**1.76**	**4.41**	**5.83**	**6.42**	**0.61**					**99.47**	**41.0**

Table 17: Major element analyses of glass shards in wt.% of core 17681

Core	Depth (cm)	SiO_2	TiO_2	Al_2O_3	FeO^T	MnO	MgO	CaO	Na_2O	K_2O	P_2O_5	Cr	F	Cl	SO_2	Total	Mg#
17681	344.6(cg)	74.42	0.29	11.64	1.69	0.07	0.31	1.66	3.98	1.64	0.06	0.01	0.05	0.18	0.06	96.07	31.7
17681	344.6(cg)	75.80	0.32	11.72	1.59	0.08	0.31	1.66	3.03	1.60	0.08	0.01	0.05	0.20	0.00	96.25	32.5
17681	344.6(cg)	75.31	0.32	11.60	1.66	0.08	0.30	1.65	3.93	1.59	0.10	0.01	0.07	0.19	0.00	96.62	31.4
17681	344.6(cg)	74.10	0.32	11.36	1.65	0.09	0.30	1.68	3.39	1.55	0.01	0.01	0.07	0.18	0.06	94.51	31.4
17681	344.6(cg)	73.81	0.29	11.57	1.65	0.08	0.33	1.70	4.04	1.63	0.05	0.03	0.05	0.18	0.07	95.22	33.6
17681	344.6(cg)	72.95	0.30	11.34	1.55	0.10	0.35	1.79	3.68	1.77	0.08	0.02	0.04	0.20	0.09	93.99	35.8
17681	344.6(cg)	74.50	0.26	11.58	1.64	0.09	0.30	1.69	3.75	1.64	0.09	0.03	0.04	0.22	0.06	95.61	31.0
17681	344.6(cg)	73.71	0.28	11.55	1.58	0.10	0.31	1.73	4.17	1.60	0.07	0.05	0.07	0.26	0.04	95.17	32.6
17681	344.6(cg)	75.05	0.25	12.14	2.71	0.13	0.16	1.67	3.48	1.63	0.06	0.03	0.08	0.14	0.05	97.39	13.0
17681	344.6(cg)	75.25	0.26	11.87	1.62	0.04	0.31	1.69	4.10	1.67	0.08	0.02	0.07	0.19	0.00	96.97	32.4
17681	344.6(cg)	73.60	0.32	11.27	1.62	0.08	0.28	1.72	4.01	1.56	0.08	0.04	0.08	0.21	0.05	94.60	30.0
17681	344.6(cg)	72.76	0.25	11.41	1.57	0.08	0.32	1.65	3.96	1.61	0.09	0.03	0.06	0.20	0.12	93.76	33.5
17681	344.6(cg)	74.67	0.30	11.56	1.66	0.08	0.30	1.59	4.04	1.67	0.07	0.03	0.03	0.19	0.06	96.00	31.0
17681	344.6(cg)	74.09	0.32	11.35	1.60	0.06	0.31	1.65	4.05	1.56	0.08	0.04	0.04	0.18	0.02	95.14	32.6
17681	344.6(cg)	74.27	0.31	11.60	1.65	0.12	0.30	1.59	4.15	1.67	0.11	0.01	0.02	0.19	0.04	95.83	31.1
17681	344.6(cg)	74.15	0.32	11.59	1.61	0.12	0.30	1.60	4.09	1.72	0.11	0.03	0.03	0.19	0.00	95.68	32.1
17681	344.6(cg)	73.00	0.33	11.42	1.66	0.09	0.30	1.67	4.13	1.63	0.08	0.02	0.04	0.19	0.00	94.37	31.4
17681	344.6(cg)	72.61	0.28	11.22	1.65	0.10	0.35	1.59	3.81	1.64	0.06	0.03	0.13	0.19	0.00	93.36	34.5
17681	344.6(cg)	73.64	0.29	11.55	1.64	0.09	0.29	1.67	4.00	1.69	0.07	0.01	0.03	0.19	0.03	94.99	31.0
17681	344.6(cg)	73.94	0.30	11.58	1.59	0.09	0.30	1.65	4.21	1.62	0.07	0.03	0.07	0.23	0.02	95.41	32.0
17681	344.6(cg)	74.76	0.33	11.62	1.60	0.09	0.30	1.78	3.99	1.58	0.07	0.02	0.03	0.23	0.07	96.18	32.0
17681	344.6(cg)	75.01	0.26	11.55	1.64	0.04	0.31	1.63	4.12	1.63	0.08	0.00	0.08	0.21	0.09	96.35	32.1
17681	344.6(cg)	75.03	0.29	11.51	1.63	0.07	0.30	1.76	4.05	1.65	0.08	0.02	0.08	0.19	0.05	96.43	31.8
17681	344.6(cg)	74.25	0.28	11.35	1.55	0.09	0.32	1.68	3.92	1.62	0.03	0.01	0.05	0.20	0.05	95.16	33.7
17681	344.6(cg)	73.32	0.28	11.24	1.57	0.07	0.28	1.62	3.88	1.71	0.08	0.04	0.07	0.18	0.00	94.12	31.1
17681	344.6(cg)	75.93	0.32	11.53	1.52	0.10	0.29	1.64	3.77	1.58	0.09	0.02	0.04	0.18	0.05	96.82	32.0
17681	344.6(cg)	74.10	0.29	11.29	1.62	0.04	0.29	1.55	3.81	1.51	0.09	0.03	0.03	0.18	0.00	94.66	31.1
17681	344.6(cg)	74.21	0.28	11.44	1.71	0.08	0.30	1.62	3.97	1.56	0.06	0.03	0.07	0.18	0.08	95.29	30.6
17681	344.6(cg)	74.22	0.28	11.56	1.65	0.08	0.31	1.64	4.00	1.69	0.08	0.02	0.06	0.16	0.00	95.59	32.0
17681	344.6(cg)	75.27	0.29	11.58	1.58	0.05	0.28	1.66	2.98	1.61	0.10	0.01	0.05	0.18	0.08	95.46	30.8
17681	344.6(cg)	74.71	0.27	11.33	1.62	0.07	0.29	1.59	4.01	1.52	0.10	0.03	0.04	0.18	0.09	95.58	30.6
17681	344.6(cg)	75.57	0.26	11.33	1.64	0.08	0.28	1.58	3.85	1.66	0.11	0.02	0.09	0.16	0.06	96.44	30.2
17681	344.6(cg)	74.62	0.29	11.45	1.63	0.10	0.29	1.52	4.06	1.67	0.06	0.02	0.04	0.19	0.02	95.76	30.4
17681	344.6(cg)	74.85	0.29	11.39	1.65	0.05	0.30	1.65	4.01	1.62	0.10	0.03	0.07	0.18	0.03	95.98	31.6
17681	344.6(cg)	75.89	0.28	11.60	1.55	0.08	0.31	1.66	3.89	1.57	0.11	0.02	0.04	0.19	0.04	96.99	33.0
stdev		0.87	0.02	0.18	0.19	0.02	0.03	0.06	0.28	0.06	0.02	0.01	0.02	0.02	0.03	0.97	
av (n=35)		**74.38**	**0.29**	**11.51**	**1.65**	**0.08**	**0.30**	**1.65**	**3.89**	**1.63**	**0.08**	**0.02**	**0.06**	**0.19**	**0.04**	**95.77**	**31.2**

cg = clear glass

Table 9.17: 17681 (continued)

Core	Depth (cm)	SiO_2	TiO_2	Al_2O_3	FeO^T	MnO	MgO	CaO	Na_2O	K_2O	P_2O_5	Cr	F	Cl	SO_2	Total	Mg#
17681	344.6 (bg)	66.92	0.62	14.53	2.57	0.13	0.66	1.87	3.85	3.80	0.12	0.03	0.10	0.25	0.06	95.19	39.1
17681	344.6 (bg)	69.31	0.64	15.11	2.71	0.16	0.62	1.81	4.57	3.92	0.14	0.01	0.07	0.25	0.05	99.11	36.5
17681	344.6 (bg)	67.64	0.62	14.72	2.74	0.13	0.66	1.93	4.64	3.93	0.17	0.04	0.07	0.27	0.08	97.29	37.5
17681	344.6 (bg)	68.51	0.60	14.84	2.76	0.14	0.64	1.85	4.65	3.97	0.17	0.03	0.08	0.25	0.14	98.25	36.6
17681	344.6 (bg)	68.61	0.63	14.94	2.63	0.15	0.67	1.79	4.61	3.95	0.20	0.02	0.10	0.24	0.00	98.29	38.7
17681	344.6 (bg)	68.47	0.62	14.86	2.83	0.18	0.65	1.82	4.43	3.98	0.23	0.02	0.07	0.24	0.10	98.20	36.5
17681	344.6 (bg)	68.39	0.60	14.70	2.68	0.14	0.65	1.80	4.73	3.98	0.11	0.04	0.10	0.26	0.04	97.89	37.6
17681	344.6 (bg)	68.67	0.62	14.95	2.77	0.14	0.62	1.81	4.77	3.99	0.18	0.02	0.02	0.27	0.04	98.65	36.0
17681	344.6 (bg)	68.07	0.61	14.70	2.71	0.16	0.62	1.85	4.79	4.07	0.16	0.02	0.03	0.26	0.04	97.84	36.3
17681	344.6 (bg)	67.09	0.58	14.58	2.66	0.15	0.63	1.94	4.74	3.92	0.16	0.03	0.05	0.26	0.06	96.56	37.2
17681	344.6 (bg)	69.12	0.65	15.03	2.74	0.14	0.64	1.83	4.60	3.90	0.17	0.04	0.09	0.25	0.09	98.93	37.0
17681	344.6 (bg)	67.80	0.63	14.69	2.78	0.15	0.63	1.84	4.71	3.94	0.15	0.03	0.10	0.24	0.02	97.43	36.2
17681	344.6 (bg)	66.31	0.61	14.22	2.56	0.14	0.59	1.74	4.57	3.92	0.17	0.01	0.12	0.24	0.02	94.95	36.5
17681	344.6 (bg)	67.77	0.64	14.50	2.73	0.15	0.63	1.78	4.23	3.84	0.19	0.03	0.12	0.26	0.05	96.58	36.8
17681	344.6 (bg)	66.40	0.64	14.35	2.76	0.16	0.62	1.82	4.73	3.90	0.17	0.02	0.04	0.20	0.04	95.66	36.1
17681	344.6 (bg)	67.22	0.63	14.76	2.51	0.16	0.64	1.76	4.53	3.87	0.13	0.03	0.08	0.24	0.04	96.32	38.7
17681	344.6 (bg)	67.45	0.64	14.63	2.66	0.15	0.65	1.86	4.30	3.88	0.20	0.01	0.06	0.22	0.06	96.52	37.9
17681	344.6 (bg)	67.11	0.63	14.59	2.57	0.19	0.63	1.81	4.37	3.91	0.16	0.03	0.07	0.23	0.03	96.08	38.1
17681	344.6 (bg)	66.65	0.62	14.59	2.62	0.13	0.63	1.74	4.35	3.89	0.17	0.02	0.07	0.24	0.07	95.50	37.6
17681	344.6 (bg)	67.47	0.63	14.72	2.77	0.10	0.69	1.92	4.34	3.82	0.15	0.00	0.05	0.24	0.07	96.73	38.3
17681	344.6 (bg)	67.52	0.62	14.57	2.60	0.14	0.63	1.85	4.43	3.88	0.21	0.03	0.09	0.23	0.06	96.56	37.9
17681	344.6 (bg)	67.78	0.66	14.68	2.72	0.14	0.61	1.81	4.59	4.08	0.12	0.02	0.05	0.23	0.12	97.29	35.9
17681	344.6 (bg)	67.01	0.67	14.85	2.99	0.15	0.76	2.14	4.57	3.86	0.20	0.00	0.09	0.22	0.03	97.32	38.8
17681	344.6 (bg)	66.34	0.77	15.46	3.87	0.19	1.17	2.96	4.64	3.75	0.32	0.01	0.06	0.18	0.06	99.63	43.0
17681	344.6 (bg)	66.79	0.71	14.54	2.97	0.18	0.69	1.84	4.69	3.43	0.22	0.03	0.08	0.16	0.07	96.19	36.8
17681	344.6 (bg)	67.86	0.64	14.60	2.76	0.15	0.62	1.82	4.21	3.61	0.15	0.03	0.07	0.22	0.13	96.53	36.0
17681	344.6 (bg)	68.42	0.61	14.73	2.66	0.18	0.63	1.77	4.74	3.95	0.16	0.04	0.08	0.21	0.07	97.96	37.4
17681	344.6 (bg)	68.42	0.65	14.99	2.69	0.16	0.63	1.83	4.62	3.93	0.13	0.04	0.08	0.24	0.08	98.15	36.9
17681	344.6 (bg)	68.81	0.63	14.87	2.66	0.11	0.59	1.77	4.76	3.97	0.17	0.03	0.06	0.25	0.00	98.45	35.8
17681	344.6 (bg)	68.74	0.67	15.00	2.63	0.17	0.63	1.76	4.65	3.96	0.14	0.01	0.07	0.24	0.02	98.47	37.4
17681	344.6 (bg)	68.44	0.59	14.90	2.69	0.14	0.62	1.77	4.64	3.91	0.12	0.04	0.06	0.25	0.07	97.94	36.7
17681	344.6 (bg)	68.13	0.60	14.69	2.68	0.16	0.61	1.80	4.50	4.00	0.10	0.01	0.09	0.24	0.12	97.39	36.3
17681	344.6 (bg)	67.60	0.59	14.58	2.66	0.18	0.62	1.82	4.65	3.85	0.15	0.05	0.11	0.26	0.14	96.80	36.8
17681	344.6 (bg)	67.29	0.66	14.53	2.60	0.15	0.63	1.74	4.38	3.74	0.15	0.03	0.08	0.26	0.17	95.98	37.9
stdev		0.82	0.04	0.23	0.22	0.02	0.10	0.21	0.20	0.12	0.04	0.01	0.02	0.02	0.04	1.17	
av (n=34)		**67.77**	**0.63**	**14.74**	**2.73**	**0.15**	**0.65**	**1.86**	**4.55**	**3.89**	**0.17**	**0.02**	**0.08**	**0.24**	**0.07**	**97.54**	**37.4**
bg = brownish glass																	
17681	444.0	75.74	0.29	11.51	1.56	0.07	0.30	1.65	3.81	1.52	0.11	0.04	0.07	0.21	0.00	96.63	32.2
17681	444.0	75.08	0.31	11.52	1.65	0.09	0.31	1.65	4.07	1.65	0.10	0.04	0.05	0.20	0.04	96.50	31.7
17681	444.0	75.28	0.29	11.49	1.60	0.05	0.31	1.65	2.71	1.57	0.09	0.03	0.06	0.24	0.21	95.11	32.9
17681	444.0	74.50	0.29	11.47	1.58	0.09	0.27	1.66	3.83	1.54	0.09	0.00	0.03	0.19	0.07	95.38	30.2
17681	444.0	75.48	0.30	11.36	1.64	0.08	0.25	1.59	3.95	1.51	0.05	0.03	0.08	0.18	0.10	96.27	27.8
17681	444.0	75.57	0.30	11.69	1.55	0.07	0.29	1.64	4.02	1.63	0.07	0.00	0.03	0.19	0.06	96.89	31.8
17681	444.0	74.19	0.27	11.29	1.64	0.11	0.27	1.67	4.24	1.58	0.05	0.03	0.01	0.18	0.08	95.36	29.1
17681	444.0	75.23	0.30	11.44	1.60	0.09	0.31	1.68	4.01	1.65	0.13	0.01	0.06	0.20	0.09	96.50	32.6
17681	444.0	75.80	0.28	11.52	1.60	0.06	0.30	1.66	3.97	1.57	0.07	0.02	0.05	0.19	0.10	96.89	32.1
17681	444.0	75.36	0.30	11.60	1.56	0.05	0.29	1.70	3.95	1.57	0.09	0.04	0.09	0.20	0.04	96.54	31.9
17681	444.0	73.75	0.27	11.40	1.61	0.12	0.30	1.62	4.11	1.57	0.08	0.02	0.07	0.18	0.07	94.90	31.5
17681	444.0	75.35	0.28	11.76	1.74	0.08	0.32	1.61	3.94	1.64	0.05	0.02	0.03	0.20	0.00	96.85	31.7
17681	444.0	74.46	0.30	11.56	1.63	0.11	0.29	1.62	4.16	1.52	0.09	0.00	0.05	0.20	0.09	95.81	30.7
17681	444.0	74.72	0.31	11.54	1.58	0.04	0.30	1.63	3.96	1.53	0.09	0.01	0.04	0.21	0.05	95.77	32.5
17681	444.0	74.36	0.32	11.42	1.57	0.09	0.30	1.63	3.79	1.56	0.04	0.03	0.05	0.16	0.06	95.15	32.5
17681	444.0	73.81	0.30	11.12	1.64	0.05	0.26	1.54	3.81	1.52	0.03	0.01	0.06	0.21	0.06	94.15	28.3
17681	444.0	75.11	0.29	11.20	1.59	0.10	0.29	1.60	2.98	1.51	0.05	0.02	0.02	0.19	0.09	94.77	31.5
17681	444.0	74.99	0.31	11.52	1.62	0.07	0.29	1.68	4.12	1.57	0.08	0.00	0.09	0.21	0.01	96.31	31.3
17681	444.0	75.16	0.33	11.45	1.57	0.09	0.30	1.59	3.99	1.62	0.07	0.06	0.09	0.19	0.01	96.25	32.6
17681	444.0	74.45	0.28	11.68	1.66	0.06	0.31	1.63	4.02	1.57	0.09	0.04	0.08	0.20	0.06	95.81	31.8
17681	444.0	74.70	0.30	11.39	1.61	0.07	0.29	1.61	3.73	1.56	0.06	0.02	0.07	0.20	0.04	95.41	31.1
stdev		0.59	0.02	0.15	0.04	0.02	0.02	0.04	0.37	0.05	0.03	0.02	0.02	0.02	0.05	0.79	
av (n=21)		**74.91**	**0.30**	**11.47**	**1.61**	**0.08**	**0.29**	**1.63**	**3.87**	**1.57**	**0.07**	**0.02**	**0.06**	**0.20**	**0.06**	**96.14**	**31.3**

Table 18: Major element analyses of glass shards in wt.% of core 17682

Core	Depth (cm)	SiO_2	TiO_2	Al_2O_3	FeO^T	MnO	MgO	CaO	Na_2O	K_2O	P_2O_5	Cr	F	Cl	SO_2	Total	Mg#
17682	9.2	69.02	0.74	14.72	4.16	0.14	0.94	2.72	3.72	3.20	0.25					99.61	36.2
17682	9.2	70.63	0.62	14.77	3.78	0.07	0.78	2.13	3.89	3.37	0.15					100.18	33.9
17682	9.2	69.57	0.77	14.52	4.02	0.13	0.88	2.66	3.66	3.12	0.24					99.58	35.4
stdev		0.82	0.08	0.13	0.19	0.04	0.08	0.33	0.12	0.13	0.05					0.34	
av (n=3)		**69.74**	**0.71**	**14.67**	**3.99**	**0.11**	**0.87**	**2.51**	**3.76**	**3.23**	**0.21**					**99.79**	**35.2**
17682	23.2	78.37	0.25	11.65	1.32	0.07	0.23	1.28	2.62	1.69	0.04					97.52	30.2
17682	23.2	78.04	0.24	11.75	1.27	0.05	0.22	1.28	2.37	1.78	0.03					97.03	30.2
17682	23.2	78.84	0.22	11.43	1.27	0.09	0.24	1.33	2.60	1.75	0.04					97.81	31.6
17682	23.2	78.08	0.24	11.68	1.25	0.06	0.23	1.31	2.21	1.75	0.05					96.86	31.3
17682	23.2	78.17	0.24	11.60	1.28	0.04	0.22	1.33	2.55	1.81	0.06					97.31	30.4
17682	23.2	80.06	0.24	11.67	1.36	0.05	0.23	1.35	2.52	1.82	0.02					99.31	29.4
17682	23.2	77.97	0.24	11.62	1.27	0.04	0.22	1.30	2.61	1.79	0.02					97.08	30.6
17682	23.2	78.55	0.26	11.56	1.21	0.06	0.21	1.29	2.63	1.73	0.04					97.52	30.2
17682	23.2	78.16	0.22	11.51	1.33	0.08	0.22	1.28	2.43	1.74	0.05					97.01	29.2
stdev		0.66	0.01	0.10	0.05	0.02	0.01	0.03	0.14	0.04	0.01					0.75	
av (n=9)		**78.47**	**0.24**	**11.61**	**1.28**	**0.06**	**0.22**	**1.31**	**2.50**	**1.76**	**0.04**					**97.50**	**30.3**
17682	38.6	68.12	0.75	15.11	3.24	0.00	0.88	2.66	3.66	3.12	0.24					97.79	40.5
17682	38.6	69.75	0.80	14.94	3.68	0.11	0.95	2.74	2.77	3.28	0.19					99.22	39.1
17682	38.6	67.36	0.81	14.89	3.74	0.16	0.96	2.74	3.13	3.23	0.23					97.25	39.0
17682	38.6	67.54	0.77	14.83	3.64	0.14	0.94	2.68	2.29	3.26	0.22					96.30	39.2
17682	38.6	67.76	0.76	14.80	3.56	0.12	0.91	2.58	3.04	3.32	0.21					97.07	39.0
17682	38.6	68.12	0.79	15.14	3.66	0.12	0.98	2.81	2.81	3.34	0.24					98.00	40.0
stdev		0.86	0.02	0.14	0.18	0.06	0.03	0.08	0.46	0.08	0.02					0.99	
av (n=6)		**68.11**	**0.78**	**14.95**	**3.59**	**0.11**	**0.93**	**2.70**	**2.95**	**3.26**	**0.22**					**97.61**	**39.4**
17682	311.2	76.34	0.30	11.83	1.59	0.11	0.34	1.81	3.84	1.43	0.09	0.01	0.04	0.15	0.07	97.93	34.6
17682	311.2	77.10	0.23	11.77	1.57	0.07	0.33	1.92	3.90	1.40	0.14	0.03	0.08	0.11	0.02	98.66	34.3
17682	311.2	76.48	0.20	11.72	1.57	0.09	0.35	1.90	3.93	1.36	0.09	0.02	0.05	0.13	0.07	97.96	35.4
17682	311.2	75.38	0.28	11.66	1.70	0.06	0.30	1.93	4.10	1.36	0.08	0.04	0.06	0.11	0.04	97.10	30.5
17682	311.2	75.41	0.24	11.70	1.57	0.06	0.33	1.88	3.68	1.36	0.11	0.03	0.10	0.12	0.04	96.63	34.0
17682	311.2	75.39	0.25	11.59	1.61	0.10	0.33	1.81	3.73	1.38	0.10	0.01	0.06	0.13	0.03	96.52	34.1
17682	311.2	77.03	0.25	11.77	1.58	0.05	0.35	1.79	3.72	1.25	0.06	0.04	0.02	0.11	0.00	98.02	35.8
17682	311.2	76.39	0.23	11.69	1.52	0.07	0.33	1.84	3.77	1.27	0.07	0.01	0.02	0.12	0.04	97.38	34.8
17682	311.2	74.67	0.26	11.58	1.57	0.08	0.35	2.66	3.96	1.34	0.10	0.01	0.08	0.14	0.14	96.93	36.1
17682	311.2	75.28	0.24	11.81	1.64	0.09	0.38	2.04	4.06	1.37	0.06	0.02	0.06	0.15	0.02	97.22	36.4
17682	311.2	76.15	0.25	11.84	1.57	0.11	0.34	1.88	3.91	1.35	0.10	0.03	0.03	0.10	0.06	97.70	35.1
17682	311.2	76.48	0.27	11.77	1.58	0.10	0.33	1.90	3.79	1.38	0.09	0.03	0.09	0.13	0.09	98.01	34.1
17682	311.2	77.57	0.23	11.94	1.70	0.07	0.34	1.87	3.87	1.43	0.09	0.02	0.06	0.12	0.03	99.33	33.3
17682	311.2	76.52	0.25	11.84	1.60	0.06	0.33	1.81	3.77	1.39	0.06	0.04	0.08	0.12	0.04	97.90	33.7
17682	311.2	74.97	0.23	11.78	1.52	0.09	0.31	1.86	3.77	1.39	0.13	0.03	0.02	0.11	0.10	96.32	34.0
17682	311.2	74.53	0.24	11.51	1.58	0.07	0.32	1.87	3.75	1.38	0.11	0.03	0.05	0.12	0.03	95.59	33.9
17682	311.2	75.34	0.23	11.84	1.62	0.07	0.35	1.86	3.70	1.36	0.10	0.05	0.08	0.13	0.04	96.77	35.1
17682	311.2	77.35	0.29	11.92	1.59	0.07	0.34	1.91	3.85	1.36	0.06	0.00	0.05	0.14	0.02	98.97	34.6
17682	311.2	76.73	0.23	11.72	1.60	0.09	0.33	1.93	3.84	1.37	0.12	0.02	0.08	0.13	0.02	98.21	34.3
17682	311.2	75.39	0.23	11.54	1.55	0.10	0.32	1.88	3.85	1.41	0.06	0.01	0.02	0.11	0.02	96.48	33.9
17682	311.2	75.28	0.25	11.74	1.63	0.08	0.31	1.86	3.75	1.38	0.06	0.03	0.05	0.11	0.05	96.57	32.3
17682	311.2	75.35	0.26	11.41	1.58	0.09	0.32	1.86	3.50	1.37	0.11	0.00	0.06	0.13	0.07	96.10	33.6
stdev		0.89	0.02	0.14	0.05	0.02	0.02	0.18	0.13	0.04	0.02	0.01	0.02	0.01	0.03	0.97	
av (n=22)		**75.96**	**0.25**	**11.73**	**1.66**	**0.08**	**0.33**	**1.91**	**3.82**	**1.37**	**0.09**	**0.02**	**0.06**	**0.12**	**0.05**	**97.44**	**33.4**

Table 9.18: 17682 (continued)

Core	Depth (cm)	SiO_2	TiO_2	Al_2O_3	FeO^T	MnO	MgO	CaO	Na_2O	K_2O	P_2O_5	Cr	F	Cl	SO_2	Total	Mg#
17682	327.8	72.90	0.41	13.22	3.43	0.16	0.64	2.92	4.16	1.11	0.18	0.00	0.06	0.15	0.12	99.46	31.7
17682	327.8	71.58	0.40	13.13	3.33	0.15	0.62	2.99	4.31	1.09	0.17	0.04	0.06	0.14	0.06	98.08	31.9
17682	327.8	73.24	0.38	13.43	3.32	0.16	0.66	2.94	2.97	1.14	0.21	0.00	0.06	0.14	0.07	98.73	33.2
17682	327.8	72.17	0.41	13.16	3.33	0.14	0.62	2.86	4.25	1.06	0.18	0.04	0.04	0.15	0.03	98.42	31.9
17682	327.8	72.07	0.44	13.45	3.46	0.13	0.71	3.12	4.16	1.13	0.20	0.03	0.08	0.12	0.02	99.13	33.9
17682	327.8	70.95	0.45	13.29	3.60	0.15	0.75	3.23	4.40	1.07	0.16	0.02	0.03	0.14	0.01	98.22	34.2
17682	327.8	70.10	0.47	13.70	4.19	0.14	0.96	3.65	4.18	1.03	0.22	0.02	0.04	0.16	0.12	98.99	36.5
17682	327.8	71.83	0.40	13.29	3.59	0.19	0.75	3.23	4.22	1.11	0.19	0.02	0.07	0.14	0.02	99.04	34.2
17682	327.8	72.74	0.49	13.85	3.85	0.15	0.86	3.47	4.07	1.07	0.20	0.00	0.07	0.15	0.08	101.04	35.8
17682	327.8	72.43	0.40	13.31	3.43	0.16	0.69	3.26	3.10	1.15	0.21	0.00	0.08	0.17	0.06	98.44	33.5
17682	327.8	70.43	0.44	13.13	3.84	0.13	0.75	3.56	4.14	1.08	0.17	0.00	0.02	0.14	0.02	97.84	32.6
17682	327.8	72.22	0.48	13.64	3.81	0.15	0.85	3.21	3.50	1.13	0.19	0.02	0.06	0.13	0.01	99.40	35.7
stdev		0.97	0.04	0.24	0.27	0.02	0.11	0.25	0.48	0.04	0.02	0.02	0.02	0.01	0.04	0.85	
av (n=12)		**71.89**	**0.43**	**13.38**	**3.75**	**0.15**	**0.74**	**3.20**	**3.95**	**1.10**	**0.19**	**0.02**	**0.06**	**0.14**	**0.05**	**99.05**	**33.0**
17682	712.6	69.29	0.67	14.15	2.89	0.13	0.62	2.05	2.66	4.02	0.17					96.65	34.9
17682	712.6	67.93	0.66	14.46	2.86	0.12	0.64	2.15	1.90	3.89	0.14					94.75	35.9
17682	712.6	68.52	0.66	14.49	2.80	0.14	0.61	1.99	2.37	3.87	0.15					95.58	35.2
17682	712.6	68.76	0.65	14.79	2.83	0.11	0.64	1.97	1.82	3.85	0.13					95.56	36.2
17682	712.6	69.08	0.67	14.88	2.82	0.12	0.64	1.98	2.81	3.93	0.12					97.05	36.4
17682	712.6	67.70	0.68	14.76	2.84	0.13	0.63	2.06	2.76	4.01	0.13					95.70	35.8
17682	712.6	67.87	0.63	14.79	2.76	0.11	0.63	2.06	2.87	4.01	0.15					95.88	36.3
17682	712.6	67.38	0.65	14.68	2.70	0.12	0.65	2.06	2.66	3.96	0.15					95.02	37.7
17682	712.6	68.47	0.65	14.63	2.80	0.11	0.62	2.04	2.79	3.99	0.12					96.23	35.8
17682	712.6	68.75	0.64	14.80	2.79	0.14	0.65	2.05	2.87	4.04	0.14					96.88	36.8
17682	712.6	69.08	0.67	15.01	2.78	0.14	0.65	1.89	3.17	4.06	0.15					97.58	36.8
17682	712.6	67.70	0.66	14.34	2.83	0.11	0.62	1.98	2.92	4.06	0.13					95.36	35.5
17682	712.6	67.08	0.68	14.92	2.80	0.12	0.66	2.03	2.70	4.01	0.13					95.13	37.0
stdev		0.71	0.01	0.25	0.05	0.01	0.01	0.06	0.39	0.07	0.01					0.87	
av (n=14)		**68.28**	**0.66**	**14.67**	**2.81**	**0.12**	**0.64**	**2.03**	**2.64**	**3.98**	**0.14**					**95.95**	**36.2**

Table 19: Major element analyses of glass shards in wt.% of core 17684

Core	Depth (cm)	SiO_2	TiO_2	Al_2O_3	FeO^T	MnO	MgO	CaO	Na_2O	K_2O	P_2O_5	Total	Mg#
17684	29.9	67.23	0.87	14.95	4.27	0.16	1.01	2.75	3.08	3.04	0.26	97.62	37.1
17684	29.9	67.48	0.77	14.59	4.04	0.10	0.94	2.70	2.41	3.25	0.21	96.50	36.8
17684	29.9	68.68	0.81	14.91	4.15	0.13	0.97	2.74	2.18	3.35	0.23	98.15	36.8
17684	29.9	69.15	0.81	15.03	4.21	0.18	1.00	2.80	2.62	3.40	0.25	99.44	37.2
17684	29.9	69.20	0.76	14.92	4.16	0.15	0.96	2.84	2.32	3.33	0.22	98.86	36.6
stdev		0.93	0.04	0.17	0.08	0.03	0.03	0.05	0.35	0.14	0.02	1.13	
av (n=5)		**68.35**	**0.81**	**14.88**	**4.17**	**0.14**	**0.97**	**2.77**	**2.52**	**3.27**	**0.23**	**98.11**	**36.9**
17684	129.6	52.35	0.52	19.74	6.84	0.18	2.09	5.27	5.09	5.44	0.76	98.29	43.3
17684	129.6	52.45	0.64	19.02	7.27	0.21	1.68	4.52	5.91	5.03	0.68	97.40	36.7
17684	129.6	53.73	1.16	19.95	7.12	0.20	1.50	4.51	5.17	5.72	0.53	99.59	34.4
stdev		0.77	0.34	0.49	0.22	0.01	0.30	0.44	0.45	0.35	0.12	1.10	
av (n=3)		**52.84**	**0.77**	**19.57**	**7.08**	**0.20**	**1.76**	**4.77**	**5.39**	**5.40**	**0.66**	**98.43**	**38.3**
17684	239.2	51.13	0.50	19.78	7.33	0.19	2.00	4.83	5.88	6.33	0.72	98.67	40.5
17684	239.2	51.06	0.50	19.69	7.52	0.21	2.04	5.12	5.83	5.65	0.71	98.34	40.5
17684	239.2	51.23	0.56	19.31	7.92	0.21	2.27	5.43	5.74	5.63	0.85	99.15	41.7
17684	239.2	52.24	0.48	19.56	7.62	0.21	1.94	4.72	6.05	6.28	0.75	99.84	38.9
17684	239.2	52.18	0.47	19.82	7.41	0.22	2.07	5.02	5.73	6.07	0.78	99.76	41.1
17684	239.2	52.54	0.49	19.63	7.42	0.23	1.97	4.92	6.44	5.78	0.76	100.18	39.9
stdev		0.66	0.03	0.18	0.21	0.01	0.12	0.25	0.27	0.31	0.05	0.72	
av (n=6)		**51.73**	**0.50**	**19.63**	**7.54**	**0.21**	**2.05**	**5.01**	**5.94**	**5.95**	**0.76**	**99.32**	**40.4**
17684	248.4	55.40	0.48	20.59	5.43	0.15	1.42	3.35	6.00	6.89	0.43	100.14	39.5
17684	248.4	53.50	0.54	19.69	6.87	0.19	1.91	4.51	5.25	6.72	0.69	99.89	41.0
17684	248.4	54.20	0.58	20.37	6.32	0.17	1.46	3.73	6.52	6.79	0.57	100.71	36.6
17684	248.4	54.24	0.58	20.06	5.69	0.18	1.46	3.67	6.06	6.11	0.58	98.63	39.1
17684	248.4	53.84	0.52	19.58	7.36	0.17	2.12	5.06	5.22	6.59	0.78	101.23	41.8
stdev		0.72	0.04	0.43	0.81	0.01	0.32	0.70	0.56	0.30	0.13	0.98	
av (n=5)		**54.24**	**0.54**	**20.06**	**6.33**	**0.17**	**1.67**	**4.07**	**5.81**	**6.62**	**0.61**	**100.12**	**39.8**
17684	290.7	52.41	0.48	19.12	6.94	0.20	1.94	4.78	5.72	6.22	0.77	98.57	41.1
17684	290.7	52.91	0.49	19.56	6.81	0.17	1.84	4.48	6.51	5.55	0.69	99.03	40.3
17684	290.7	52.43	0.50	18.96	6.83	0.21	2.07	5.00	5.40	6.17	0.78	98.34	43.1
17684	290.7	52.90	0.51	19.90	7.61	0.19	1.96	4.91	6.07	5.56	0.80	100.41	39.2
17684	290.7	53.68	0.48	19.82	6.95	0.20	1.95	4.83	6.11	5.91	0.74	100.67	41.3
17684	290.7	53.22	0.49	19.76	6.73	0.18	1.95	4.90	5.94	6.27	0.70	100.15	42.1
17684	290.7	53.67	0.50	19.67	6.75	0.21	2.01	4.97	5.60	6.50	0.79	100.66	42.7
17684	290.7	53.16	0.50	19.31	7.19	0.20	1.98	5.18	5.93	6.13	0.78	100.37	40.8
stdev		0.49	0.01	0.34	0.30	0.01	0.07	0.20	0.34	0.34	0.04	0.97	
av (n=8)		**53.05**	**0.49**	**19.51**	**6.98**	**0.19**	**1.96**	**4.88**	**5.91**	**6.04**	**0.76**	**99.78**	**41.3**

Table 20: Composition of feldspar

Core	Depth (cm)	SiO_2	TiO_2	Al_2O_3	FeO^T	MnO	MgO	CaO	Na_2O	K_2O	P_2O_5	Total	n	*An*	*Ab*	*Or*	Xeno	Matrix
17675	12.1	56.69	0.05	27.22	0.67	0.02	0.07	10.19	5.58	0.32	0.10	100.92	1	*49.3*	*48.9*	*1.8*	x	
17675	21.5	59.67	0.01	25.64	0.35	0.03	0.01	8.32	6.65	0.14	0.12	100.93	3	*40.5*	*58.6*	*0.9*	x	
17675	21.5	59.18	0.02	25.44	0.37	0.01	0.03	8.31	6.64	0.15	0.10	100.24	4	*40.5*	*58.6*	*0.9*	x	
17676	20.3	58.46	0.01	26.14	0.40	0.01	0.02	9.41	6.26	0.12	0.12	100.96	2	*45.1*	*54.3*	*0.6*	x	
17677	6.8	60.72	0.04	25.32	0.40	0.02	0.02	7.69	6.51	0.17	0.11	100.98	2	*39.1*	*59.9*	*1.0*		x
17677	6.8	60.18	0.01	25.10	0.35	0.01	0.03	7.66	6.88	0.18	0.10	100.49	3	*37.7*	*61.3*	*1.0*	x	
17677	6.8	59.90	0.01	25.42	0.37	0.01	0.01	7.92	6.80	0.17	0.11	100.72	4	*38.8*	*60.2*	*1.0*	x	
17677	51.5	54.02	0.02	29.17	0.50	0.02	0.03	11.61	4.70	0.09	0.12	100.29	3	*57.4*	*42.1*	*0.5*	x	
17677	157.6	61.34	0.02	24.50	0.50	0.02	0.02	6.00	6.92	1.45	0.06	100.83	3	*29.6*	*61.8*	*8.6*	x	
17677	183.3	52.71	0.03	29.47	0.66	0.01	0.05	12.49	3.87	0.54	0.16	99.99	2	*62.0*	*34.8*	*3.2*		x
17677	183.3	53.53	0.04	29.27	0.49	0.02	0.05	12.58	4.03	0.29	0.14	100.41	3	*62.2*	*36.1*	*1.7*	x	
17677	183.3	55.61	0.03	28.20	0.55	0.02	0.04	10.65	4.78	0.76	0.14	100.78	3	*52.7*	*42.8*	*4.5*	x	
17677	183.3	54.45	0.04	28.20	0.51	0.02	0.04	11.26	4.74	0.70	0.14	100.12	3	*54.5*	*41.5*	*4.0*	x	
17677	231.1	55.59	0.04	27.60	0.57	0.00	0.05	10.97	4.70	0.79	0.13	100.44	4	*53.7*	*41.7*	*4.6*	x	
17677	231.1	55.07	0.01	28.20	0.26	0.00	0.00	11.96	4.77	0.16	0.14	100.57	3	*57.5*	*41.5*	*1.0*	x	
17677	231.1	54.90	0.02	28.13	0.60	0.03	0.02	10.92	4.92	0.42	0.10	100.06	3	*53.7*	*43.8*	*2.5*	x	
17677	345.5	54.41	0.06	27.76	0.52	0.00	0.04	10.67	4.74	0.92	0.14	99.27	2	*52.5*	*42.5*	*5.3*	x	
17677	345.5	54.79	0.03	28.03	0.46	0.01	0.02	11.18	4.81	0.50	0.12	99.97	3	*54.6*	*42.5*	*2.9*	x	
17682	38.6	51.92	0.04	29.43	1.56	0.00	0.21	13.80	3.44	0.07	0.17	100.62	2	*68.6*	*31.0*	*0.4*	x	
17682	38.6	54.85	0.00	28.75	0.48	0.01	0.02	11.55	5.03	0.09	0.12	100.90		*55.6*	*43.8*	*0.6*		x
17682	327.8	53.85	0.02	28.00	1.61	0.01	0.07	11.69	4.74	0.22	0.21	100.42	2	*56.9*	*41.8*	*1.3*	x	
17684	29.9	54.44	0.05	27.83	0.61	0.00	0.05	10.83	4.67	0.93	0.13	99.54	3	*53.1*	*41.5*	*5.4*	x	
17684	129.6	56.52	0.03	26.78	0.51	0.02	0.02	8.78	6.19	0.72	0.10	99.67	3	*42.1*	*53.8*	*4.1*		x
17684	248.4	58.76	0.02	25.82	0.50	0.00	0.02	8.53	6.26	0.85	0.10	100.85	3	*40.9*	*54.3*	*4.8*	x	
17684	248.4	58.62	0.05	25.40	0.53	0.00	0.03	8.28	6.26	0.84	0.10	100.12	4	*40.2*	*55.0*	*4.8*	x	

Table 21: Composition of pyroxene

Core	Depth (cm)	SiO_2	TiO_2	Al_2O_3	FeO^T	MnO	MgO	CaO	Na_2O	K_2O	P_2O_5	Total	n	*Wo*	*En*	*Fs*
17677	51.5	48.52	0.72	5.44	6.40	0.14	14.07	23.73	0.33	0.00	0.27	99.62	3	*49.0*	*40.4*	*10.5*
17677	51.5	52.06	0.32	2.04	4.62	0.12	16.39	23.91	0.19	0.01	0.27	99.95	3	*47.4*	*45.2*	*7.3*
17677	157.6	50.83	0.55	3.18	6.74	0.38	14.25	22.98	0.64	0.01	0.32	99.88	2	*47.5*	*41.0*	*11.5*
17677	157.6	48.26	0.87	5.34	8.00	0.25	12.71	22.84	0.52	0.01	0.31	99.12	3	*48.6*	*37.7*	*13.7*
17677	157.6	50.83	0.55	3.18	6.74	0.38	14.25	22.98	0.64	0.01	0.32	99.88	2	*47.5*	*41.0*	*11.5*
17677	157.6	48.26	0.87	5.34	8.00	0.25	12.71	22.84	0.52	0.01	0.31	99.12	3	*48.6*	*37.7*	*13.7*
17677	157.6	50.45	0.65	3.67	6.65	0.31	13.94	22.86	0.58	0.00	0.27	99.39	3	*47.9*	*40.7*	*11.4*
17677	157.6	51.14	0.56	3.04	6.53	0.39	14.42	22.90	0.62	0.01	0.27	99.89	3	*47.3*	*41.5*	*11.2*
17677	183.3	51.14	0.59	3.53	7.02	0.32	14.27	22.60	0.66	0.00	0.25	100.39	2	*46.9*	*41.2*	*11.9*
17677	183.3	49.54	0.78	5.71	8.14	0.19	12.69	22.38	0.46	0.01	0.29	100.20	3	*48.1*	*37.9*	*14.0*
17677	272.4	49.91	0.81	4.71	7.28	0.27	13.21	22.95	0.56	0.00	0.29	100.01	3	*48.6*	*38.9*	*12.5*
17677	272.4	49.68	0.71	4.33	6.70	0.24	13.57	23.38	0.47	0.00	0.27	99.40	3	*49.0*	*39.6*	*11.4*
17677	272.4	49.60	0.80	4.47	7.02	0.28	13.17	22.99	0.52	0.01	0.27	99.36	4	*48.9*	*39.0*	*12.1*
17677	345.5	48.63	0.65	4.61	7.50	0.20	13.39	23.12	0.44	0.01	0.29	98.83	4	*48.4*	*39.0*	*12.6*
17677	345.5	48.90	0.89	5.27	7.96	0.33	12.89	23.72	0.50	0.01	0.29	100.74	4	*49.3*	*37.3*	*13.4*
17677	345.5	49.44	0.78	4.56	7.46	0.30	13.09	23.38	0.49	0.00	0.28	99.79	3	*49.1*	*38.2*	*12.7*
17684	29.9	48.91	0.94	5.41	8.22	0.26	12.60	23.24	0.56	0.00	0.35	100.49	3	*49.0*	*37.0*	*14.0*
17684	29.9	49.62	0.71	4.53	7.83	0.30	13.30	23.43	0.51	0.01	0.31	100.54	3	*48.5*	*38.3*	*13.2*
17684	29.9	49.23	0.93	5.15	7.89	0.28	12.69	23.39	0.59	0.00	0.29	100.45	3	*49.3*	*37.2*	*13.5*
17684	129.6	48.26	0.90	5.86	8.18	0.28	12.45	23.33	0.66	0.00	0.32	100.24	3	*49.4*	*36.7*	*14.0*
17684	129.6	49.42	0.68	4.17	7.43	0.33	13.69	23.48	0.59	0.00	0.27	100.06	3	*48.3*	*39.2*	*12.5*
17684	129.6	48.14	0.85	4.34	8.81	0.36	12.08	23.88	0.77	0.01	0.27	99.51	3	*49.9*	*35.1*	*15.0*
17684	239.2	50.65	0.63	4.56	7.43	0.26	12.41	23.52	0.59	0.03	0.30	100.37	4	*50.3*	*36.9*	*12.8*
17684	239.2	50.37	0.64	4.21	7.66	0.25	12.57	23.69	0.43	0.00	0.30	100.12	3	*50.0*	*36.9*	*13.0*
17684	239.2	51.41	0.48	3.25	7.39	0.14	13.43	24.18	0.29	0.00	0.29	100.85	3	*49.6*	*38.3*	*12.1*
17684	248.4	49.33	0.74	4.74	8.01	0.27	11.21	24.02	0.51	0.01	0.29	99.12	3	*52.1*	*33.8*	*14.0*
17684	248.4	51.36	0.66	3.20	6.59	0.30	12.85	23.78	0.69	0.01	0.27	99.71	3	*50.6*	*38.0*	*11.4*
17684	290.7	49.66	0.62	4.77	7.18	0.21	13.15	23.02	0.45	0.01	0.31	99.37	6	*48.9*	*38.9*	*12.2*
17684	290.7	48.31	0.92	5.71	8.60	0.23	11.55	23.66	0.53	0.01	0.29	99.80	3	*50.7*	*34.5*	*14.8*
17684	290.7	47.87	0.80	5.63	8.63	0.18	12.08	23.48	0.52	0.00	0.30	99.48	2	*49.8*	*35.6*	*14.6*
17684	290.7	48.16	0.76	5.38	8.37	0.27	11.72	23.69	0.48	0.01	0.25	99.09	3	*50.7*	*34.9*	*14.4*

Table 22: Composition of olivine

Core	Depth (cm)	SiO_2	TiO_2	Al_2O_3	FeO^T	MnO	MgO	CaO	Na_2O	K_2O	P_2O_5	Total	n	*Fo*
17676 *	20.3	52.52	0.12	0.41	20.11	1.57	20.39	1.03	0.00	0.01	0.02	98.66	3	*50.3*
17676	20.3	53.54	0.11	0.46	19.99	1.47	21.54	1.06	0.01	0.01	0.02	100.69	3	*51.9*
17677 *	6.8	53.84	0.28	0.77	15.73	0.94	24.54	1.61	0.03	0.00	0.04	99.74	3	*61.0*
17677	6.8	54.67	0.25	0.56	15.23	1.21	24.30	1.51	0.04	0.01	0.03	99.69	3	*61.5*
17677	6.8	53.86	0.11	0.42	19.63	1.63	21.43	1.02	0.02	0.01	0.03	100.58	3	*52.2*
17677	75	37.15	0.02	0.03	23.05	0.81	35.37	0.43	0.02	0.00	0.06	99.78	3	*60.6*
17677	183.3	38.12	0.03	0.03	20.52	1.02	35.94	0.34	0.01	0.01	0.06	98.62	3	*63.7*

* Rim analysis

Table 23: Composition of phlogopite

Core	Depth (cm)	SiO_2	TiO_2	Al_2O_3	FeO^T	MnO	MgO	CaO	Na_2O	K_2O	P_2O_5	Total	n	Mg#
17677	51.5	39.42	0.50	15.05	7.00	0.06	22.85	0.59	0.86	8.43	0.65	95.95	3	89.1
17677	56.8	40.32	0.34	16.76	5.54	0.02	23.61	0.48	1.12	9.12	0.43	98.06	3	91.4

9.7 Trace element statistics

Table 24: ICP-MS measurements of two samples dissolved in duplicate to check the reproducibility

Core	17682	17682
Depth (cm)	712.6	712.6 dupl.
Co	2.6	2.9
Ga	18.2	18.7
Rb	76.3	79.1
Sr	210.4	220.2
Y	36.1	37.7
Zr	219.0	229.1
Nb	4.88	5.26
Cs	2.16	2.25
Ba	515.2	533.4
Hf	5.60	5.64
Ta	0.23	0.26
Tl	0.30	0.31
Pb	12.47	13.84
Th	3.64	3.81
U	2.18	2.28
La	15.74	16.15
Ce	33.68	35.00
Pr	4.79	4.99
Nd	19.95	20.75
Sm	5.05	5.33
Eu	1.28	1.28
Gd	5.20	5.41
Tb	0.87	0.90
Dy	5.60	5.83
Ho	1.22	1.27
Er	3.61	3.72
Tm	0.57	0.59
Yb	3.93	4.03
Lu	0.61	0.63

Table 25: Trace element analyses of standard rocks (Jenner et al., 1990; Govindaraju, 1994; Jochum et al., 2000)

	StHs6/80-G this work	StHs6/80-G Jochum et al. 2000	BHVO-1 this work	BHVO-1 Govindaraju 1994	BHVO-1 Jenner 1990
Co	15.8	13.0	46.6	45.0	–
Ni	22.9	27.0	117.9	121.0	–
Cu	46.6	47.0	141.7	136.0	–
Zn	72.0	65.0	110.4	105.0	–
Ga	24.2	21.0	22.6	21.0	–
Rb	29.2	29.9	9.8	11.0	9.2
Sr	510.2	486.0	417.9	403.0	396.0
Y	12.0	11.3	25.7	27.6	25.6
Zr	124.1	120.0	170.7	179.0	190.0
Nb	7.07	7.10	17.68	17.11	19.00
Cs	1.50	1.89	0.10	0.13	0.11
Ba	305.9	302.0	133.2	139.0	133.0
Hf	3.27	3.16	4.71	4.38	4.60
Ta	0.42	0.42	1.10	1.10	1.20
Pb	10.37	10.20	2.04	2.08	2.00
Th	2.23	2.22	1.22	1.10	1.20
U	1.01	1.03	0.44	0.43	0.43
La	12.12	11.90	15.55	15.80	15.40
Ce	25.09	25.70	37.76	39.00	37.70
Pr	3.22	3.17	5.45	5.70	5.25
Nd	12.69	12.70	24.36	25.20	24.40
Sm	2.84	2.79	6.20	6.20	6.00
Eu	0.93	0.97	2.06	2.06	2.20
Gd	2.66	2.64	6.27	6.40	6.20
Tb	0.40	0.37	0.96	0.86	0.96
Dy	2.26	2.19	5.35	5.20	5.40
Ho	0.44	0.42	1.00	0.99	1.05
Er	1.21	1.17	2.64	2.40	2.54
Tm	0.18	0.17	0.34	0.33	0.32
Yb	1.15	1.11	2.02	2.02	2.01
Lu	0.18	0.17	0.28	0.29	0.28

9.8 Trace element analyses

Table 26: Trace element concentrations of glass shards in ppm

Core	17674	17675	17675	17675	17675	17676	17676	17676	17677	17677	17677
Depth (cm)	44.4	12.1	18.3	21.5	138.4	10.3	20.3	22.2	116.6	228.9	231.1
Co	4.6	4.9	2.7	3.5	5.6	2.7	2.1	1.7	3.7	1.1	29.3
Ni	9.9	11.8	14.0	13.6	14.3	9.9	6.5	5.5	6.3	5.4	10.9
Cu	34.0	20.4	16.1	30.2	37.9	16.2	13.2	13.5	11.5	73.0	238.1
Ga	17.1	16.2	14.9	15.7	18.4	16.2	14.1	13.1	15.6	17.4	22.1
Rb	51.1	36.9	25.6	32.7	56.1	28.1	24.0	23.9	16.1	72.5	97.4
Sr	197.7	239.1	153.4	246.7	197.6	197.3	138.0	142.8	243.7	132.1	1898.0
Y	33.2	34.0	32.8	35.1	35.7	37.0	33.0	31.8	22.9	41.0	19.3
Zr	200.4	152.6	149.1	159.8	218.0	167.8	143.6	143.3	74.3	225.5	84.2
Nb	4.14	2.99	2.20	2.88	4.56	2.54	2.16	2.19	0.77	4.76	3.46
Cs	1.43	0.99	0.86	1.01	1.58	1.00	0.85	0.85	0.91	1.92	1.64
Ba	479.0	430.2	368.1	659.4	505.0	431.8	361.3	360.7	160.2	551.5	392.2
Hf	5.31	4.08	4.05	4.51	5.90	4.60	3.89	3.85	2.16	5.98	1.96
Ta	0.20	0.12	0.11	0.15	0.20	0.13	0.11	0.08	0.05	0.23	0.15
Tl	0.28	0.21	0.19	0.21	0.31	0.22	0.18	0.18	0.15	0.30	0.28
Pb	11.64	8.81	6.85	9.47	12.57	7.46	5.93	5.96	5.45	12.76	11.84
Th	2.47	1.78	1.29	1.66	2.73	1.43	1.24	1.21	0.40	3.57	2.39
U	1.55	1.10	0.89	1.06	1.74	0.98	0.85	0.82	0.39	2.17	1.78
La	14.63	12.74	9.99	12.39	15.83	11.32	9.91	9.62	3.50	17.45	20.50
Ce	32.36	28.29	22.30	27.60	34.78	25.34	22.47	21.35	8.92	37.87	39.51
Pr	4.59	4.17	3.28	3.99	4.98	3.68	3.29	3.13	1.45	5.42	5.33
Nd	19.15	17.94	13.95	17.28	20.71	15.67	14.30	13.46	7.13	22.49	21.57
Sm	4.68	4.62	3.59	4.46	4.95	4.17	3.71	3.51	2.33	5.68	4.89
Eu	1.03	1.16	0.77	1.07	1.08	0.88	0.75	0.72	0.78	1.20	1.43
Gd	4.73	4.80	4.06	4.82	5.09	4.58	4.21	3.85	3.00	5.87	4.33
Tb	0.79	0.82	0.71	0.83	0.85	0.80	0.73	0.69	0.53	1.01	0.62
Dy	5.12	5.27	4.79	5.38	5.50	5.45	4.88	4.62	3.63	6.44	3.38
Ho	1.11	1.14	1.09	1.19	1.21	1.24	1.10	1.04	0.81	1.41	0.66
Er	3.37	3.39	3.34	3.65	3.60	3.78	3.34	3.21	2.39	4.18	1.84
Tm	0.54	0.54	0.56	0.58	0.59	0.62	0.55	0.52	0.37	0.66	0.28
Yb	3.78	3.70	3.88	4.01	4.01	4.35	3.85	3.69	2.54	4.57	1.83
Lu	0.58	0.56	0.61	0.63	0.63	0.69	0.61	0.59	0.39	0.71	0.27

Table 10.21:Trace element concentrations of glass shards in ppm (continued)

Core	17677	17677	17677	17681	17681	17682	17682	17682	17684	17684
Depth (cm)	264.8	270.0	272.4	344.6*	444.0	311.2	327.8	712.6	248.4	290.7
Co	20.9	15.5	20.3	2.2	2.9	2.1	3.6	2.7	29.6	25.8
Ni	3.9	6.6	12.2	8.0	6.7	5.3	8.9	11.3	8.2	9.3
Cu	201.3	204.3	206.6	19.7	11.2	11.4	11.8	11.3	212.6	185.7
Ga	21.9	19.6	25.1	12.9	17.3	12.1	15.3	18.4	21.4	19.2
Rb	101.0	88.2	111.6	26.3	19.4	22.4	17.5	77.7	90.4	81.4
Sr	1378.1	1683.2	1326.3	151.5	202.9	218.8	224.4	215.3	2227.9	2073.5
Y	16.0	15.5	17.8	26.8	25.7	17.8	24.0	36.9	17.9	15.5
Zr	67.5	74.5	108.2	109.3	76.5	71.6	79.4	224.1	61.7	76.9
Nb	4.03	3.17	5.85	1.14	1.04	1.06	0.89	5.07	2.54	2.99
Cs	1.77	1.67	2.14	1.06	0.94	0.83	0.96	2.21	1.48	1.35
Ba	367.9	412.5	439.3	283.4	215.6	229.5	172.7	524.3	465.2	465.0
Hf	1.30	1.68	2.33	3.24	2.15	2.07	2.29	5.62	1.26	1.80
Ta	0.09	0.13	0.25	0.06	0.06	0.06	0.05	0.24	0.07	0.15
Tl	0.11	0.14	0.17	0.23	0.18	0.20	0.17	0.30	0.11	0.15
Pb	11.42	16.37	14.25	6.48	6.10	5.79	6.21	13.15	11.32	12.59
Th	2.70	2.53	3.22	0.61	0.48	0.55	0.44	3.72	2.31	2.52
U	1.88	1.80	2.25	0.59	0.51	0.52	0.38	2.23	1.67	1.88
La	21.04	19.98	23.06	4.84	4.59	4.73	3.66	15.95	22.14	22.22
Ce	39.71	37.69	43.12	11.79	10.27	10.68	9.23	34.34	42.75	42.15
Pr	5.17	4.94	5.57	1.94	1.59	1.63	1.52	4.89	5.64	5.53
Nd	20.06	19.53	21.39	8.93	7.83	7.42	7.40	20.35	23.01	22.20
Sm	4.28	4.12	4.56	2.83	2.27	2.14	2.48	5.19	4.99	4.68
Eu	1.25	1.25	1.30	0.63	0.66	0.53	0.75	1.28	1.52	1.45
Gd	3.72	3.62	3.87	3.35	3.37	2.35	3.17	5.30	4.39	4.12
Tb	0.51	0.49	0.53	0.60	0.56	0.41	0.58	0.88	0.60	0.55
Dy	2.76	2.68	2.96	4.06	3.67	2.72	3.86	5.72	3.22	2.94
Ho	0.54	0.52	0.60	0.91	0.78	0.60	0.87	1.24	0.62	0.56
Er	1.53	1.44	1.69	2.76	2.31	1.82	2.52	3.67	1.69	1.56
Tm	0.23	0.22	0.26	0.44	0.36	0.29	0.39	0.58	0.25	0.23
Yb	1.53	1.47	1.72	3.01	2.63	2.04	2.69	3.98	1.63	1.52
Lu	0.23	0.22	0.26	0.48	0.40	0.32	0.42	0.62	0.25	0.23

* Clear glass